Remote Sensing of Mangrove Composition and Structure in the Galapagos Islands

Benjamin W. Heumann
Dissertation

A dissertation submitted to the faculty of the University of North Carolina at Chapel Hill in partial fulfillment of the requirement for the degree of Doctor of Philosophy in the Department of Geography

Chapel Hill
2011

Approved by
Dr. Stephen J. Walsh
Dr. Conghe Song
Dr. Aaron Moody
Dr. George P. Malanson
Dr. Dean Urban

Abstract

Benjamin W. Heumann: Remote sensing of mangrove composition and structure in the
Galapagos Islands
(Under the direction of Dr. Stephen J. Walsh)

Mangroves are unique inter-tidal ecosystems that provide valuable ecosystem goods and

services. This dissertation investigates new methods of characterizing mangrove forests using

remote sensing with implications for mapping and modeling ecosystem goods and services.

Specifically, species composition, leaf area, and canopy height are investigated for mangroves in

the Galapagos Islands. The Galapagos Islands serve as an interesting case study where

environmental conditions are highly variable over short distances producing a wide range of

mangrove composition and structure to examine. This dissertation reviews previous mangrove

remote sensing studies and seeks to address missing gaps. Specifically, this research seeks to

examine pixel and object-based methods for mapping mangrove species, investigate the

usefulness of spectral and spatial metrics to estimate leaf area, and compare existing global

digital surface models with a digital surface model extracted from new very high resolution

imagery. The major findings of this research include the following: 1) greater spectral

separability between true mangrove and mangrove associate species using object-based image

analysis compared to pixel-based analysis, but a lack of separability between individual

mangrove species, 2) the demonstrated necessity for novel machine-learning classification

techniques rather than traditional clustering classification algorithms, 3) significant but weak

relationships between spectral vegetation indices and leaf area, 4) moderate to strong

relationships between grey-level co-occurrence matrix image texture and leaf area at the

individual species level, 5) similar accuracy between a very high resolution stereo optical digital

surface model a coarse resolution InSAR product to estimate canopy height with improved accuracy using a hybrid model of these two products. The results demonstrate advancements in remote sensing technology and technique, but further challenges remain before these methods can be applied to monitoring and modeling applications. Based on these results, future research should focus on emerging technologies such as hyperspectral, very high resolution InSAR, and LiDAR to characterize mangrove forest composition and structure.

To my loving wife Carla,

Acknowledgements

Preface

The proposed title of this dissertation research was "Mapping suitable habitat of the critically endangered mangrove finch using remote sensing". The aim of this research was to generate the spatial data for a habitat model using remote sensing and use the output from the habitat model to help inform the Charles Darwin Research Station on where the best locations to establish new population of the mangrove finch would be. The creation of these spatial data were experimental, new types of imagery, and methods for mangroves were tested since existing methods had largely failed to accurately describe mangroves. The end result is a thorough assessment of the remote sensing of mangrove species composition, leaf area, and canopy. This research has contributed in a significant manner towards furthering remote sensing data and techniques. Unfortunately, the remote sensing data products did not provide sufficient accuracy that I felt them suitable for input into a habitat model that would be used to make conservation management decisions for a critically endangered bird. Thus, I have framed my research around finding a methodology for assessing ecosystem goods and services including, but not specifically, habitat.

Table of Contents

List of Tables

List of Figures

List of Abbreviations

ALI - Advanced Land Imager

ALOS - Advanced Land Observation Sensor

ASTER GDEM - Advanced Spaceborne Thermal Emission and Reflection Radiometer Global Digital Elevation Model

DEM - Digital Elevation Model

DSM - Digital Surface Model

EG&S - Ecosystem Goods and Services

eLAI - Effective Leaf Area Index

EVI - Enhanced Vegetation Index

FCC - Fraction Canopy Cover

GCP – Ground Control Point

GLOM - Grey-Level Occurrence Matrix

GLCM - Grey-Level Co-Occurrence Matrix

IGM - National Geographic Institute, Ecuador

InSAR - Synthetic Aperture Radar Interferometry

IRSR - Infrared Simple Ratio

LAI- Leaf Area Index

MLC – Maximum Likelihood Classification

NDMI - Normalized Difference Moisture Index

NDVI - Normalized Difference Vegetation Index

NIR- Near-Infrared

OBIA - Object-Based Image Analysis

PolSAR - Polarmetric Synthetic Aperture Radar

PRISM - Panchromatic Remote-sensing Instrument for Stereo Mapping

ROC - Receiver Operating Characteristic

RMSE - Root Mean Square Error

RPC - Rational Polynomial Coefficient

RPM - Rational Polynomial Model

r_s = Spearman ranked correlation

SAR - Synthetic Aperture Radar

SPOT - Satellite Pour l'Observation de la Terre

SR - Simple Ratio

SRTM - Shuttle Radar Topographic Mission

SVM - Support Vector Machine

SWIR - Short-wave Infrared

tLAI - true Leaf Area Index

VHR - Very High Resolution

Chapter 1: Introduction

Mangroves are unique in that they are the foundational species of a woody intertidal ecosystem that links terrestrial and marine systems and support biodiversity across systems. Mangroves are an assemblage of woody halophytes (i.e. salt tolerant plants) that are the foundational species of dense inter-tidal forest ecosystems that occur along tropical and sub-tropical coastlines, estuaries, lagoons, and rivers (Tomlinson, 1986; Smith 1992; Hogarth, 2007). While mangrove forest composition is often characterized by a strong zonation in community composition based on primarily on soil salinity related to tidal inundation (Tomlinson, 1986), other geomorphic, edaphic, climatic, and biotic factors can create more complex patterns (Onuf, 1977; Ewel et al., 1998; Farnsworth, 1998; Lee et al., 1998; Duke et al., 1996; Ellison 2002). For example, crabs can alter community structure through seed predation and alteration of soil nutrients and aeration through bioturbulation (Lee et al., 1998), mangrove trees themselves may alter local edaphic conditions contributing to spatial patterns (McKee, 1993), and that typical lateral zonation based on soil salinity can be absent in high precipitation regions (Ewel et al., 1998). The extent to which biotic and abiotic factors create patterns is debated. For instance, Ellison et al. (2002) found that although geomorphic and edaphic factors were significantly correlated with mangrove patterns, there was not any detectable zonation in species.

As Tomlinson (1986) describes, mangroves tend to have biological characteristics associated with pioneer terrestrial trees such as a large number of propagules, wide dispersal, fast growth rates, light as a limiting resource, uniform crown shape, and prolonged flowering period. Mangrove communities also have many pioneer characteristics such as low species richness, low stratification, and few climbers or epiphytes. However, mangroves trees and communities do have some mature characteristics as well such as long life span, low leaf palatability, medium leaf size, hard wood, and the absence of undergrowth. Ward et al. (2006) found that mangrove forests demonstrate a negative scaling relationship between mean stem diameter and stem density,

2

typical of self-thinning theory of mono-specific stands, as well as asymptotic standing biomass accumulation typical of upland tree communities. Furthermore, mangrove trees have strong allometric relationships between stem diameter, tree height, and above ground biomass (Fromard et al., 1998; Smith et al., 2006). Thus, mangrove forests tend to form distinguishable patterns of community composition and predictable canopy structure.

Mangrove forests provide a variety of valuable ecosystem goods and services. Examples of mangrove ecosystem goods and services include as timber and fuel (Walters et al., 2010), carbon sequestration (Komiyama, 2008), nutrient cycling to marine systems (Duarte et al., 1996), habitat for rare terrestrial fauna (Dvorak et al., 2004), economically important fisheries (Laegdsgaard et al., 2001; Mumby et al., 2004; Nagelkerken et al., 2000), filtration of pollution (Harbison, 1986), and a potential reduction in the impact of tsunami and storm surge (Granek and Ruttenberg, 2007; Danielsen et al., 2005). Costanza et al. (1997) estimated that these ecosystem goods and services are worth about US $10,000 per hectare per year or about US $180 billion globally.

According to the Millennium Ecosystem Assessment framework (Corvalán, 2005), ecosystem goods and services can be broadly divided among four categories - supporting, regulating, provisional, and cultural (see figure 1). Ecosystems provide valuable goods and services that support and regulate climate, biodiversity, and human well-being (Corvalán, 2005). The creation of sustainability policy requires clear definition and assessment of ecosystem goods and services and a method of accounting (Lele, 1991). The Earth system sciences and physical geography are well placed to develop quantitative assessment methods and to link them to broader sustainability policy (Leemans et al., 2009). In particular, space-based remote sensing provides the tools for wide-scale, repeatable methods to quantify and monitor ecosystem goods and services from local to national scales (Carpenter et al., 2009). As such, the advancement of remote sensing techniques that characterize composition and structure is crucial for future mapping, modeling, and monitoring of ecosystem goods and

services of mangroves. For example, consistent, accurate and repeatable measurements of canopy height can provide estimates of carbon storage as a component of climate regulation.

Supporting
Primary Production
Soil Formation
Habitat

Provisional
Food
Fuel
Medicine

Regulating
Climate
Water
Disease

Cultural
Spiritual
Recreation
Aesthetics
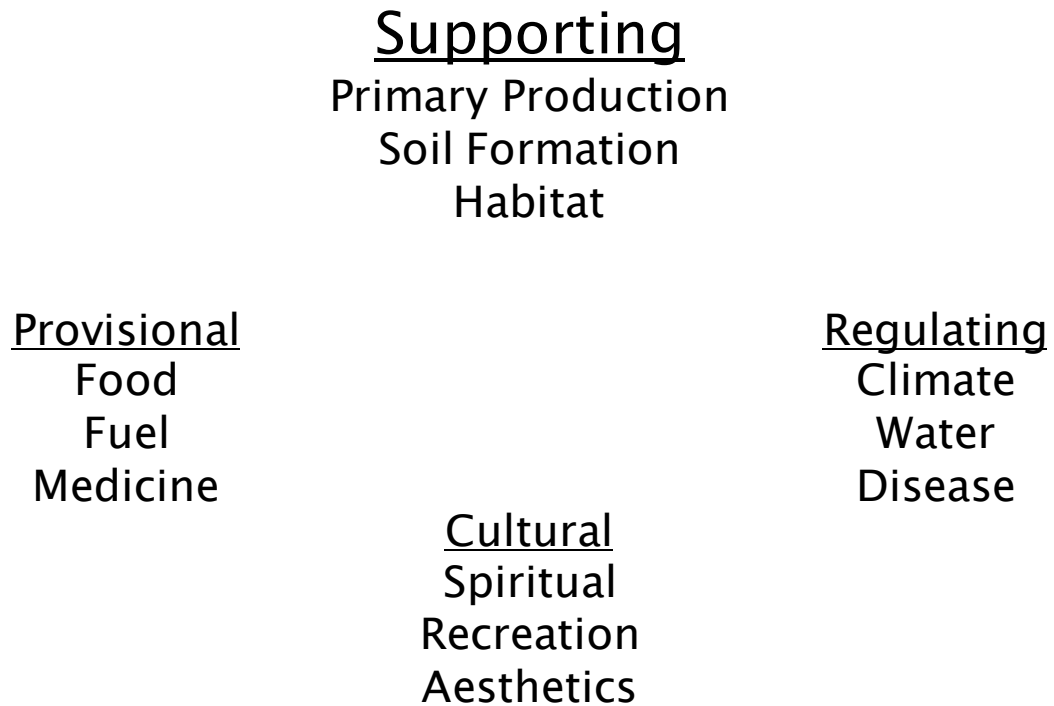
Figure 1.1: Examples of Ecosystem Goods and Services (after Corvalán, 2005).

The Galapagos Islands are renowned for biodiversity, especially high levels of species endemism such as Darwin's Finches. Located 1000-km off the coast of Ecuador, the Galapagos Islands, are an archipelago consisting of 13 large islands, 4 of which have human populations, and 188 small islands and rocks. The Galapagos Islands were declared a national park in 1959 (the park consists of 97% of land area), a UNESCO World Heritage Site in 1978, and a UNESCO Biosphere Reserve in 1987. Despite its reputation, relatively little research has been conducted

at the landscape scale to describe patterns and processes of ecosystems. The mangroves are no exception.

The Galapagos Islands lie on the western edge of the Atlantic-East Pacific mangrove complex. Mangrove forests consist of three true species common in this region: *Rhizophora mangle* (red), *Avicennia germinans* (black), *and Laguncularia racemosa* (white), and as well as the associate species such as *Conocarpus erectus* (button or buttonwood mangrove) and *Hippomane mancinella* (manzanillo), or other halophytes growing on nearby sand flats or dunes (Van der Werff and Andsersen, 1993). In the Galapagos Islands, mangrove forest form dense, but small patches in protected coves and lagoons along an otherwise barren or arid coast. Mangroves grow on a range of substrates from aa lava to sand or silty-clay. Mangrove forests in the study area can be described primarily as fringe mangroves forming along the coastline or basin mangroves along hyper-saline lagoons. While mangroves are generally observed to have clear zonation of species along the hydroperiod or salinity gradient, the pattern is most evident for large mangrove forests in riverine setting when the mixing of substantial freshwater and salt water occurs along a long, flat delta. In the Galapagos Islands, mangroves are situated along a geologically young coastline with highly variable micro-topography, small freshwater inputs, and a relatively narrow inter-tidal zone. As such, the pattern of species zonation is less distinct as conditions of hydroperiod, salinity, and wave action are variable over short distances.

Very little information about mangroves in Galapagos is available in English. With the exception of a book chapter about dry coastal ecosystems in Galapagos (Van der Werff and Andsersen, 1993), mangroves are simply the setting rather than the subject of research. For example, there is a series of papers about the critically endangered mangrove finch (Grant and Grant, 1998; Dvorak et al., 2004; Fessl et al., 2010). As Dvorak et al. (2004) note in their analysis of mangrove finch habitat, there is little information about the extent, species composition, or structure of mangrove forests in the Galapagos Islands. To date, there have been two sets of maps that include mangroves as a land cover classification. However, these

maps were derived from coarse resolution air photos or satellite imagery and field scientists have found the accuracy of these products unsatisfactory. Thus, accurate maps of mangrove forest extent, structure, and canopy structure are the first steps to understanding the role of mangrove forests in the Galapagos Islands and establishing a baseline for future monitoring. Although the role and importance of mangrove ecosystem goods and services beyond habitat in the Galapagos Islands is likely minor due to their limited extent, the Galapagos Islands represent a highly variable and often marginal environment for mangroves. The Galapagos Islands host a wide range of mangrove forms within species and thus provide a good range of conditions from which to understand the relationships between remote sensing data and mangrove composition and structure.

The remote sensing of mangroves presents many challenges including mixed pixel effects with variable backgrounds, similar spectral signatures between mangrove species as well as landward vegetation, variable structure based on environmental conditions, and difficulty obtaining widespread field data. For mangroves growing in arid regions, these problems are complicated by often sparse vegetation (mixed pixel effects), and a truncation of the zonation between species along the topographic gradient. Traditional satellite remote sensing approaches (e.g. Landsat and SPOT) are largely limited to mapping the extent of large mangrove forest. The remote sensing of forest parameters related to ecosystem goods and services requires more advance data and techniques. These issues are discussed in further detail in Chapter 2.

Research Objectives

The objective of this dissertation is to map mangrove forests and characterize composition and structure. The following three sets of characteristics have been selected: 1) forest extent and species composition as parameters important to basic mapping of mangrove forests in terms of distribution as well as habitat, 2) leaf area defined by either

fraction canopy cover or leaf area index as an important parameter for net primary productivity, evapotranspiration, and nutrient flux, and 3) canopy height as a proxy for standing biomass (carbon storage) and habitat quality. This research emphasizes the use of new sensors and a shift from pixel-based analysis to spatial based analysis through image texture or OBIA. The research seeks to address the following sets of questions:

1) Can individual mangrove and associate species be accurately mapped using very high resolution satellite imagery? What improvement does the new Worldview-2 sensor provide over Quickbird? Does OBIA improve spectral separability between classes?

2) Do spectral or spatial characteristics better predict leaf area? Is spatial resolution or the range of spectral bands more important? At what scales and resolutions does image texture capture leaf area? Are there species-specific relationships?

3) Can a digital surface model derived from VHR stereo provide accurate estimates of canopy height? How does the accuracy of the VHR optical DSM compare to a coarse resolution InSAR DSM? Can these two products be merged to enhance canopy height estimates?

Dissertation Outline

Chapter 2 is a review paper on the remote sensing of mangroves published in *Progress in Physical Geography*, February, 2011. This chapter provides an overview of traditional approaches to mangrove remote sensing, recent advances in remote sensing technology and methods as applied to mangroves, and future opportunities from new sensors or methods not yet examined for mangrove forests. This chapter provides the rationale for the methods and techniques used is subsequent chapters.

Chapter 3 explores new methods to map mangrove extent and species composition. An exploratory multispectral separability analysis demonstrates the spectral confusion

between mangrove species and mangrove associate species and tests the differences between Quickbird and the new Worldview-2 sensors. Based on the results of the exploratory analysis, a hybrid decision-tree / support vector machine classification is created using an OBIA framework.

Chapter 4 compares spectral and spatial techniques to estimate mangrove canopy leaf area. The spectral techniques include spectral vegetation indices using Quickbird and Advanced Land Imager data. Spatial techniques include an analysis of image texture using grey-level occurrence matrices (GLOM) and grey-level co-occurrence matrices (GLCM). Leaf area is examined based on individual species and groups as well as background substrate. The best predictors are used to create a parametric model.

Chapter 5 examines the potential for using optical stereo satellite imagery for mapping global mangrove canopy height including fringe mangroves by comparing a DSM extracted from ALOS PRISM imagery with the ASTER GDEM and the SRTM global DEM product. The ALOS PRIM DSM is examined at the pixel and object-level.

Chapter 6 reviews the findings from results chapters and reflects on the contributions made. The future opportunities outlined in Chapter 2 are revisited given the results. The dissertation concludes with an outlook on the future state of mangroves in the Galapagos Islands and future research directions.

Contributions

This dissertation contributes to the broader interdisciplinary research on sustainability science by addressing methodological issues on the remote sensing of ecosystem goods and services. While there are many conceptualizations of sustainability, remote sensing plays in important role as the best available source of data to assess and monitor ecosystems at local, regional, and global scales in consistent and repeatable ways. Mangroves are but one of many valuable ecosystems that are being degraded or destroyed

through land conversion, pollution, and modification of hydrologic processes with potentially far reaching consequences. This research contributes towards improving the methods available to assess and monitor mangrove forests and providing repeatable spatial measures of ecosystem goods and services over larger and generally inaccessible settings. This research also addresses a broader call for more research that explicitly considers the use of new remote sensing technologies in physical geography (Mather, 2011). This dissertation contributes to these areas in the following ways:

1) Chapter 2 contributes a review of current literature on the remote sensing of mangrove forests. A review on this topic has not been published in the last decade and this review addresses many of the advances in remote sensing technology and techniques since the last reviews. Furthermore, it outlines future opportunities for research and applications and establishes a rational for the subsequent chapters.

2) Two new sensors, ALOS PRISM and Worldview-2, are used. This is the first application of these sensors for mangrove research and demonstrates both the potential and limitations of these sensors to address the assessment of canopy height and species composition. Specifically, this research compares the utility of Worldview-2 to Quickbird and a VHR stereo DSM to a coarse resolution InSAR DSM.

3) This research also contributes to the growing trend from pixel-based image analysis to spatial or object based image analysis. Each chapter demonstrates how a spatial or object-based approach exceeds a pixel based approach. This research presents the first application of GLCM image texture to mangrove leaf area and contributes to issues of parameterizing GLCM image texture to measure leaf area.

4) Fringe mangrove are often omitted from remote sensing analysis due to their small areal extent. This small extent poses challenges for remote sensing using coarser resolution imagery due to mixed pixels. The small extent also can marginalize the importance of fringe mangroves. This research explicitly considers fringe mangroves and seeks to find robust methods for their mapping and monitoring.

5) Finally, this research contributes to the discussion of scale in remote sensing. Identified in this research is the need for very high resolution products that are suitable for the remote sensing of fringe mangrove forests, but that are globally available. These two needs are in opposition from a technological perspective as high spatial resolution generally means a smaller extent and longer global coverage and repeat image acquisition time. The tradeoffs between spatial resolution and sensor sensitivity are examined and discussed.

References

Carpenter, S. R., H. A. Mooney, J. Agard, D. Capistrano, R. S. DeFries, S. Diaz, T. Dietz, A. K. Duraiappah, A. Oteng-Yeboah, H. M. Pereira, C. Perrings, W. V. Reid, J. Sarukhan, R. J. Scholes & A. Whyte (2009) Science for managing ecosystem services: Beyond the Millennium Ecosystem Assessment. *Proceedings of the National Academy of Sciences of the United States of America,* 106**,** 1305-1312.

Corvalán, C. F. (2005) Ecosystems and human well-being: a report of the millennium ecosystem assessment. 53.

Danielsen, F., M. K. Sorensen, M. F. Olwig, V. Selvam, F. Parish, N. D. Burgess, T. Hiraishi, V. M. Karunagaran, M. S. Rasmussen, L. B. Hansen, A. Quarto & N. Suryadiputra (2005) The Asian tsunami: A protective role for coastal vegetation. *Science,* 310**,** 643.

Duarte, C. M. & J. Cebrian (1996) The fate of marine autotrophic production. *Limnology and Oceanography,* 41**,** 1758.

Duke, N. C., M. C. Ball & J. C. Ellison. (1996) Factors influencing biodiversity and distributional gradients in mangroves. In *International Workshop on Biodiversity and Ecosystem Function in Marine Ecosystems*, 27-47. Palo Alto, California.

Dvorak, M., H. Vargas, B. Fessl & S. Tebbich (2004) On the verge of extinction: a survey of the mangrove finch Cactospiza heliobates and its habitat on the Galapagos Islands. *Oryx,* 38**,** 171.

Ellison, A. M. (2002) Macroecology of mangroves: large-scale patterns and processes in tropical coastal forests. *Trees-Structure and Function,* 16**,** 181.

Ewel, K. C., S. F. Zheng, Z. S. Pinzon & J. A. Bourgeois (1998) Environmental effects of canopy gap formation in high-rainfall mangrove forests. *Biotropica,* 30**,** 510-518.

Farnsworth, E. J. (1998) Issues of spatial, taxonomic and temporal scale in delineating links between mangrove diversity and ecosystem function. *Global Ecology and Biogeography,* 7**,** 15-25.

Fessl, B., H. G. Young, R. P. Young, J. Rodriguez-Matamoros, M. Dvorak, S. Tebbich & J. E. Fa (2010) How to save the rarest Darwin's finch from extinction: the mangrove finch on Isabela Island. *Philosophical Transactions of the Royal Society B-Biological Sciences,* 365**,** 1019-1030.

Fromard, F., H. Puig, E. Mougin, G. Marty, J. L. Betoulle & L. Cadamuro (1998) Structure, above-ground biomass and dynamics of mangrove ecosystems: new data from French Guiana. *Oecologia,* 115**,** 39-53.

Granek, E. F. & B. I. Ruttenberg (2007) Protective capacity of mangroves during tropical storms: a case study from 'Wilma' and 'Gamma' in Belize. *Marine Ecology-Progress Series,* 343**,** 101.

Grant, P. R. & B. R. Grant (1997) The rarest of Darwin's finches. *Conservation Biology,* 11**,** 119-126.

Harbison, P. (1986) Mangrove Muds - a Sink and a Source for Trace-Metals. *Marine Pollution Bulletin,* 17**,** 246.

Hogarth, P. (2007) The Biology of Mangroves and Seagrasses. Oxford University Press.

Komiyama, A., J. E. Ong & S. Poungparn (2008) Allometry, biomass, and productivity of mangrove forests: A review. *Aquatic Botany,* 89**,** 128-137.

Laegdsgaard, P. & C. Johnson (2001) Why do juvenile fish utilise mangrove habitats? *Journal of Experimental Marine Biology and Ecology,* 257**,** 229.

Lee, S. Y. (1998) Ecological role of grapsid crabs in mangrove ecosystems: a review. *Marine and Freshwater Research,* 49**,** 335.

Leemans, R., G. Asrar, A. Busalacchi, J. Canadell, J. Ingram, A. Larigauderie, H. Mooney, C. Nobre, A. Patwardhan, M. Rice, F. Schmidt, S. Seitzinger, H. Virji, C. Vorosmarty & O. Young (2009) Developing a common strategy for integrative global environmental change research and outreach: the Earth System Science Partnership (ESSP) Strategy paper. *Current Opinion in Environmental Sustainability,* 1**,** 4-13.

Lele, S. M. (1991) Sustainable Development - A Critical-Review. *World Development,* 19**,** 607-621.

Mather, P. M. (2010) Is there any sense in remote sensing? *Progress in Physical Geography,* 34**,** 739-740.

McKee, K. L. (1993) Soil Physicochemical Patterns and Mangrove Species Distribution - Reciprocal Effects. *Journal of Ecology,* 81**,** 477.

Mumby, P. J., A. J. Edwards, J. E. Arias-Gonzalez, K. C. Lindeman, P. G. Blackwell, A. Gall, M. I. Gorczynska, A. R. Harborne, C. L. Pescod, H. Renken, C. C. C. Wabnitz & G. Llewellyn (2004) Mangroves enhance the biomass of coral reef fish communities in the Caribbean. *Nature,* 427**,** 533.

Nagelkerken, I., G. van der Velde, M. W. Gorissen, G. J. Meijer, T. van't Hof & C. den Hartog (2000) Importance of mangroves, seagrass beds and the shallow coral reef as a nursery for important coral reef fishes, using a visual census technique. *Estuarine Coastal and Shelf Science,* 51**,** 31.

Onuf, C. P., J. M. Teal & I. Valiela (1977) Interactions of Nutrients, Plant-Growth and Herbivory in a Mangrove Ecosystem. *Ecology,* 58**,** 514.

Smith, T. 1992. Forest Structure. In *Tropical Mangrove Ecosystems,* ed. R. A. I. a. D. M. Alongi. American Geophysical Union.

Smith, T. J., III & K. R. T. Whelan (2006) Development of allometric relations for three mangrove species in South Florida for use in the Greater Everglades Ecosystem restoration. *Wetlands Ecology and Management,* 14**,** 409-419.

Tomlinson, P. B. 1986. *The botany of mangroves*. Cambridge Cambridgeshire; New York: Cambridge University Press.

Van Der Werff, H. H. & H. Adsersen (1993) Dry coastal ecosystems of the Galapagos Islands. *Ecosystems of the World; Dry coastal ecosystems: Africa, America, Asia and Oceania***,** 459-475.

Walters, B. B., P. Ronnback, J. M. Kovacs, B. Crona, S. A. Hussain, R. Badola, J. H. Primavera, E. Barbier & F. DahdouhGuebas (2008) Ethnobiology, socio-economics and management of mangrove forests: A review. *Aquatic Botany,* 89**,** 220.

Ward, G. A., T. J. Smith, K. R. T. Whelan & T. W. Doyle (2006) Regional processes in mangrove ecosystems: spatial scaling relationships, biomass, and turnover rates following catastrophic disturbance. *Hydrobiologia,* 569**,** 517.

Chapter 2 : Satellite remote sensing of mangrove forests: Recent advances and future opportunities

[This chapter first appeared as a journal article in *Progress in Physical Geography*, 35:1, 2011. All permissions from SAGE publications have been obtained.]

Abstract

Mangroves are salt tolerant woody plants that form highly productive intertidal ecosystems in tropical and subtropical regions. Despite the established importance of mangroves to the coastal environment, including fisheries, deforestation continues to be a major threat due to pressures for wood and forest products, land conversion to aquaculture, and coastal urban development. Over the past 15 years, remote sensing has played a crucial role in mapping and understanding changes in the areal extent and spatial pattern of mangrove forests related to natural disasters and anthropogenic forces. This paper reviews recent advancements in remote-sensed data and techniques and describes future opportunities for integration or fusion of these data and techniques for large-scale monitoring in mangroves as a consequence of anthropogenic and climatic forces. While traditional pixel-based classification of Landsat, SPOT, and ASTER imagery has been widely applied for mapping mangrove forest, more recent types of imagery such as very high resolution (VHR), Polarmetric Synthetic Aperture Radar (PolSAR), hyperspectral, and LiDAR systems and the development of techniques such as Object Based Image Analysis (OBIA), spatial image analysis (e.g. image texture), Synthetic Aperture Radar Interferometry (InSAR), and machine-learning algorithms have demonstrated the potential for reliable and detailed characterization of mangrove forests including species, leaf area, canopy height, and stand biomass. Future opportunities include the application of existing sensors such as the hyperspectral HYPERION, the application of existing methods from terrestrial forest remote sensing, investigation of new sensors such as ALOS PRISM and PALSAR, and overcoming challenges to the global monitoring of mangrove forests such as wide-scale data availability, robust and consistent methods, and capacity-building with scientists and organizations in developing countries.

Introduction

Mangrove forests and shrubland, or mangroves, form important intertidal ecosystems that link terrestrial and marine systems and provide valuable ecosystem goods and services (Alongi, 2002). For example, mangroves are a foundation assemblage of trees that provide habitat for numerous terrestrial and marine species including economically and ecologically important fisheries (Nagelkerken et al., 2008). Despite the economic and ecological value of mangroves to the coastal environment including fisheries, more than 25% of global mangrove area was cleared between 1980 and 2000 (Wilkie and Fortuna, 2003). Detailed and accurate characterizations of mangroves are important to support ecological understanding and management of mangroves. Remote sensing has had a crucial role in monitoring mangroves, but the vast majority of the applications have been used to map areal extent and patterns of change at local scales. Recent advances in data and techniques have not only demonstrated the potential for improved accuracy of land cover classification and change-detection, but the capacity to characterize stand characteristics such as leaf area, canopy closure, species composition, canopy height, and standing biomass. This paper describes the following: (1) the traditional approaches of mapping mangrove areal extent and change using remote sensing; (2) recent advancements in remotely sensed data and analysis techniques for characterizing mangroves in terms of leaf area, species composition, and standing biomass; and (3) future opportunities for integration of these recent advancements and wide-scale application to provide regional and global monitoring of mangroves and indicators of ecological goods and services in the context of continued and growing threats from deforestation, natural disasters, and global climate change, especially sea-level rise.

Mangrove vegetation and ecosystems

Mangroves are an assemblage of woody halophytes (i.e. salt tolerant plants) that are the foundational species of intertidal forest and shrubland ecosystems that occur along tropical and subtropical coastlines, estuaries, lagoons, and river deltas (Hogarth, 2007; Smith, 1992; Tomlinson, 1986). While mangrove composition is often characterized by a strong zonation in community composition, based primarily on soil salinity related to tidal inundation (Tomlinson, 1986), other geomorphic, edaphic, climatic, and biotic factors can create more complex patterns (Duke et al., 1998; Ellison, 2002; Ewel et al., 1998; Farnsworth, 1998; Lee, 1999; Onuf et al., 1977).

As Tomlinson (1986) describes, mangroves tend to have biological characteristics associated with pioneer terrestrial trees such as large numbers of propagules, wide dispersal, fast growth rates, light as a limiting resource, uniform crown shape, and a prolonged flowering period. Mangrove communities also have many pioneer characteristics such as low species richness, low stratification, and few climbers or epiphytes. However, mangrove trees and communities have some characteristics of mature forests as well, such as a long life span, low leaf palatability, medium leaf size, hard wood, and the absence of undergrowth. Mangroves demonstrate a negative scaling relationship between mean stem diameter and stem density, typical of the self-thinning theory of mono-specific stands as well as asymptotic standing biomass accumulation typical of upland tree communities (Ward et al., 2006). Furthermore, mangrove trees have strong allometric relationships between stem diameter, tree height, and above-ground biomass (Fromard et al., 1998; Smith and Whelan, 2006). Thus, mangrove forests tend to form distinguishable patterns of community composition and predictable canopy structure.

The ecosystem goods and services that mangroves provide include carbon sequestration, the support of biodiversity through structure, nutrients and primary productivity, filtration of pollutants, and the potential to reduce the impacts of hurricanes

and tsunamis (Alongi, 2002). Primary productivity of mangroves can rival terrestrial, tropical rainforests (Alongi, 2002). Even though most productivity in mangroves is attributed to mangrove trees or bacteria in the soils, roughly 9% and 30% of carbon is consumed through herbivory or exported to the near- shore, respectively (Duarte and Cebrian, 1996). Mangroves provide protection from predators and increased food availability for marine fauna (Laegdsgaard and Johnson, 2001) and they have been linked to increased fish biomass (Mumby et al., 2004) as well as overall fish populations (Nagelkerken et al., 2008). Furthermore, many other marine species rely directly or indirectly on litter fall for food. These ecosystem goods and services are estimated to be worth about US $10,000 per hectare per year or about US $180 billion globally (Costanza et al., 1997). Major threats to mangroves include logging for fuel and timber, land conversion to aquaculture, primarily shrimp ponds, coastal development for shipping, and the direct and indirect effects of urban development including fresh water diversions (Gopal and Chauhan, 2006). The value of mangroves has been recognized by many governmental and non-governmental organizations (Wilkie and Fortuna, 2003). Efforts to manage mangroves require wide- scale monitoring to track changes in areal extent, health, and ecological functioning. Remote sensing plays a crucial role in the monitoring of mangroves to track deforestation (e.g. Giri et al., 2007; Lee and Yeh, 2009; Manson et al., 2001; Mantri and Mishra, 2006; Paling et al., 2008; Thu and Populus, 2007), the impact of natural disasters such as hurricanes (Doyle et al., 2009; Erftemeijer, 2002) and tsunamis (Giri et al., 2008; Olwig et al., 2007; Sirikulchayanon et al., 2008), reforestation projects (Al Habshi et al., 2007; Beland et al., 2006) and natural coastal dynamics (Fromard et al., 2004).

Traditional approaches to mangrove remote sensing

Aerial photography (AP) and legacy high resolution systems such as Landsat and SPOT are by far the most common approaches to mangrove remote sensing (Newton et al.,

2009). AP has been widely used in the mapping and assessment of mangroves (see table 1). AP can be more cost effective over small areas than satellite remote sensing (Mumby et al., 1999) and can provide fine grain imagery unavailable from satellite remote sensing due to government restrictions. Furthermore, historical imagery allows for change-detection well before the availability of satellite remote sensing. AP is more accessible to developing nations in which the majority of the world's mangroves grow and AP can provide very rapid assessments for monitoring change (Dahdouh-Guebas et al., 2006) in times of crisis. Most studies have used visual interpretation of AP to map the extent of mangrove and detect change between images, although digital AP now allows for computational classification (see table 2). Dahdouh-Guebas et al. (2006) demonstrated that fine grain AP can be successfully used to detect and map individual species. Major limitations to AP are the limited areal extent and relatively high costs of data acquisition over large geographic areas as well as the possible inconsistencies inherent in AP data such as uneven brightness and parallax distortion. Satellite-based remote sensing is essential for cost effective and repeatable mapping and monitoring of mangroves across geographic scales.

The vast majority of mangrove remote sensing studies (see table 1) have employed high resolution satellite imagery (i.e. spatial resolution between 5 and 100 m) such as Landsat (MSS, TM, or ETM+), SPOT (HVR, HRVIR, or HRG), ASTER, or IRS (1C or 1D). Table 3 provides further details on these sensor systems. The techniques used to detect and delineate mangrove have primarily involved unsupervised classification techniques such as the ISODATA approach, supervised classification techniques such as the maximum likelihood classification (MLC), mahalanobis distance, or other techniques commonly available in commercial image processing software, or a hybrid unsupervised/supervised classification scheme (see table 2 for a list of studies). Other common approaches for the classification of mangroves using multispectral imagery include pre- processing steps such as spectral transformations such as principal components analysis (PCA) or Tassel-Cap

Transformation (Crist and Cicone, 1984), or spectral vegetation indices such as Normalized Difference Vegetation Index (NDVI) or Simple Ratio (SR). In a comparison of classification techniques and data types, Green et al. (1998) found that the classification of PCA data performed significantly better than classifications using raw satellite bands. Additionally, the authors reported that the difference in classification accuracy using either Landsat or high resolution airborne imagery was small.

Using traditional data and techniques, reported classification accuracies of mangroves classes ranged from 75% to 90% for producer's and user's accuracies, though many applied studies omit detailed accuracy assessments. The omission of accuracy assessments is likely due to disconnect between the remote sensing and other disciplines (e.g. Newton et al., 2009). Accuracies tend to be higher for classifications using contemporary imagery with ground data than classifications using spectral library for land cover types with historical imagery (Giri et al., 2007). Despite the wide application of these traditional remote sensing data and techniques, there remain several limitations and challenges to traditional approaches to mangrove remote sensing. Confusion between mangroves and other vegetation is a commonly reported source of classification error (Al Habshi et al., 2007; Benfield et al., 2005; Gao, 1998). Another source of classification error is the omission of fringe mangroves that are less than the pixel size, resulting in mixed pixels (Manson et al., 2001). While the discrimination of mangrove density is possible with high resolution multispectral imagery (e.g. Green et al., 1998; Al Habshi et al., 2007), detection of individual species or estimation of canopy structure remain a challenge. For example, Ramsey and Jensen (1996) found no significant relationship between the spectral responses of different mangrove species using spectral bands available from Landsat. While estimation of canopy structure may be possible with high resolution imagery (Li et al., 2007), there are a number of challenges including mixed pixels (Green et al., 1997) and spectral saturation effects at higher biomass levels (Li et al., 2007) that limit the potential accuracy of these

data. Furthermore, reliance on a single grain of analysis can skew detection, analysis, and interpretation of landscape patterns and change (Wang et al., 2009).

Table 2.1: Traditional remote sensing sensors and mangrove studies

Sensor(s)	Studies
Aerial Photography	Benfield et al. (2005); Chauvaud et al. (1998); Dahdouh-Guebas et al. (2006); Eslami-Andargoli et al. (2009); Everitt et al. (2007); Fromard et al. (2004); Hossain et al. (2009); Jones et al. (2004); Krause et al. (2004); Manson et al. (2001); Murray et al. (2003)
Landsat MSS, TM, or ETM+	Beland et al. (2006); Cornejo et al. (2005); Green et al. (1998); Giri et al. (2008); James et al. (2007); Krause et al. (2004); Lee and Yeh (2009); Liu et al. (2008); Long and Skewes (1996); Manson et al. (2001); Mumby et al. (1999); Paling et al. (2008); Ruiz-Luna and Berlanga-Robles (2003); Vasconcelos et al. (2002)
SPOT HVR, HRVIR, or HRG	Chauvaud et al. (2001); Gao (1998); Gao (1999); Green et al. (1998); Lee and Yeh (2009); Mumby et al. (1999); Rasolofoharinoro et al. (1998); Saito et al. (2003)
ASTER	Al Habshi et al. (2007); Vaiphasa et al. (2006)
IRS C or D	Mantri and Mishra (2006); Pattanaik et al. (2008); Reddy and Pattanaik (2007); Ramachandran et al. (1998)

Table 2.2: Traditional remote sensing techniques and mangrove studies

Technique	Studies
Visual Interpretation	Benfield et al. (2005); Dahdouh-Guebas et al. (2006); Fromard et al. (2004); Murray et al. (2003)
Classification of Digital AP	Chauvaud et al. (1998); Everitt et al. (2007); Krause et al. (2004)
Unsupervised Classification	Bhatt et al. (2009); Green et al. (1998); James et al. (2007); Murray et al. (2003)
Supervised Classification	Al Habshi et al. (2007); Chauvaud et al. (2001); Cornejo et al. (2005); Gao (1999); Giri et al. (2007); Green et al. (1998); Lee and Yeh (2009); Ruiz-Luna and Berlanga-Robles (2003); Saito et al. (2003); Thu and Populus (2007)
Hybrid Classification	Giri et al. (2008); Hossain et al. (2009); Paling et al. (2008)
Spectral Transformation	Green et al. (1998); Krause et al. (2004); Mantri and Mishra (2006); Paling et al. (2008); Manson et al. (2001)
Spectral Vegetation Indices	Krause et al. (2004); Lee and Yeh (2009); Mantri and Mishra (2006); Rasolofoharinoro et al. (1998); Thu and Populus (2007)

Table 2.3: Passive optical satellite remote sensing systems (B =blue; G= green; R= red; NIR= near-infrared; SWIR= shortwave)

Sensor/System	Platform	# of Band(s)	Spectral Range	MSS	Pan.
High Resolution Sensors					
MSS (Multi Spectral Sensor)	Landsat 1, 2, 3	4	B,G,R,NIR	~80m	
TM (Thematic Mapper)	Landsat 4, 5	6	B,G,R,NIR,SWIR	30m	
ETM+ (Enhanced Thematic Mapper Plus)	Landsat 7	6	VNIR,SWIR	30m	15m
HVR (High Resolution Visibility)	SPOT (Satellite Pour l'Observation de la Terre) 1, 2, 3	3	G,R,NIR	20m	10m
HRVIR (High Resolution Visible and Infrared)	SPOT (Satellite Pour l'Observation de la Terre) 4	4	G,R,NIR,SWIR	20m	10m
HRG (High Resolution Geometrical)	SPOT (Satellite Pour l'Observation de la Terre) 5	4	G,R,NIR,SWIR	10m (VNIR); 20m (SWIR)	2.5
ASTER*	Terra	10	G,R,NIR; 6-SWIR	15m (VNIR); 30m (SWIR)	
IRS (Indian Remote-Sensing Satellite) 1C, 1D		4	G,R,NIR,SWIR	23m	5.8m
ALI (Advanced Land Imager)	EO-1 (Earth Observing)	9	2-B,G,R,2-NIR,2-SWIR	30m	15m
Very High Resolution Sensors					
Quickbird		4	VNIR; Pan	2.4m	0.6m
IKONOS		4	VNIR; Pan	4m	1m
PRISM**	ALOS (Advanced Land Observation System)	1	Pan	N/A	2.5m
WorldView-2		8	VNIR; Pan	< 2m ***	< 0.5m ***
GeoEye-1		4	VNIR; Pan	1.65m	0.41m
Other Optical Sensors					
GLAS (Geoscience Laser Altimeter System)	IceSAT (Ice, cloud and land elevation Satellite)	LiDAR, 2	Green (532 nm), NIR(1064 nm)	70m footprint; 170m spacing	
HYPERION	EO-1 (Earth Observing)	Hyper-spectral: 220	400 - 2500nm	30m	

*Advanced Spaceborne Thermal Emission and Reflectance Radiometer

**Panchromatic Remote-sensing Instrument for Stereo Mapping

*** maximum resolution limited by U.S. government

Recent advances

Traditional remote sensing approaches can provide important information for monitoring the areal extent and change of mangroves. New satellite sensors and techniques can potentially improve the accuracy of mangrove classifications, detect individual species, and provide reliable estimates of structure such as leaf area, canopy height, and biomass. There has been very rapid development of new remote sensing sensors and systems in recent years (e.g. Gillespie et al., 2008; Wooster, 2007). The new types of satellite sensors include very high resolution (VHR) systems (e.g. Quickbird, IKONOS, GeoEye-1 Worldview-2, and ALOS PRISM), Synthetic Aperture Radar systems (e.g. ALOS PALSAR, ASAR ENVISAT, and the Radarsat satellites), and LiDAR systems such as IceSAT/GLAS (see Tables 3 and 4 for details). Airborne sensors have been used to demonstrate the potential for satellite-based sensors such as the hyperspectral Airborne Visible/Infrared Imaging Spectrometer (AVIRIS), TOPSAR and AIRSAR (Polarmetric SAR), and various commercial wave-form LiDAR systems. Several new analysis techniques have been developed such as Object-Based Image Analysis (OBIA), and image texture metrics, such as lacunarity, use spatial information to improve image classification that can be applied to newer and traditional remote sensing imagery. Techniques such as genetic algorithms, spectral angular mapping, or neural networks have been developed and adapted to deal with new types of data (e.g. hyperspectral data or fusion of multiple types of data). The following sections will describe recent advances of data and techniques by remote sensing objective.

Table 2.4: Synthetic Aperture Radar (SAR) remote sensing systems. Polarization indicated by transmit and receive polarizations, respectively (H = horizontal polarization; V= vertical polarization)

Sensor	Platform	Band(s)	Polarization(s)	Spatial Resolution
Synthetic Aperture Radar (SAR)				
SIR-C (Space-borne Imaging Radar)	Space Shuttle	C, L, X	HH,VH, VV	10 - 200m
ERS-1 (European Remote-Sensing Satellite)	European Remote-Sensing Satellite	C	VV	25m - 100m
JERS-1 (Japanese Earth Resource Satellite)	Japanese Earth Resource Satellite	L	HH	25m - 100m
Radarsat-1		C	HH	8 - 100m
Radarsat-2		C	HH,HV,VH, VV	3 - 100m
ASAR (Advanced Synthetic Aperture Radar)	ENVISAT	C	HH, VH, HV, VV	25 - 150m
PALSAR (Phased Array type L-band Synthetic Aperture Radar)	ALOS (Advanced Land Observation System)	L	HH, HV, VH, VV	10 - 100m

Traditionally, multispectral remote sensing has been relatively effective at mapping the areal extent of mangroves but is limited in terms of spatial resolution or spectral resolution of sensors, or the inability of optical sensors to penetrate cloud cover. Newer types of imagery can address these limitations. For example, VHR imagery such as Quickbird or IKONOS can reduce the number of mixed pixels, hyperspectral imagery such as HYPERION can potentially detect fine differences in spectral signatures, and SAR imagery from sensors such as Radarsat or ASAR ENVISAT can penetrate cloud cover. While VHR imagery has been used to map mangrove extent, this type of imagery has been used almost exclusively for mapping individual species and characterizing canopy structure (see sections VI and VII). The few studies that have used VHR to map mangrove extent have relied upon visual interpretation over small geographic areas as a form of accuracy assessment of classifications derived from less expensive and coarser resolution imagery applied over a larger area (Giri et al., 2007; Howari et al., 2009).

Hyperspectral imagery provides detailed fine spectral resolution data that can be used to detect subtle differences in spectral reflectance. To date, the only satellite-based hyperspectral sensor, HYPERION on the EO-1 platform, has not been applied to mangrove studies. However, two studies have used airborne hyperspectral imagery to map the extent of mono-specific mangrove stands. While both D'Iorio et al. (2007) and Yang et al. (2009) demonstrate that hyper- spectral imagery can produce very high accuracy classifications, D'Iorio et al. (2007) found that the improvement in accuracy of supervised classifications to detect red mangrove (*Rhizophora mangle*) using NASA's AVIRIS sensor was insignificant compared to classifications of imagery from ASTER imagery or aerial photography. These limited results suggest that further studies are needed to determine the effectiveness of mapping multispecific mangroves using hyperspectral imagery compared to other types of imagery.

A common problem inherent to passive optical remote sensing, particularly in humid tropical regions, is cloud cover. Synthetic Aperture Radar (SAR) is an active form of remote sensing in which a microwave signal is directed towards an object and the strength (i.e. amplitude) of the reflected signal is measured. Signal strength is altered through transmittance and reflectance of different media based on thickness and dielectric properties of the media as well as the wavelength and polarization of the microwave beam. For example, SAR can penetrate cloud cover, but reflects off solid surfaces like soil or stems. For more complex media such as forest canopy, the relative amount of signal transmittance through the canopy versus signal scattering is a function of the signal wavelength. In general, longer wavelengths have high transmittance. Hence, the architecture of mangrove trees, local geomorphic conditions and the specifications of the SAR system are critical elements to this type of remote sensing. For a more detailed background of SAR remote sensing, see Henderson and Lewis (1998).

SAR imagery from SIR-C, JERS-1, ERS-1, and Radarsat-1 has been successfully used to delineate mangrove extent (Fromard et al., 2004; Lucas et al., 2007; Pasqualini et al., 1999; Simard et al., 2002). Pasqualini et al. (1999) examined the potential of C and L band Polarmetric SAR (PolSAR) using vertical (VV) and cross polarization (VH) from SIR-C and found that only the L-band with VH polarization could accurately discriminate between diffuse, dense, and recessive mangroves and other land cover types. Simard et al. (2002) used a decision tree classifier to map coastal land cover, including low and high mangroves, and compare the effectiveness of the JERS, ERS, and combined imagery. They found that the combined imagery improved overall accuracy by 18% to 84%, though the authors note considerable confusion between low mangrove and other flooded forest classes. Souza-Filho and Paradella (2003) were able to visually interpret mangrove extent and the relative stage of growth using Radarsat imagery. In a follow-up study, Souza-Filho and Paradella (2005)

were not able to statistically differentiate between land cover types including mangrove, based solely on Radarsat backscatter.

In recent years, new techniques have been developed or adapted to improve the accuracy of mapping the extent of mangrove and detecting change over time using either a data fusion approach to integrate different types of data or an Object-Based Image Analysis (OBIA) approach. Data fusion techniques can improve classification accuracy by drawing upon different data sources to maximize the dimensionality of available information. While a few studies have used visual interpretation of fused data (e.g. Souza-Filho and Paradella, 2005), most studies use multiple data sources within a rule-based classification scheme. Rule-based classifications separate out individual or groups of classes based on user-defined rules rather than solely on the spectral distance relationships used in many unsupervised and supervised classification schemes. Rule-based classifications are often invoked using a decision-tree that refines the separation of classes with each level. For example, DEM data are used to distinguish mangrove vegetation from neighboring terrestrial vegetation (Fatoyinbo et al., 2008; Islam et al., 2008; Liu et al., 2008). Additionally, rule-based classifications can utilize spatial information such as distance surfaces to separate mangrove from terrestrial vegetation based on a distance from ocean rule (Gao et al., 2004; Liu et al., 2008) The results of a rule-based classification can substantially improve classification accuracy over traditional methods. Gao et al. (2004) report substantial improvement in the classification accuracy of stunted mangroves (from 46.7% to 83.3%) and lush mangroves (from 68.3% to 96.7%). It is important to note that differences in the spatial resolution of multiple data sets can be a major challenge to data fusion techniques, especially when using archived data. For example, Manson et al. (2001) found that the use of an archived DEM did not accurately represent the topography of intertidal areas at an appropriate scale for mangrove mapping.

OBIA is a classification technique that uses objects rather than just individual pixels for image analysis. Objects are contiguous pixels that are grouped based on image properties or GIS data through an image segmentation process. Objects can be created at different levels. For example, lower-level objects could represent individual tree crowns; mid-level objects could represent a group of tree crowns of the same species and age; and high-level objects could represent a mangrove forest patch (e.g. Krause et al., 2004). Few studies have used OBIA to map the areal extent and change of mangroves as this approach is more commonly applied to species mapping (see section VI).

In a study by Conchedda et al. (2008), an OBIA approach was examined for effectiveness of detecting mangrove extent as well as change- detection between two images. The OBIA classification yielded very high accuracy for classifying mangroves with a user's accuracy greater than 97%. However, the effectiveness of change-detection using an integrated OBIA approach, in which two images are segmented together then classified, was less than a traditional image-difference change-detection technique. The traditional approach had an overall accuracy of 79.2% compared to 66.0% for the integrated OBIA approach. Conchedda et al. (2008) note that the segmentation process balances the size and number of objects, and in the case of the multidate segmentation, the objects were not sufficiently small to separate varying degrees of change between images.

Species composition

Species composition is an important characteristic of mangroves. Mangrove individuals often exhibit strong zonation patterns based on biotic and abiotic factors, and they can serve as a good indicator of geomorphic and environmental change (Souza-Filho and Paradella, 2005). Furthermore, habitat selection by animal can be a function of mangrove species, in additional to other factors (e.g. Dvorak et al., 2004). To detect individual species, spectral (e.g. leaf physiology) or spatial characteristics (e.g. crown shape

or canopy pattern) of individual species must be detectable via remote sensing. Traditional satellite-based remote sensing techniques and data have been unable to detect species with needed confidence, given spatial and/or spectral constraints. However, newer data and techniques have demonstrated a number of methods in which the mapping of mangrove species is possible including VHR and hyperspectral imagery. The Quickbird and IKONOS sensors are used almost exclusively where satellite-based VHR are used due to their long-mission life and substantial archived imagery. Although the spectral information available from Quickbird and IKONOS is limited to the blue, green, red and near-infrared bands that are similar to those of Landsat TM or ETM+, the very high spatial resolution (see table 3) may reduce the number and effect of mixed pixels and provide sufficient detail for the analysis of image texture as a metric of canopy structure. In a comparison of Quickbird and IKONOS imagery, Wang et al. (2004b) found that the IKONOS panchromatic and multispectral data outperformed Quickbird data for texture analysis and MLC, respectively, although both sensors are useful for mapping species.

A variety of sophisticated classification techniques have been used with VHR imagery to detect and classify mangrove species, including fuzzy classifications (Neukermans et al., 2008), Neural Networks (Wang et al., 2004a, 2008), support machine vectors (Huang et al., 2009), post-classification data fusion (Vaiphasa et al., 2006) and OBIA (Krause et al., 2004; Myint et al., 2008; Wang et al., 2004a, 2004b). Results from the few studies above indicate that spectral-only information for classification of individual species is often insufficient. For example, Neukermans et al. (2008) report an overall accuracy of 72% based of the mapping of four mangrove species and the surrounding land cover using Quickbird multispectral imagery and a fuzzy classification scheme. Similarly, Wang et al. (2004b) report an overall classification accuracy of nearly 75% or less for three mangrove species using Quickbird or IKONOS imagery with a MLC technique. Moreover, the user's accuracy for some individual

species was as low as 55%, further demonstrating the limitations of distinguishing between mangrove species using just spectral data.

Classification accuracy of species is greatly improved when spatial information, such as image texture, is used. Image texture is often measured using first- and second-order metrics, computed from the grey-level co-occurrence matrix within a given window, lag distance, and direction (Barber and Ledrew, 1991; Haralick et al., 1973; Kayitakire et al., 2006). Wang et al. (2004b) report that image texture enhances image classification in both Quickbird and IKONOS imagery. Similarly, Wang et al. (2004a) found in a comparison of MLC and OBIA nearest neighbor classification techniques that while the pixel-based classification had an overall accuracy higher than that of the OBIA method (i.e. 88.9% versus 80.4%), due to classification confusion of white mangroves in the OBIA method, a hybrid approach provided the highest accuracy. The hybrid approach had an overall accuracy of 74%, 92%, and 98% for red (*Rhizophora mangle*), black (*Avicennia germinans*), and white (*Laguncularia racemosa*) mangrove canopies, respectively. In a comparison of MLC and neural network classification techniques, Wang et al. (2008) also found that the inclusion of image texture information improved the accuracies for the MLC and neural network techniques. Using a different machine learning method (i.e. support machine vector), Huang et al. (2009) report classification accuracies greater than 90% for red, black, and white based on spectral and image texture data.

Another approach to measuring image texture is lacunarity. Lacunarity is a metric of the fractal dimensionality of the whole or subset of an image and can be used to describe the pattern of canopy crowns and gaps (Myint et al., 2008). Similar to other metrics of image texture, lacunarity can be calculated based on varying window sizes, lags, and directions. In as study by Myint et al. (2008) used lacunarity transformed images were used during for the image segmentation process of an OBIA classification of individual mangrove species. Results showed an overall accuracy greater than 90% compared to an overall accuracy of

62.8% using a traditional pixel-based spectral classification. To date, there has not been a study to investigate the use of lacunarity to classify mangrove species using pixel- or object-based methods.

In a data fusion approach, Vaiphasa et al. (2006) used known relationships between mangroves species and soil pH to improve post- classification accuracy with a typical Bayesian probability model and pH map. Despite an overall classification accuracy improvement (i.e. from 76% to 88%), classification accuracy of some species remained low (<70%), likely due to the relatively coarse spatial resolution of the ASTER imagery.

Although there have not been any studies that have used satellite-based hyperspectral remote sensing to detect and map mangrove species, lab experiments indicate that discrimination between multiple species is possible. Vaiphasa et al. (2005) were able to discriminate between 14 different species common to Thailand using the Jeffries-Matusita distance technique, although there was reported confusion among Rhizophora species. Vaiphasa et al. (2007) used a genetic algorithm to find just six hyperspectral channels that were able to distinguish between 16 mangrove species. While the laboratory studies demonstrate the potential for hyperspectral remote sensing of species, a number of real world challenges remain, such as mixed pixels (e.g. canopy gaps and shadows, and tidal water), atmospheric distortion and contamination, and variance in leaf reflectance due to biotic and environment conditions. Similarly, Wang and Sousa (2009) found using linear discrimination analysis that six hyper- spectral channels could discriminate between three common species in the Americas with very high accuracy (i.e. kappa >0.9). However, the six channels reported by Wang and Sousa (2009) do not agree with those reported by Vaiphasa et al. (2007).

Leaf area and canopy closure

   Leaf area and canopy closure are important biophysical parameters for assessing evapotranspiration, carbon cycling, habitat conditions, and forest health (e.g. Kercher and Chambers, 2001; Kovacs et al., 2008; Pasher et al., 2007). While the remote sensing of leaf area and canopy closure are major areas of research for terrestrial forests, relatively little research has been done on mangroves. In fact, all but one satellite-based mangrove leaf area remote sensing study has been conducted in the same estuary - the Agua Brava Lagoon in Mexico. In a series of studies, leaf area index (LAI) has been estimated using empirical relationships between ground-based measurements and VHR spectral vegetation indices or SAR backscatter. Using IKONOS, Kovacs et al. (2004) found strong significant relationships between LAI of red and white mangroves and the Simple Ratio (SR) and the Normalized Difference Vegetation Index (NDVI). Both indices produced similar results; NDVI explained 71% of variance in LAI with a standard error of 0.63 while SR explained 73% of variance with a standard error of 0.65. In a follow-up study on black mangroves, Kovacs et al. (2005) found similar results - NDVI and SR explained 63% and 65% of LAI variance, respectively. The extent of saturation effects for the remote sensing of LAI in mangroves is unknown. While Green et al. (1997) reported LAI values from 0.8 to 7.0, other studies have not observed high LAI values associated with saturation effects (see Chapter 3; Kovacs et al., 2004). While Kovacs et al. (2004) observed relatively high uncertainty for low LAI values, Kovacs et al. (2005) reported similar uncertainty for both healthy and degraded mangrove forests. Kovacs et al. (2009) used spectral vegetation indices from the Quickbird sensor and found very similar results to previous IKONOS studies. Kovacs et al. (2008) found a stronger relationship between cross-polarmetric C-Band SAR data and LAI (r^2 = 0.82) than previous VHR spectral relationships. Despite the strength of these findings, the study site of these studies is relatively species poor and much of the study area is degraded, according to the

authors. These methods should therefore be replicated in other areas to test the consistency and variability of these empirical relationships across species and conditions.

Height and biomass

Estimates of tree and forest biomass provide valuable insights into the carbon storage and cycling in forests (Litton et al., 2007). Canopy height and biomass have been shown in field studies to be strongly related for many mangrove species (Fromard et al., 1998; Smith and Whelan, 2006). Biomass can be estimated directly using PolSAR or indirectly using VHR image texture to detect canopy structure or SAR Interferometry (InSAR), stereo imagery, or LiDAR to estimate canopy height.

Proisy et al. (2007) used Fourier-based textual ordination (i.e. principal components analysis of Fourier spectra) with IKONOS near-infrared and panchromatic imagery to estimate biomass based on detection of canopy structure. Results show a significant non-linear relationship between the tree stage (e.g. pioneer, mature, dead) and the principal components of the Fourier spectra. The best model used the panchromatic imagery with a 30 m window and explained over 90% of the total and trunk biomass with a relative error of 16.9%. The authors note that they did not find any 'saturation effect' at high biomass levels, often observed in spectral response of dense terrestrial vegetation (Huete et al., 1997).

Most studies that estimate height or biomass from satellite remote sensing use SAR. Several studies have used airborne SAR sensors, such as AIRSAR, to demonstrate the potential of SAR to estimate canopy characteristics (Lucas et al., 2007; Mougin et al., 1999; Proisy et al., 2000, 2002). PolSAR methods use the values and differences of horizontal, vertical, and cross polarizations as the SAR signal scatters and reflects with different forest components. For example, reflection off trunks and soil may produce a single or double bounce interactions while the signal may scatter within the canopy, which is dependent on the signal wavelength (Proisy et al., 2000). The P-band PolSAR best estimates tree height

33

and above-ground biomass, although the HV polarization of L-band SAR also performs well, explaining 93%, 96%, and 94% of basal area, tree height, and above-ground biomass, respectively (Mougin et al., 1999). The relationships between PolSAR coefficients and biomass are, however, non-linear and change sign multiple times over the biomass range. In a follow-up study by Proisy et al. (2000), PolSAR signal modeling illustrated difficulties predicting the interaction of PolSAR with three-dimential heterogeneous components, specifically interactions between soil surface, trunk, and canopy volume components. These findings were confirmed by Proisy et al. (2002). In pioneer and declining mangrove stands, a substantial fraction of scattering was due to the interaction of surface and canopy volume components. For example, between 30% and 90% of the scattering mechanism of L-band PolSAR was associated with the interactive component, depending upon the polarization and stand characteristics. Proisy et al. (2002) conclude based on model results that statistical relationships of PolSAR to biomass are limited to homogeneous closed canopies where interaction effects are less pronounced. In a separate study using AIRSAR to assess the potential of space-borne L-band PolSAR, Lucas et al. (2007) note that L-band HV data can delineate different mangrove zones based on species and biomass/stage, but that the separation of surface, volume, and interaction components from the PolSAR signal remains a significant challenge due to inconsistent empirical results. The implications of these results suggest that a given SAR signal results from different combinations of forest structure. Although Li et al. (2007) are able to separate surface and trunk components of Radarsat-1 imagery (C-Band, HH) using a genetic algorithm, the SAR data only explained about 45% of biomass variance, although these results were better than NDVI as a predictor of biomass.

A different SAR technique is InSAR. InSAR can produce millimeter accurate digital surface models of bare terrain by analyzing the signal phase between two offset SAR images (e.g. tandem sensors or repeat-track image acquisition). For additional information on InSAR, see Hanssen (2001) or Rott (2009). While InSAR is widely used in geology for high

accuracy topographic mapping of volcanic and earthquake deformation, it can also be used to estimate canopy height. Under the assumption that the ground elevation is at mean sea level as all mangroves must grow in intertidal conditions, InSAR can be used to create a digital surface model of the canopy surface from which canopy height can be estimated (Fatoyinbo et al., 2008; Mitchell et al., 2007; Simard et al., 2006, 2008). InSAR processing for vegetation studies can be very complicated and difficult due to an often low coherence (i.e. agreement in signal phase) between images due to inconsistent scattering in the canopy volume. A globally available InSAR digital surface model, the Shuttle Topographic Radar Mission (SRTM) data set, has been demonstrated to provide reasonable estimates of mangrove canopy heights (Fatoyinbo et al., 2008; Simard et al., 2006, 2008). While the SRTM DSM can be calibrated using field measurements (Fatoyinbo et al., 2008; Simard et al., 2008), air borne LiDAR (Simard et al., 2006) or space-borne LiDAR from IceSAT/GLAS (Simard et al., 2008) can better characterize the vertical canopy structure.

The accuracy of this approach is best for tall mature mangroves where the relative error is less (Simard et al., 2006) as the reported root mean square error ranges from 1.5 to 2.0 m, well within local topographic ranges within the inter- tidal zone. All three studies use a generalized allometric relationship to convert canopy height to standing biomass, because species information was unavailable. While the SRTM product has a spatial resolution of 30 m over the United States, global coverage is reduced to 90 m, limiting its applicability to very large homogenous mangroves.

Productivity

Mangroves can be as productive as terrestrial rainforests, yet productivity can vary greatly due to environmental conditions (Komiyama et al., 2008; Lovelock et al., 2004). While many field and greenhouse studies have investigated the rate and mechanisms of mangrove productivity, practically no research has been conducted to map mangrove

productivity. In a field study using a hand-held spectroradiometer, Nichol et al. (2006) found a significant relationship between Photochemical Reflectance Index (PRI) and effective quantum yield, a metric of photosynthetic activity, thus demonstrating the potential for hyperspectral remote sensing of mangrove photosynthesis and productivity. In a similar study, Song et al. (2011) found that there was a significant relationship between soil-water salinity and PRI, further suggesting the potential of remote sensing to detect productivity and stress in mangroves.

Conclusions and future opportunities

Recent advances in the remote sensing of mangroves have demonstrated practical methods to improve classification accuracy, estimate leaf area, map individual species, and measure canopy height impossible with traditional remote sensing approaches. Newer types of imagery such as VHR and SAR provide new types of data which can be used separately or in conjunction with traditional remote sensing data. New techniques have been developed to exploit new types of data from VHR and SAR. Spatial patterns measured using image texture metrics or lacunarity can be related to canopy structure to detect individual species. InSAR has been used to directly measure canopy height and indirectly estimate standing biomass via allometric relationships. OBIA has been shown to outperform traditional pixel-based classifications in many cases and provides an environment in which other techniques such as data fusion and hierarchical rule-based classifications can be developed and applied. The science for remote sensing of mangroves has rapidly advanced in the last decade. Many of the challenges are not unique to mangroves and have been identified as challenges in other applications of terrestrial remote sensing (Wang et al., 2009). While recent advances have overcome many of the limitations of traditional remote sensing approaches, there remain many opportunities to further the science and application of mangrove remote sensing. The following is a list of suggested opportunities to improve and apply these advances.

There are some existing sensors that have not been applied to mangrove remote sensing studies such as the Advanced Land Imager (ALI) and HYPERION on the EO-1 platform (see table 3 for details). ALI is similar to the Landsat TM and ETM sensors with additional bands in the blue, NIR and SWIR. Although the spatial resolution of this sensor is relatively coarse, it can serve as a Landsat-compatible sensor for change-detection given the sensor malfunctions of Landsat ETM+ (e.g. scan line corrector) and ASTER (e.g. SWIR sensor). Of interest is the hyperspectral HYPERION sensor. HYPERION has 220 bands in the visible, NIR, and SWIR spectra. Given that HYPERION has been used to detect tree genera or species in tropical environments (e.g Christian and Krishnayya, 2009; Papes et al., 2010; Walsh et al., 2008) and laboratory studies have been able to distinguish between mangrove studies using hyperspectral imaging (Vaiphasa et al., 2005, 2007), there is great potential for mapping individual species using hyperspectral imagery. Furthermore, hyperspectral remote sensing could be used to estimate photosynthetic productivity and forest health (e.g. Nichol et al., 2006) as has been done for other tropical environments (e.g. Asner et al., 2006). Due to the relatively coarse spatial resolution of the HYPERION sensor (i.e. 30 m), spectral unmixing techniques will be required to reduce the effects of mixed pixel components (Walsh et al., 2008) such as soil, water, shadow, and various mangrove species.

Use of existing methods from terrestrial forests

There are a number of remote sensing methods that have been developed for terrestrial forests that have not been adapted or tested for mangroves. For example, image texture has been used to estimate canopy structure and leaf area in temperate terrestrial forests (e.g. Colombo et al., 2003; Song and Dickinson, 2008; Wulder et al., 1998). While image texture has been used to map mangrove species, it has not been tested for other forest

characteristics. Similarly, spectral unmixing techniques are often used in the remote sensing of terrestrial forests to separate the spectral end-members of mixed pixels. While studies have investigated the effect of background end-members (e.g. soil and water) on vegetation indices in mangrove forests (Diaz and Blackburn, 2003), to date there has not been a study that applies spectral unmixing to the remote sensing of mangrove forests. Finally, although considerable research has been conducted to develop process-based algorithms to model biophysical parameters such as LAI (Liang, 2007), these algorithms have not been applied to the remote sensing of mangroves.

Investigation of new sensors

The launch of several new sensors (e.g. ALOS PALSAR and PRISM, Radarsat-2, Worldview- 2 and GeoEye-1) offer new opportunities (see Tables 3 and 4 for sensor details). ALOS PALSAR is an L-band PolSAR sensor with 10-30 m resolution, depending on polarization. L-band PolSAR has been demonstrated to be among the best SAR configurations to map mangrove structure. Furthermore, the ALOS PALSAR mission seeks repeat-track image acquisition, ideal for InSAR and relatively high resolution mapping of mangrove height compared to the 90 m global SRTM product. However, there remain challenges in obtaining high coherence between images within the canopy due to the relatively high transmittance of L-band SAR though the forest canopy (Rott, 2009).

Radarsat-2 is another new PolSAR sensor. Radarsat-2 is a C-band sensor with the option for very high spatial resolution imagery as fine as 1 m. Some of the previous challenges to SAR remote sensing are reduction in image 'speckling' from signal noise and mixed pixels. The very high resolution imagery from Radarsat-2 may reduce the effect of both of these effects. However, the potential for mangrove studies is limited as C-band PolSAR has been shown to be the least sensitive to mangrove canopy structure compared to

other SAR wavelengths (e.g. Mougin et al., 1999), although the potential for high resolution InSAR applications exceed that of ALOS PALSAR in term of spatial resolution.

Another potential sensor for mapping mangrove canopy height is ALOS PRISM. PRISM is a very high resolution panchromatic sensor (e.g. 2.5 m) that acquires triplet sets of images (e.g. front, nadir, backward) for stereo DEM extraction. While this method has a lower vertical accuracy than InSAR, stereo methods of DEM extraction are relatively simple and are available with many commercial remote sensing software packages.

A new generation of VHR sensors has recently been launched as a continuation of the legacy of IKONOS and Quickbird. The successor of IKONOS, GeoEye-1, has four multispectral bands with a multispectral spatial resolution of 1.65 m and a panchromatic resolution of 0.41 m. The improved spatial resolution (i.e. less than half the pixel size of IKONOS), provides new opportunities of further investigation of spatial information in mangrove remote sensing using image texture, lacunarity, and image segmentation in OBIA. The successor to Quickbird, Worldview-2, has similar spatial resolutions to GeoEye-1 (less than 2 m in the multispectral and less than 0.5 m in the panchromatic bands, but finer resolutions are restricted by the US government), but has eight multispectral channels including bands in the yellow and red edge spectral ranges designed for vegetation studies. However, since both new VHR sensors have only recently been launched, the amount of archive imagery is relatively small and the cost of tasking image acquisition is very high compared to other remote sensing imagery.

Data fusion and integration

Data fusion is a promising methodology that aims to reduce data limitations by integrating multiple types of data. While data fusion has been used for mangrove studies to improve classification accuracy (Wang and Sousa-Filho, 2009), data fusion has yet to be incorporated into other areas of mangrove remote sensing such as mapping canopy height or

stand biomass. The current dominant technique for mapping canopy height is SRTM elevation data. This product can have a high vertical accuracy in flat terrain (Gorokhovich and Voustianiouk, 2006) but has a coarse resolution (e.g. 90 m) outside the United States where the vast majority of mangrove occurs. A less common approach outlined in the previous section uses stereo optical imagery to extract a DEM. While this approach is generally less accurate than InSAR techniques, the spatial resolution is potentially much higher, especially when VHR imagery is used. A global 30 m DEM product using the ASTER sensor was recently released by NASA. Fusion of DEM data from optical stereo imagery such as ASTER or ALOS PRISM with coarse resolution SRTM data could integrate the strengths of both data sets. High resolution canopy height maps can also help improve classification accuracy using a data fusion approach in OBIA (e.g. Ke et al., 2010) to distinguish between mangrove stages and species. Another opportunity is the fusion of species and canopy structure data. Mangrove trees have strong allometric relationships (e.g. canopy height versus biomass or leaf area), but these relationships vary by species (e.g. Smith and Whelan, 2006). Previous studies have relied on generalized allometric relationships. For example, Simard et al. (2006) estimate above- ground biomass based on canopy height. The fusion of species maps and canopy height could improve this technique through the use of species-specific allometric relationships.

Monitoring: Local to global

Perhaps the greatest challenge, and yet the greatest opportunity, is global monitoring of mangroves. To date, most studies have focused on local monitoring, although a few studies have provided regional assessments of South Asia. These local and regional monitoring projects are very important to their locals, but their scope is limited. Recently, Giri et al. (2011) mapped mangroves globally for the first time exclusively using satellite remote sensing data. This work demonstrates substantial advancement toward global

monitoring efforts. Global monitoring will not only provide a comprehensive overview of the state and change of mangroves, but will also provide consistent data between regions to help track not only mangrove extent, but structure, function, and maybe even ecosystem services as well. In order to achieve global monitoring, the following steps are needed:

1) Transition from experimentation to application. Traditional remote sensing data and techniques are now regularly applied through the world for mangrove studies. However, traditional remote sensing has many serious limitations. Recent advances also need to be incorporated into applied studies to provide improved monitoring.

2) Collaboration among scientists. Collaboration is needed between remote sensing specialist for fusion and integration of different types of remote sensing such as PolSAR, InSAR and VHR spatial imagery into accessible and available products. Furthermore, to advance the links between remote sensing and ecology, increased collaboration is needed between field and remote sensing scientists (Newton et al., 2009) as field inventory is a critical component for the calibration, validation, and interpretation of remote sensing products.

(3) Wide-scale data acquisition. Although global coverage is not necessary for monitoring purposes as a targeted sampling scheme could produce good assessment, data acquisition must be pan-tropical to cover different types of mangroves. Furthermore, repeated image acquisition is required to produce time series of imagery to understand the dynamics of change, rather than just snapshots of change (Gillanders et al., 2008).

4)The digital divide. The vast majority of the world's mangroves exist in developing nations. While some developing nations like India and Brazil have produced their own satellite remote sensing programs, most nations rely on the developed nations for access to remote sensing technology, not to mention barriers due to the costs of infrastructure and training. While Dahdouh-Guebas et al. (2006) show that aerial photography can provide inexpensive

high quality data, satellite based remote sensing has greater potential for coverage, repeatability, and consistency. While free access to imagery for scientific has improved in recent years (e.g. the Landsat archive, or to certain developing nations the China-Brazil Earth Resources Satellite), more effort is needed to improve training in remote sensing techniques and provide accessibility to remote sensing imagery, products, and requisite technology such as software and computers to scientists in the developing world.

References

Al Habshi A, Youssef T, Aizpuru M, and Blasco F (2007). New mangrove ecosystem data along the UAE coast using remote sensing. Aquatic Ecosystem Health and Management 10: 309-319.

Alongi DM (2002) Present state and future of the world's mangrove forests. Environmental Conservation 29: 331-349.

Asner GP, Martin RE, Carlson KM, Rascher U, and Vitousek PM (2006). Vegetation-climate interactions among native and invasive species in Hawaiian rainforest. Ecosystems 9: 1106-1117.

Barber DG and Ledrew EF (1991). SAR sea ice discrimination using texture statistics - a multivariate approach. Photogrammetric Engineering and Remote Sensing 57(4): 385-395.

Beland M, Goita K, Bonn F, and Pham TTH (2006). Assessment of land-cover changes related to shrimp aquaculture using remote sensing data: A case study in the Giao Thuy District, Vietnam. International Journal of Remote Sensing 27: 1491-1510.

Benfield SL, Guzman HM, and Mair JM (2005) Temporal mangrove dynamics in relation to coastal development in Pacific Panama. Journal of Environmental Management 76: 263-276.

Bhatt S, Shah DG, and Desai N (2009) The mangrove diversity of Purna Estuary, South Gujarat, India. Tropical Ecology 50: 287-293.

Chauvaud S, Bouchon C, and Maniere R (1998) Remote sensing techniques adapted to high resolution mapping of tropical coastal marine ecosystems (coral reefs, seagrass beds and mangrove). International Journal of Remote Sensing 19: 3625-3639.

Chauvaud S, Bouchon C, and Maniere R (2001) Thematic mapping of tropical marine communities (coral reefs, seagrass beds and mangroves) using SPOT data in Guadeloupe Island. Oceanologica Acta 24: S3-S16.

Christian B and Krishnayya NSR (2009) Classification of tropical trees growing in a sanctuary using Hyperion (EO-1) and SAM algorithm. Current Science 96: 1601-1607.

Colombo R, Bellingeri D, Fasolini D, and Marino CM (2003) Retrieval of leaf area index in different vegetation types using high resolution satellite data. Remote Sensing of Environment 86: 120-131.

Conchedda G, Durieux L, and Mayaux P (2008) An object-based method for mapping and change analysis in mangrove ecosystems. ISPRS Journal of Photogrammetry and Remote Sensing 63: 578-589.

Cornejo, R. H., N. Koedam, A. R. Luna, M. Troell & F. Dahdouh-Guebas (2005) Remote sensing and ethnobotanical assessment of the Mangrove forest changes in the Navachiste-San Ignacio-Macapule lagoon complex, Sinaloa, Mexico. Ecology and Society, 10, 16.

Dahdouh-Guebas F (2005) Remote sensing and ethno- botanical assessment of the mangrove forest changes in the Navachiste-San Ignacio-Macapule lagoon complex, Sinaloa, Mexico. Ecology and Society 10: 16.

Costanza, R., R. dArge, R. deGroot, S. Farber, M. Grasso, B. Hannon, K. Limburg, S. Naeem, R. V. Oneill, J. Paruelo, R. G. Raskin, P. Sutton & M. vandenBelt (1997) The value of the world's ecosystem services and natural capital. Nature, 387, 253.

Crist EP and Cicone RC (1984) Application of the Tasseled Cap Concept to simulated thematic mapper data. Photogrammetric Engineering and Remote Sensing 50: 343-352.

Dahdouh-Guebas F, Verheyden A, Kairo JG, Jayatissa LP, and Koedam N (2006) Capacity building in tropical coastal resource monitoring in developing countries: A re-appreciation of the oldest remote sensing method. International Journal of Sustainable Development and World Ecology 13: 62-76.

Diaz BM and Blackburn GA (2003) Remote sensing of mangrove biophysical properties: Evidence from a laboratory simulation of the possible effects of background variation on spectral vegetation indices. International Journal of Remote Sensing 24: 53-73.

D'Iorio M, Jupiter SD, Cochran SA, and Potts DC (2007) Optimizing remote sensing and GIS tools for mapping and managing the distribution of an invasive mangrove (Rhizophora mangle) on South Molokai, Hawaii. Marine Geodesy, 30: 125-144.

Doyle TW, Krauss KW, and Wells CJ (2009) Landscape analysis and pattern of hurricane impact and circulation mangrove forests of the Everglades. Wetlands 29: 44-53.

Duarte CM and Cebrian J (1996) The fate of marine autotrophic production. Limnology and Oceanography 41: 1758-1766.

Duke NC, Ball MC, and Ellison JC (1998) Factors influencing biodiversity and distributional gradients in mangroves. Global Ecology and Biogeography Letters 7: 27-47.

Dvorak M, Vargas H, Fessl B, and Tebbich S (2004) On the verge of extinction: A survey of the mangrove finch Cactospiza heliobates and its habitat on the Galapagos Islands. Oryx 38: 171-179.

Ellison AM (2002) Macroecology of mangroves: Large-scale patterns and processes in tropical coastal forests. Trees - Structure and Function 16: 181-194.

Erftemeijer PLA (2002) A new technique for rapid assessment of mangrove degradation: A case study of shrimp farm encroachment in Thailand. Trees - Structure and Function 16: 204-208.

Eslami-Andargoli L, Dale P, Sipe N, and Chaseling J (2009) Mangrove expansion and rainfall patterns in Moreton Bay, Southeast Queensland, Australia.

Estuarine Coastal and Shelf Science 85: 292-298.

Everitt JH , Yang C , Summy K R , Judd F W , and Davis MR (2007) Evaluation of color-infrared photography and digital imagery to map black mangrove on the Texas gulf coast. Journal of Coastal Research 23: 230-235.

Ewel KC, Zheng SF, Pinzon ZS, and Bourgeois JA (1998) Environmental effects of canopy gap formation in high rainfall mangrove forests. Biotropica 30: 510-518.

Farnsworth EJ (1998) Issues of spatial, taxonomic and temporal scale in delineating links between mangrove diversity and ecosystem function. Global Ecology and Biogeography Letters 7: 15-25.

Fatoyinbo TE, Simard M, Washington-Allen RA, and Shugart HH (2008) Landscape-scale extent, height, biomass, and carbon estimation of Mozambique's mangrove forests with Landsat ETM+ and Shuttle Radar Topography Mission elevation data. Journal of Geophysical Research - Biogeosciences 113: G02S06.

Fromard F, Puig H, Mougin E, Marty G, Betoulle JL, and Cadamuro L (1998) Structure, above-ground biomass and dynamics of mangrove ecosystems: New data from French Guiana. Oecologia 115: 39-53.

Fromard F, Vega C, and Proisy C (2004) Half a century of dynamic coastal change affecting mangrove shorelines of French Guiana: A case study based on remote sensing data analyses and field surveys. Marine Geology 208: 265-280.

Gao J (1998) A hybrid method toward accurate mapping of mangroves in a marginal habitat from SPOT multispectral data. International Journal of Remote Sensing 19: 1887-1899.

Gao J (1999) A comparative study on spatial and spectral resolutions of satellite data in mapping mangrove forests. International Journal of Remote Sensing 20: 2823-2833.

Gao J, Chen HF, Zhang Y, and Zha Y (2004) Knowledge- based approaches to accurate mapping of mangroves from satellite data. Photogrammetric Engineering and Remote Sensing 70: 1241-1248.

Gillanders SN, Coops NC, Wulder MA, Gergel SE, and Nelson T (2008) Multitemporal remote sensing of landscape dynamics and pattern change: Describing natural and anthropogenic trends. Progress in Physical Geography 32: 503-528.

Gillespie TW, Foody GM, Rocchini D, Giorgi AP, and Saatchi S (2008) Measuring and modelling biodiversity from space. Progress in Physical Geography 32: 203-221.

Giri, C., E. Ochieng, L. L. Tieszen, Z. Zhu, A. Singh, T. Loveland, J. Masek & N. Duke (2011) Status and distribution of mangrove forests of the world using earth observation satellite data. *Global Ecology and Biogeography,* 20**,** 154-159.

Giri C, Pengra B, Zhu ZL, Singh A, and Tieszen LL (2007) Monitoring mangrove forest dynamics of the Sundarbans in Bangladesh and India using multi-temporal satellite data from 1973 to 2000. Estuarine Coastal and Shelf Science 73: 91-100.

Giri C, Zhu Z, Tieszen LL, Singh A, Gillette S, and Kelmelis JA (2008) Mangrove forest distributions and dynamics (1975-2005) of the tsunami-affected region of Asia. Journal of Biogeography 35: 519-528.

Gopal B and Chauhan M (2006) Biodiversity and its conservation in the Sundarban Mangrove Ecosystem. Aquatic Sciences 68: 338-354.

Gorokhovich Y and Voustianiouk A (2006) Accuracy assessment of the processed SRTM-based elevation data by CGIAR using field data from USA and Thailand and its relation to the terrain characteristics. Remote Sensing of Environment 104(4): 409-415.

Green EP, Clark CD, Mumby PJ, Edwards AJ, and Ellis AC (1998) Remote sensing techniques for mangrove mapping. International Journal of Remote Sensing 19: 935-956.

Green EP, Mumby PJ, Edwards AJ, Clark CD, and Ellis AC (1997) Estimating leaf area index of mangroves from satellite data. Aquatic Botany 58: 11-19.

Hanssen RF (2001) Data Interpretation and Error Analysis. Dordrecht: Kluwer Academic.

Haralick RM, Shanmuga K, and Dinstein I (1973) Textural features for image classification. IEEE Transactions on Systems Man and Cybernetics SMC3: 610-621.

Henderson FM and Lewis AJ (eds) (1998) Principles and Applications of Imaging Radar. New York: Wiley.

Hogarth P (2007) The Biology of Mangroves and Seagrasses. Oxford: Oxford University Press.

Hossain MZ, Tripathi NV, and Gallardo WG (2009) Land use dynamics in a marine protected area system in lower andaman coast of Thailand, 1990-2005. Journal of Coastal Research 25: 1082-1095.

Howari FM, Jordan BR, Bouhouche N, and Wyllie-Echeverria S (2009) Field and remote-sensing assessment of mangrove forests and seagrass beds in the northwestern part of the United Arab Emirates. Journal of Coastal Research 25: 48-56.

Huang X, Zhang LP, and Wang L (2009) Evaluation of morphological texture features for mangrove forest mapping and species discrimination using multispectral IKONOS imagery. IEEE Geoscience and Remote Sensing Letters 6: 393-397.

Huete AR, Liu HQ, Batchily K, and van Leeuwen W (1997) A comparison of vegetation indices over a global set of TM images for EOS-MODIS. Remote Sensing of Environment 59: 440-451.

Islam, M. A., P. S. Thenkabail, R. W. Kulawardhana, R. Alankara, S. Gunasinghe, C. Edussriya & A. Gunawardana (2008) Semi-automated methods for mapping wetlands using Landsat ETM plus and SRTM data. International Journal of Remote Sensing, 29, 7077-7106.

James GK, Adegoke JO, Saba E, Nwilo P, and Akinyede J (2007) Satellite-based assessment of the extent and changes in the mangrove ecosystem of the Niger Delta. Marine Geodesy 30: 249-267.

Jones J, Dale PER, Chandica AL, and Breitfuss MJ (2004) Changes in the distribution of the grey mangrove Avicennia marina (Forsk.) using large scale aerial color infrared photographs: Are the changes related to habitat modification for mosquito control? Estuarine Coastal and Shelf Science 61: 45-54.

Kayitakire F, Hamel C, and Defourny P (2006) Retrieving forest structure variables based on image texture analysis and IKONOS-2 imagery. Remote Sensing of Environment 102 (3-4): 390-401.

Ke YH, Quackenbush LJ, and Im J (2010) Synergistic use of QuickBird multispectral imagery and LIDAR data for object-based forest species classification. Remote Sensing of Environment 114: 1141-1154.

Kercher JR and Chambers JQ (2001) Parameter estimation for a global model of terrestrial biogeochemical cycling by an iterative method. Ecological Modelling 139: 137-175.

Komiyama A, Ong JE, and Poungparn S (2008) Allometry, biomass, and productivity of mangrove forests: A review. Aquatic Botany 89: 128-137.

Kovacs JM, Flores-Verdugo F, Wang JF, and Aspden LP (2004) Estimating leaf area index of a degraded mangrove forest using high spatial resolution satellite data. Aquatic Botany 80: 13-22.

Kovacs JM, King JML, de Santiago FF, and Flores-Verdugo F (2009) Evaluating the condition of a mangrove forest of the Mexican Pacific based on an estimated leaf area index mapping approach. Environmental Monitoring and Assessment 157: 137-149.

Kovacs JM, Vandenberg CV, Wang J, and Flores-Verdugo F (2008) The use of multipolarised spaceborne SAR backscatter for monitoring the health of a degraded mangrove forest. Journal of Coastal Research 24: 248-254.

Kovacs JM, Wang JF, and Flores-Verdugo F (2005) Mapping mangrove leaf area index at the species level using IKONOS and LAI-2000 sensors for the Agua Brava Lagoon, Mexican Pacific. Estuarine Coastal and Shelf Science 62: 377-384.

Krause G, Bock M, Weiers S, and Braun G (2004) Mapping land-cover and mangrove structures with remote sensing techniques: A contribution to a synoptic GIS in support of coastal management in North Brazil. Environmental Management 34: 429-440.

Laegdsgaard P and Johnson C (2001) Why do juvenile fish utilise mangrove habitats? Journal of Experimental Marine Biology and Ecology 257: 229-253.

Lee SY (1999) Tropical mangrove ecology: Physical and biotic factors influencing ecosystem structure and function. Australian Journal of Ecology 24: 355-366.

Lee TM and Yeh HC (2009) Applying remote sensing techniques to monitor shifting wetland vegetation: A case study of Danshui River estuary mangrove communities, Taiwan. Ecological Engineering 35: 487-496.

Li, X., A. G. O. Yeh, S. Wang, K. Liu, X. Liu, J. Qian & X. Chen (2007) Regression and analytical models for estimating mangrove wetland biomass in South China using Radarsat images. International Journal of Remote Sensing, 28, 5567.

Liang SL (2007) Recent developments in estimating land surface biogeophysical variables from optical remote sensing. Progress in Physical Geography 31: 501-516.

Litton CM, Raich JW, and Ryan MG (2007) Carbon allocation in forest ecosystems. Global Change Biology 13: 2089-2109.

Liu K, Li X, Shi X, and Wang SG (2008) Monitoring mangrove forest changes using remote sensing and GIS data with decision-tree learning. Wetlands 28: 336-346.

Long BG and Skewes TD (1996) A technique for mapping mangroves with Landsat TM satellite data and Geographic Information System. Estuarine Coastal and Shelf Science 43: 373-381.

Lovelock CE, Feller IC, McKee KL, Engelbrecht BMJ, and Ball MC (2004) The effect of nutrient enrichment on growth, photosynthesis and hydraulic conductance of dwarf mangroves in Panama. Functional Ecology 18: 25-33.

Lucas RM, Mitchell AL, Rosenqvist A, Proisy C, Melius A, and Ticehurst C (2007) The potential of L-band SAR for quantifying mangrove characteristics and change: Case studies from the tropics. Aquatic Conservation - Marine and Freshwater Ecosystems 17: 245-264.

Manson FJ, Loneragan NR, McLeod IM, and Kenyon RA (2001) Assessing techniques for estimating the extent of mangroves: Topographic maps, aerial photographs and Landsat TM images. Marine and Freshwater Research 52: 787-792.

Mantri VA and Mishra AK (2006) On monitoring mangrove vegetation of Sagar Island by remote sensing. National Academy Science Letters - India 29: 45-48.

Mitchell AL, Lucas RM, Donnelly BE, Pfitzner K, Milne AK, and Finlayson M (2007) A new map of mangroves for Kakadu National Park, Northern Australia, based on stereo aerial photography. Aquatic Conservation - Marine and Freshwater Ecosystems 17: 446-467.

Mougin, E., C. Proisy, G. Marty, F. Fromard, H. Puig, J. L. Betoulle & J. P. Rudant (1999) Multifrequency and multipolarization radar backscattering from mangrove forests. IEEE Transactions on Geoscience and Remote Sensing, 37, 94.

Mougin, E., C. Proisy, G. Marty, F. Fromard, H. Puig, J. L. Betoulle & J. P. Rudant (1999) Multifrequency and multipolarization radar backscattering from mangrove forests. IEEE Transactions on Geoscience and Remote Sensing, 37, 94.

Mumby PJ, Green EP, Edwards AJ, and Clark CD (1999) The cost-effectiveness of remote sensing for tropical coastal resources assessment and management. Journal of Environmental Management 55: 157-166.

Murray, M. R., S. A. Zisman, P. A. Furley, D. M. Munro, J. Gibson, J. Ratter, S. Bridgewater, C. D. Minty & C. J. Place (2003) The mangroves of Belize Part 1. distribution, composition and classification. Forest Ecology and Management, 174, 265-279.

Myint SW, Giri CP, Le W, Zhu ZL, and Gillette SC (2008) Identifying mangrove species and their surrounding land use and land cover classes using an object- oriented approach with a lacunarity spatial measure. GIScience and Remote Sensing 45: 188-208.

Nagelkerken, I., S. J. M. Blaber, S. Bouillon, P. Green, M. Haywood, L. G. Kirton, J. O. Meynecke, J. Pawlik, H. M. Penrose, A. Sasekumar & P. J. Somerfield (2008) The habitat function of mangroves for terrestrial and marine fauna: A review. Aquatic Botany, 89, 155.

Neukermans G, Dahdouh-Guebas F, Kairo JG, and Koedam N (2008) Mangrove species and stand mapping in GAzi bay (Kenya) using Quickbird satellite imagery. Journal of Spatial Science 53: 75-86.

Newton AC, Hill RA, Echeverria C, Golicher D, Benayas JMR, Cayuela L, and Hinsley SA (2009) Remote sensing and the future of landscape ecology. Progress in Physical Geography 33: 528-546.

Nichol CJ, Rascher U, Matsubara S, and Osmond B (2006) Assessing photosynthetic efficiency in an experimental mangrove canopy using remote sensing and chlorophyll fluorescence. Trees-Structure and Function 20: 9-15.

Olwig, M. F., M. K. Sorensen, M. S. Rasmussen, F. Danielsen, V. Selvam, L. B. Hansen, L. Nyborg, K. B. Vestergaard, F. Parish & V. M. Karunagaran (2007) Using remote sensing to assess the protective role of coastal woody vegetation against tsunami waves. International Journal of Remote Sensing, 28, 3153.

Onuf CP, Teal JM, and Valiela I (1977) Interactions of nutrients, plant-growth and herbivory in a mangrove ecosystem. Ecology 58: 514-526.

Paling EI, Kobryn HT, and Humphreys G (2008) Assessing the extent of mangrove change caused by Cyclone Vance in the eastern Exmouth Gulf, northwestern Australia. Estuarine Coastal and Shelf Science 77: 603-613.

Papes M, Tupayachi R, Martinez P, Peterson AT, and Powell GVN (2010) Using hyperspectral satellite imagery for regional inventories: A test with tropical emergent trees in the Amazon Basin. Journal of Vegetation Science 21: 342-354.

Pasher J, King D, and Lindsay K (2007) Modelling and mapping potential hooded warbler (Wilsonia citrina) habitat using remotely sensed imagery. Remote Sensing of Environment 107: 471-483.

Pasqualini V, Iltis J, Dessay N, Lointier M, Guelorget O, and Polidori L (1999) Mangrove mapping in northwestern Madagascar using SPOT-XS and SIR-C radar data. Hydrobiologia 413: 127-133.

Pattanaik C, Reddy CS, and Prasad SN (2008) Mapping, monitoring and conservation of Mahanandi wetland ecosystem, Orissa, India using remote sensing and GIS. Proceedings of the National Academy of Sciences India Section B - Biological Sciences 78: 81-89.

Proisy C, Couteron P, and Fromard F (2007) Predicting and mapping mangrove biomass from canopy grain analysis using Fourier-based textural ordination of IKONOS images. Remote Sensing of Environment 109: 379-392.

Proisy C, Mougin E, Fromard F, and Karam MA (2000) Interpretation of polarimetric radar signatures of mangrove forests. Remote Sensing of Environment 71: 56-66.

Proisy C, Mougin E, Fromard F, Trichon V, and Karam MA (2002) On the influence of canopy structure on the radar backscattering of mangrove forests. International Journal of Remote Sensing 23: 4197-4210.

Ramachandran S, Sundaramoorthy S, Krishnamoorthy R, Devasenapathy J, and Thanikachalam N (1998) Application of remote sensing and GIS to coastal wetland ecology of Tamil Nadu and Andaman and Nicobar group of islands with special reference to mangroves. Current Science 75: 236-244.

Ramsey EW and Jensen JR (1996) Remote sensing of mangrove wetlands: Relating canopy spectra to site- specific data. Photogrammetric Engineering and Remote Sensing 62: 939-948.

Rasolofoharinoro M, Blasco F, Bellan MF, Aizpuru M, Gauquelin T, and Denis J (1998) A remote sensing based methodology for mangrove studies in Madagascar. International Journal of Remote Sensing 19: 1873-1886.

Reddy CS and Pattanaik C (2007) Mangrove vegetation assessment and monitoring in Balasore district, Orissa using remote sensing and GIS. National Academy Science Letters - India 30: 377-381.

Rott H (2009) Advances in interferometric synthetic aperture radar (InSAR) in earth system science. Progress in Physical Geography 33: 769-791.

Ruiz-Luna A and Berlanga-Robles CA (2003) Land use, land cover changes and coastal lagoon surface reduction associated with urban growth in northwest Mexico. Landscape Ecology 18: 159-171.

Saito H, Bellan MF, Al-Habshi A, Aizpuru M, and Blasco F (2003) Mangrove research and coastal ecosystem studies with SPOT-4 HRVIR and TERRA ASTER in the Arabian Gulf. International Journal of Remote Sensing 24: 4073-4092.

Simard M, De Grandi G, Saatchi S, and Mayaux P (2002) Mapping tropical coastal vegetation using JERS-1 and ERS-1 radar data with a decision tree classifier. International Journal of Remote Sensing 23: 1461-1474.

Simard M, Rivera-Monroy VH, Mancera-Pineda JE, Castaneda-Moya E, and Twilley RR (2008) A systematic method for 3D mapping of mangrove forests based on Shuttle Radar Topography Mission elevation data, ICEsat/GLAS waveforms and field data:

Application to Cienaga Grande de Santa Marta, Colombia. Remote Sensing of Environment 112: 2131-2144.

Simard, M., K. Q. Zhang, V. H. Rivera-Monroy, M. S. Ross, P. L. Ruiz, E. Castaneda-Moya, R. R. Twilley & E. Rodriguez (2006) Mapping height and biomass of mangrove forests in Everglades National Park with SRTM elevation data. Photogrammetric Engineering and Remote Sensing, 72, 299-311.

Sirikulchayanon P, Sun WX, and Oyana TJ (2008) Assessing the impact of the 2004 tsunami on mangroves using remote sensing and GIS techniques. International Journal of Remote Sensing 29: 3553-3576.

Smith TJ III (1992) Forest structure. In Robertson AI and Alongi DM (eds) Tropical Mangrove Ecosystems. Washington, DC: American Geophysical Union, 101-136.

Smith TJ III and Whelan KRT (2006) Development of allometric relations for three mangrove species in South Florida for use in the Greater Everglades Ecosystem restoration. Wetlands Ecology and Management 14: 409-419.

Song C and Dickinson MB (2008) Extracting forest canopy structure from spatial information of high resolution optical imagery: Tree crown size versus leaf area index. International Journal of Remote Sensing 29: 5605-5622.

Song C, White B, and Heumann BW (2011) Hyperspectral remote sensing of salinity stress on red (Rhizophora mangle) and white (Laguncularia racemosa) mangroves on Galapagos Islands. Remote Sensing Letters.

Souza-Filho PWM and Paradella WR (2003) Use of synthetic aperture radar for recognition of Coastal Geomorphological Features, land-use assessment and shoreline changes in Braganca coast, Para, Northern Brazil. Anais da Academia Brasileira de Ciencias 75: 341-356.

Souza-Filho PWM and Paradella WR (2005) Use of RADARSAT-1 fine mode and Landsat-5 TM selective principal component analysis for geomorphological mapping in a macrotidal mangrove coast in the Amazon region. Canadian Journal of Remote Sensing 31: 214-224.

Thu PM and Populus J (2007) Status and changes of mangrove forest in Mekong Delta: Case study in Tra Vinh, Vietnam. Estuarine Coastal and Shelf Science 71: 98-109.

Tomlinson PB (1986) The Botany of Mangroves. Cambridge: Cambridge University Press.

Vaiphasa C, Ongsomwang S, Vaiphasa T, and Skidmore AK (2005) Tropical mangrove species discrimination using hyperspectral data: A laboratory study. Estuarine Coastal and Shelf Science 65(1-2): 371-379.

Vaiphasa C, Skidmore AK, and de Boer WF (2006) A post-classifier for mangrove mapping using ecological data. ISPRS Journal of Photogrammetry and Remote Sensing 61: 1.

Vaiphasa C, Skidmore AK, de Boer WF, and Vaiphasa T (2007) A hyperspectral band selector for plant species discrimination. ISPRS Journal of Photogrammetry and Remote Sensing 62(3): 225-23.

Vasconcelos MJP, Biai JCM, Araujo A, and Diniz MA (2002) Land cover change in two protected areas of Guinea-Bissau (1956-1998). Applied Geography 22: 139-156.

Walsh, S. J., A. L. McCleary, C. F. Mena, Y. Shao, J. P. Tuttle, A. Gonzalez & R. Atkinson (2008) QuickBird and Hyperion data analysis of an invasive plant species in the. Galapagos Islands of Ecuador: Implications for control and land use management. Remote Sensing of Environment, 112, 1927-1941.

Wang K, Franklin SE, Guo XL, He YH, and McDermid GJ (2009) Problems in remote sensing of landscapes and habitats. Progress in Physical Geography 33: 747-768.

Wang L and Sousa-Filho WP (2009) Distinguishing mangrove species with laboratory measurements of hyperspectral leaf reflectance. International Journal of Remote Sensing 30: 1267-1281.

Wang L, Silvan-Cardenas JL, and Sousa WP (2008) Neural network classification of mangrove species from multi-seasonal IKONOS imagery. Photogrammetric Engineering and Remote Sensing 74: 921-927.

Wang L, Sousa-Filho WP, and Gong P (2004a) Integration of object-based and pixel-based classification for mapping mangroves with IKONOS imagery. International Journal of Remote Sensing 25: 5655-5668.

Wang L, Sousa-Filho WP, Gong P, and Biging GS (2004b) Comparison of IKONOS and QuickBird images for mapping mangrove species on the Caribbean coast of Panama. Remote Sensing of Environment 91: 432-440.

Ward GA, Smith TJ, Whelan KRT, and Doyle TW (2006) Regional processes in mangrove ecosystems: Spatial scaling relationships, biomass, and turnover rates following catastrophic disturbance. Hydrobiologia 569: 517-527.

Wilkie ML and Fortuna S (2003) Status and trends in mangrove area extent worldwide. Forest Resources Assessment Working Paper 63. Rome: Forest Resources Division, Food and Agriculture Organization of the United Nations (FAO).

Wooster M (2007) Remote sensing: sensors and systems. Progress in Physical Geography 31: 95-100.

Wulder MA, LeDrew EF, Franklin SE, and Lavigne MB (1998) Aerial image texture information in the estimation of northern deciduous and mixed wood forest leaf area index (LAI). Remote Sensing of Environment 64: 64-76.

Yang CH, Everitt JH, Fletcher RS, Jensen RR, and Mausel PW (2009) Evaluating AISA plus hyperspectral imagery for mapping black mangrove along the South Texas Gulf Coast. Photogrammetric Engineering and Remote Sensing 75: 425-435.

Chapter 3 : An Object-Based Classification of Fringe and Basin Mangroves Using a Hybrid

Decision-Tree and Support Vector Machine Approach

Abstract

Mangroves provide valuable ecosystem goods and services such as carbon sequestration, habitat for terrestrial and marine fauna, and coastal hazard mitigation. The use of satellite remote sensing to map mangroves has become widespread as it can provide accurate, efficient, and repeatable assessments. Traditional remote sensing approaches have failed to accurately map fringe mangroves and true mangrove species due to relatively coarse spatial resolution and/or spectral confusion with landward vegetation. This study demonstrates the use of the new Worldview-2 sensor, Object-based image analysis (OBIA), and support vector machine (SVM) classification to overcome both of these limitations. An exploratory spectral separability analysis revealed serious effects of mixed pixels for sparse vegetation that prevented spectral differentiation between vegetation classes. Furthermore, separability analysis showed that individual mangrove species could be not spectrally separated. An OBIA classification was used that combined a decision-tree classification with the machine-learning SVM classification. Results showed an overall accuracy greater than 94% (kappa = 0.863) for classifying true mangroves species and other dense coastal vegetation at the object level. However, when considering individual field point data, there was considerable error between the true mangrove and mangrove associate classes for black mangroves (*Avicennia germinans*) and buttonwood (*Conocarpus erectus*). The results demonstrate the improved spectral capabilities of the Worldview-2 sensor over Quickbird, especially the capacity for new spectral band ratios. However, there remain serious challenges to accurately mapping fringe mangroves using remote sensing data due to spectral similarity of mangrove and associate species, lack of clear zonation between species, and mixed pixel effects, especially for sparse vegetation.

Introduction

Mangroves are an assemblage of tropical and sub-tropical halophytes (i.e. salt loving) woody plants. Mangrove forests are among the most productive forest ecosystems in the world and unique in linking terrestrial and marine systems through the inter-tidal zone (Hogarth, 2007). Despite the low tree species diversity and simple canopy structure, mangroves provide many valuable ecosystems goods and services such as carbon sequestration, habitat for terrestrial fauna as well as economically important fisheries, and coastal hazard mitigation (Alongi, 2002). Mangrove forests can range from vast swamps across large estuarine systems such as the Ganges River Delta to narrow strips of vegetation (i.e. fringe mangroves) along arid coastlines.

Globally, satellite remote sensing has played an important role in mapping and monitoring mangroves (Heumann, 2011; Giri et al., 2010). Mapping and monitoring mangrove forests is critically important for numerous scientific areas such as carbon stock estimates of tropical coastal nations, effectively managing commercial fisheries and their mangrove nurseries, and understanding the dynamics of vegetation-coastal geomorphology and coastal hazard mitigation. Furthermore, mangroves can provide unique habitat for rare species such as the mangrove finch in the Galapagos Islands of Ecuador.

Previous studies have reported remote sensing classification accuracies between mangroves and other landcover ranging from 75% to 90%, though many studies have omitted accuracy assessments (see Heumann, 2011, for an in-depth review). There remains a number of challenges to accurately detect mangroves including spectral similarity between mangroves and nearby landward tropical vegetation including in arid or marginal environments (Al Habshi et al., 2007, Benfield et al., 2005, Gao, 1998, Simard et al., 2002) and the effect of mixed pixels for fringe mangroves (Manson et al., 2001). Detection of individual mangrove species presents an even greater challenge. Traditional remote sensing approaches generally have failed to detect individual species (e.g. Ramsey and Jensen,

1996). While Vaiphasa et al. (2005) and Wang and Sousa (2009) were able to discriminate between mangrove species in hyperspectral laboratory studies, real-world results have been mixed. Almost all recent studies utilize very high resolution imagery, though a wide variety of different techniques have been tested including fuzzy classifications (Neukermans et al., 2008), neural networks (Wang et al., 2004a; Wang et al., 2008), support machine vectors (Huang et al., 2009), post-classification data fusion (Vaiphasa et al., 2006) and OBIA (Wang et al., 2004a; Wang et al., 2004b; Myint et al., 2008; Krause et al., 2004). Studies using only multispectral data have generally reported moderate to poor results. For example, Neukermans et al. (2008) report an overall accuracy of 72 percent based on the mapping of four mangrove species and the surrounding land cover using Quickbird multispectral imagery and a fuzzy classification scheme. Similarly, Wang et al. (2004b) report an overall classification accuracy of nearly 75 percent or less for each of three mangrove species using Quickbird or IKONOS imagery with a maximum likelihood classification (MLC) technique.

The incorporation of spatial information either in the form of OBIA or pixel-based image texture (e.g. grey-level co-ocuurence matrix or lacunarity) improved the classification accuracy (Huang et al., 2009; Myint et al., 2008; Wang et al., 2004a; Wang et al., 2004b; Wang et al., 2008). Spatial information seeks to extract repeated patterns in canopy structure that can be indirectly related to species. This approach has merit as mangrove genera often differ greatly in form and structure (Tomlinson, 1986). Spatial metrics are very sensitive to edge effects and work best over continuous canopies. In the case of fringe or basin mangroves, mangrove species zonation is often not as distinct as in other environments, and high edge length to area ratio makes edge effects a serious challenge. Thus, to effectively map and monitor fringe mangrove forests, especially at local and regional scales, the challenges of spectral confusion and likely limited effectiveness of spatial metrics are constraining factors. Previous studies have reported a range of classification accuracies. Wang et al. (2004a) report that a hybrid OBIA-MLC classification outperforms

either individual approach, but accuracy for individual species still ranged from 74% to 98%. Both Huang et al. (2009) and Myint et al. (2008) report accuracies greater than 90% using spatial data as part of the classification, or as an input into the image object segmentation process.

<u>Study Objective</u>

The objective of this study was to map fringe and basin mangrove forests at the species level. First, an analysis of spectral separability of vegetation using Jeffries-Matusita separability measure was conducted to distinguish between vegetation types or groups and toevaluate the differences between Quickbird and Woldview-2 for multispectral analysis. Based on these results, a hybrid OBIA-SVM approach was designed to enhance vegetation separability. An object-based decision tree classification was used to classify classes other than dense coastal vegetation that are not central to this study. A support vector machine classification was used to classify dense coastal vegetation between true mangroves and mangrove associates. The accuracy of the results was analyzed at the object level and field plot or point level for individual vegetation types.

<u>Background</u>

Object-Based Image Analysis

Pixel-based analysis is generally conceptually simple and methods are generic across sensors. However, pixels are often not the unit of interests, but rather the default unit of measurement. For example, individual crowns and canopy gaps consist of multiple pixels and produce spatial-autocorrection within objects that can be detected using high resolution imagery (Woodcock and Strahler, 1987). OBIA seeks to create "meaningful" objects by segmenting an image into groups of pixels with similar characteristics based on spectral and spatial properties (Benz et al., 2004). In OBIA, segmented objects become the unit of

analysis, from which spectral statistics, such as spectral band means and standard deviation, or spatial information, such as image texture, can be used for further analysis including image classification. User-defined scale, shape, and compactness parameters make OBIA particularly useful for creating objects with heterogeneous pixels where a pixel based analysis would fail to capture the relationship between pixels. For example, lava with sparse vegetation or a dense canopy with small gaps can be classified as a land cover type rather than individual pixels with different classifications. Figure 3.1 illustrates the difference between high and very high resolution pixel-based classification and a very high resolution object-based classification. The high resolution classification contains many pixel with multiple classes. The very high resolution pixel-based classification resolves individual classes better, but the resolution is actually finer than the objects of interest. The OBIA classification illustrates how a forest classification can include gaps and a non-vegetation object can include isolated sparse vegetation. OBIA has been widely applied for forest remote sensing studies (Chubey et al., 2006; Desclee et al., 2006; Hay et al., 2005; Wulder et al., 2008) and has been successfully applied to mangrove studies (Conchedda et al., 2007; Myint et al., 2008, Wang et al., 2004a). However, OBIA has not been explicitly applied to fringe mangroves.
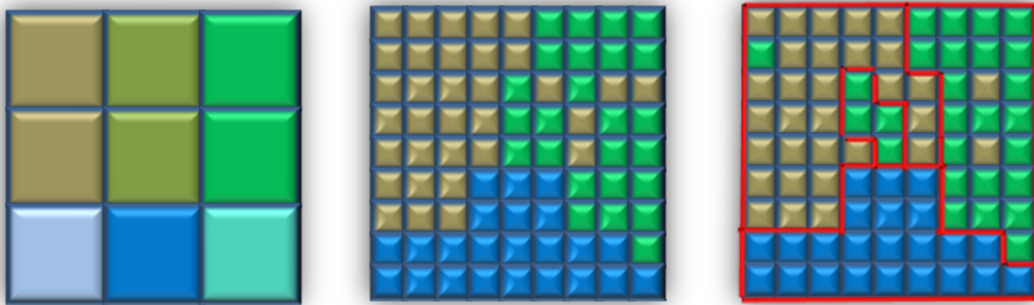
Figure 3.1: A stylized example of a) a pixel-based high resolution classification with mixed pixels, b) a pixel-based very high resolution classification, and c) an object-based very high resolution classification with objects outlined in red. Blue = Water; Brown = Soil; Green = Vegetation; Other colors are mixed pixels.

Support Vector Machine

SVM is a machine-learning technique that is well adapted to solving non-linear, high dimensional space classifications (Pal and Mather, 2005). For remote sensing, SVM is a useful tool for multispectral and hyperspectral classifications in which spectral separability is less than perfect. The mathematical formulation of SVM are described in Vapnik (1995) and a detailed assessment of SVM for remote sensing is described by Huang et al. (2002). Though still a novel method for remote sensing, SVM has been applied in many other fields such as biology, biochemistry, and economics. SVM differs from traditional classification approaches by identifying the boundary between classes in n-dimensional spectral-space rather that assigning points to a class based on mean values. SVM creates a hyperplane through n-dimensional spectral-space that separates classes based on a user defined kernel function and parameters that are optimized using machine-learning to maximize the margin from the closest point to the hyperplane. Figure 3.2 illustrates the difference between a maximum likelihood classification and a SMV. By identifying the hyperplane that separates two classes (represented by the red and blue dots) rather than using the distance between class spectral means (the black dots), SVM can produce a more accurate classification. A penalty parameter allows the SVM to vary the degree of training data misclassified due to possible data error when optimizing the hyperplane. While there are many possible kernels, four common kernels found in remote sensing packages are linear, polynomial, radial basis function, and sigmoid. Finding the best kernel and parameters can be difficult, though Hsu et al. (2010) suggest starting with a radial basis function and testing a range of parameters to identify an effective model. In a recent study by Yang (2011), it is shown that for most land cover classes, the radial basis function is the best kernel with a penalty parameter of 100.

Several studies have demonstrated the great potential for SVM. Pal and Mather (2005) found that SVM outperforms maximum likelihood and artificial neural network classifiers using Landsat TM and is well suited for small training sets and high-dimensional

data. Foody and Mathur (2004) found SVM outperforms discriminate analysis and decision-tree algorithms for airborne sensor data. Li et al. (2010) applied SVM to an OBIA with better results than standard fuzzy logic classification. Only a single study has applied SVM for analysis of mangroves. Huang et al. (2009) applied SVM as part of a fusion methodology of spectral and image texture data to map mangroves although the effectiveness of SVM for multispectral classification of mangroves remains untested.
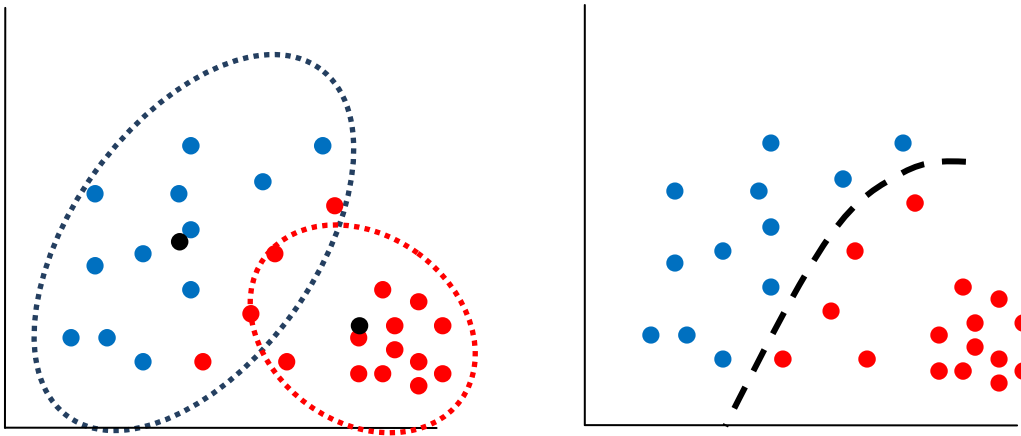
Figure 1.2: A stylized example of a maximum likelihood classification (left) and a support vector machine likelihood (right)

Methods

Study Area

The research was conducted on Isabela Island in the Galapagos Archipelago, Ecuador. The Galapagos Islands, located 1000-km off the coast of Ecuador, are an archipelago consisting of 13 large islands, 4 of which have human populations, and 188 small islands and rocks (Figure 3.3). The Galapagos Islands were declared a national park in 1959 (the park consists of 97% of land area), a UNESCO World Heritage Site in 1978, and a UNESCO Biosphere Reserve in 1987. The Galapagos Islands lie on the western edge of the Atlantic-East Pacific mangrove complex. Mangrove forests consist of three true species common in this region: *Rhizophora mangle* (red), *Avicennia germinans* (black), *and Laguncularia racemosa* (white), and as well as the associate species such as *Conocarpus erectus* (button or buttonwood mangrove) and

Hippomane mancinella (manzanillo), or other halophytes growing on nearby sand flats or dunes (Van der Werff and Andsersen, 1993). In the Galapagos Islands, mangrove forest form dense, but small patches in protected coves and lagoons along an otherwise barren or arid coast. Mangrove forests in the study site can be described primarily as fringe mangroves forming along the coastline or basin mangroves along hyper-saline lagoons. Mangroves grow on a range of substrates from aa lava to sand or silty-clay. For a more detailed description of the arid coastal environment in the Galapagos Islands, see Van der Werff and Andersen (1993).
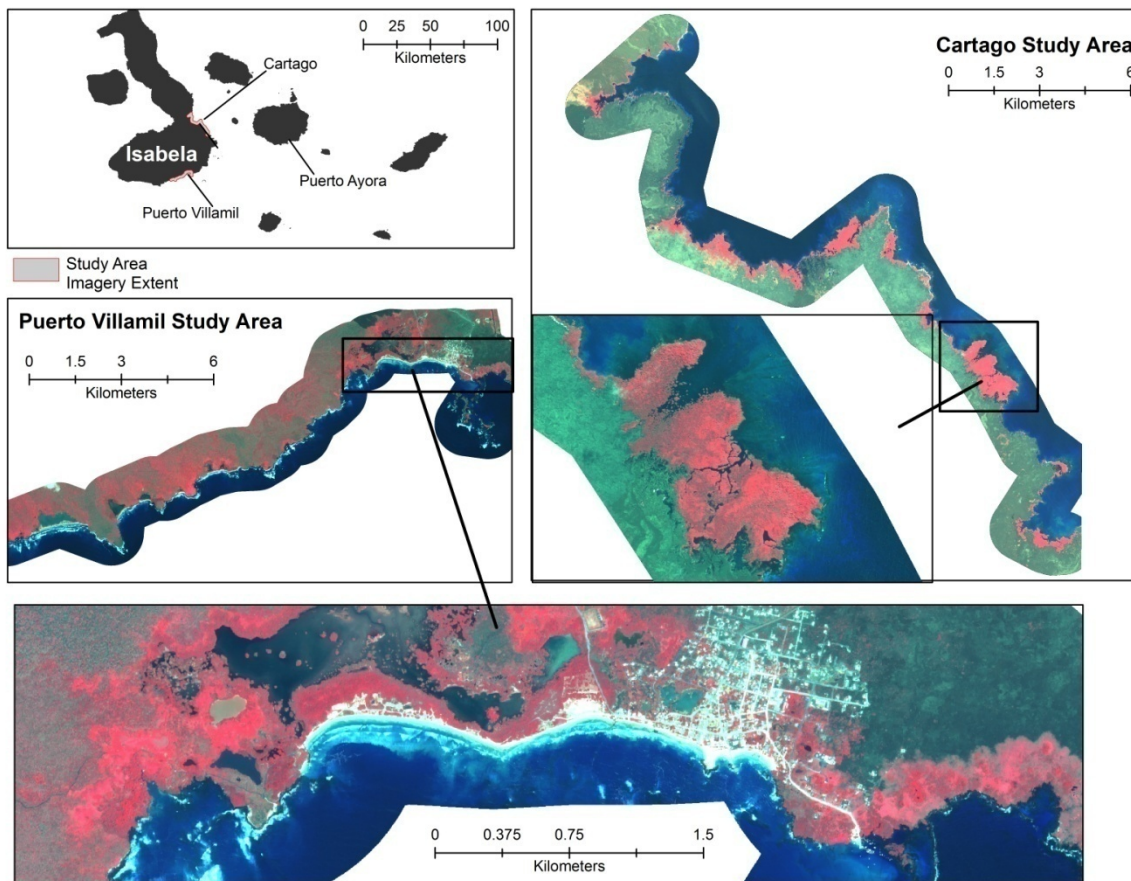
Figure 1.3: Quickbird false color composites for the Puerto Villamil and Cartago study areas on Isabela Island.

This study focuses on two study areas on Isabela Island - Puerto Villamil and Cartago (Figure 3.3). The Puerto Villamil study site is located on the southern end of Isabela Island

extending west from the town of Puerto Villamil. The study area contains some features unique to the Galapagos Islands including the largest lagoon complex in the Galapagos Islands, the longest sand beach, and complex geologic topography along the coastline. Figure 3.4 shows several examples of the mangroves in different settings from the study area. Salinity varies greatly across the study site as both fresh water springs and hyper-saline ponds occur in relatively close proximity. Field observations show that while mangrove species form patterns of zonation based on salinity and/or wave action, the mangrove and associate species co-occur in close proximity due to micro-topographical geological features (i.e. lava coastline). To the west of Puerto Villamil, the elevation increases quickly away from the shoreline towards the Sierra Negra or Cerro Azul volcanoes and the vegetation changes from barren/arid to semi-arid/semi-humid along this elevation transition. It is important to note that unlike large riverine mangrove forests like those along the coast of mainland Ecuador, the pattern of zonation between mangrove and mangrove associate species is truncated and highly variable due to the small inter-tidal zone and the geologic rather the fluvial coastal geomorphology. The Cartago study area is located on the eastern edge of Isabela Island. This area has the largest mangrove forest patches in the Galapagos (unpublished field observation, Birgit Fessl, Charles Darwin Research Station). Unlike the Puerto Villamil study area, Cartago lacks lagoons or vegetation away from the coast as the study area lies on a relatively flat lava field to the east of Sierra Negra.
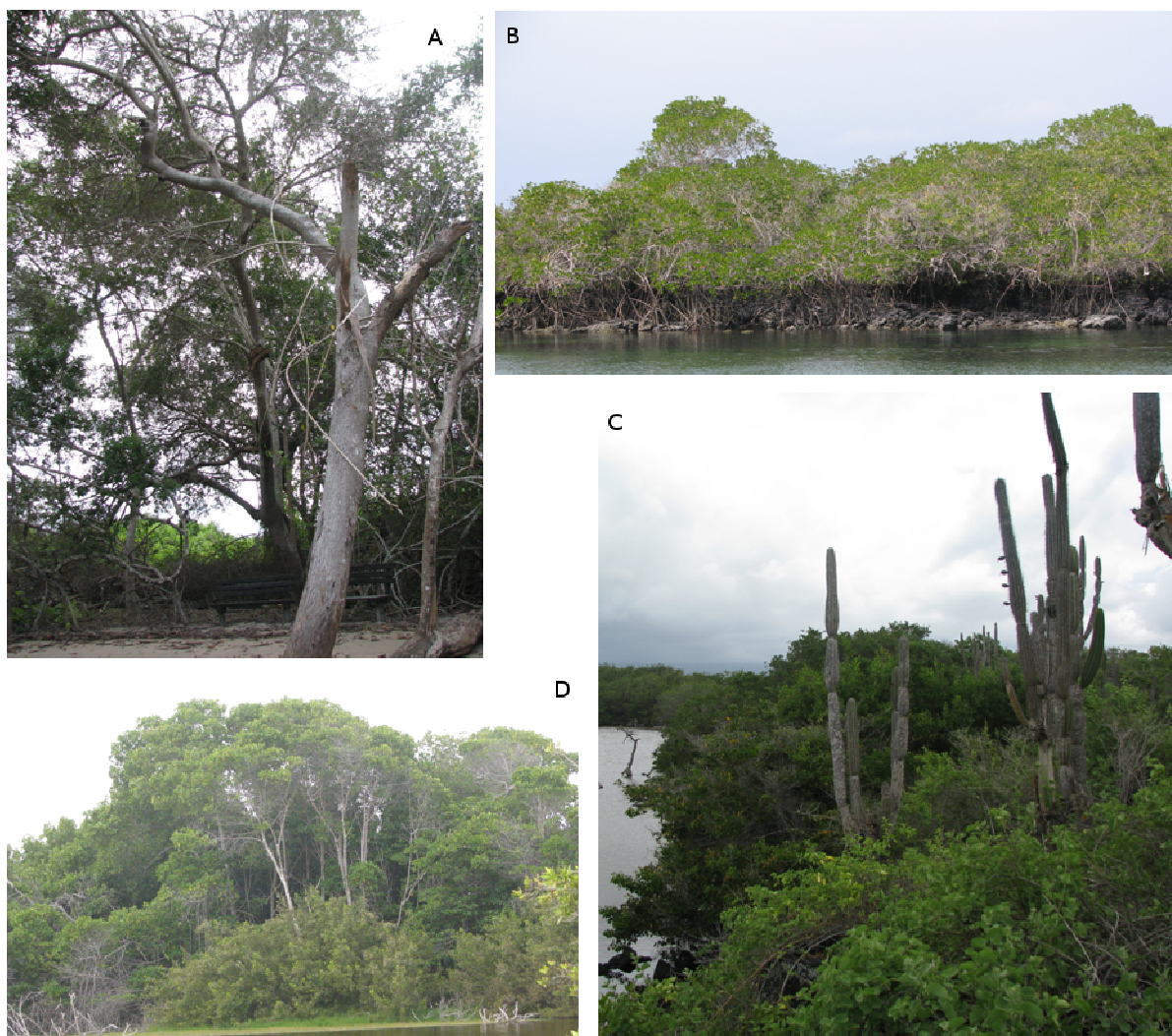
Figure 1.4: Examples of vegetation near Puerto Villamil (from upper left, clockwise): A) tall black mangroves near a fresh water spring, B) red mangroves growing on lava shoreline, C) mixed arid vegetation and mangroves along a saline pond, D) tall red mangroves mixed with white and black mangroves on a saline pond.

<u>Field Data</u>

  Field data were collected during the summer of 2009 near the town of Puerto

Villamil. Due to conservation policies within the Galapagos National Park, non-destructive

sampling was required. Mangroves form stands with dense aerial roots and branches,

making many areas inaccessible. An opportunistic sampling scheme was conducted due to

logistical constraints and efforts were made to sample a wide range of conditions for each

species (Table 3.1). A wide range of conditions were sampled from lava to sand substrates,

fresh water springs to hypersaline ponds, and short shrubs to trees over 20 meters tall. Canopy height, substrate conditions, and mangrove species were recorded at nine points for 48, 10-m diameter plot. Plot location was recorded using a Trimble GeoXT GPS unit and differentially corrected to a 95% horizontal positional accuracy of less than 1.5 meters. To extend the extent of the sampled area, an additional 481 species and height point measurements were collected Point locations were measured using a compass and laser range finder from a known GPS position. Due to the limited accuracy of the analog compass (+/- 1 deg), a maximum of 100 meters from the observer was set for all points collected. All field data points are considered representative for a 3-meter diameter circle.

Table 1.1: Vegetation Field Data

Species	Plots*	Points	Total	Percent
AC	8	27	35	3.472
MZ	43	7	50	4.960
OV	16	17	33	3.274
BW	56	55	111	11.012
RM	120	174	294	29.167
WM	146	243	389	38.591
BM	66	30	96	9.524
Total	455	553	1008	

* points taken at field plots; 9 points per plot

True Mangroves	Mangrove Associates
RM = Red Mangrove	AC = Acacia
WM = White Mangrove	MZ = Manzanillo
BM = Black Mangrove	OV = Other Vegetation
	BW = Buttonwood

Remote Sensing Data

Details of the Quickbird and Worldview-2 imagery are shown in table 3.2. The Quickbird imagery was cloud-free over coastal areas, while the Worldview-2 imagery had a few clouds over the study area. Thus, the Quickbird imagery was used for the first level of analysis. All imagery was geometrically corrected using the ENVI Rational polynomial

coefficients (RPC) with ground control points (GCP) orthorectification correction algorithm. Since all mangroves grow within the inter-tidal zone, the elevation was assumed to be at mean sea-level across the image. The root mean square error (RMSE) was found to be less than 1.5m using 16 independent GCPs. All imagery was radiometically corrected using a Dark Object Subtraction. Since consistent dark objects could not be identified between images, a 1% threshold value for each band was used. Solar angle was not found to be substantially different between images. All imagery was resampled to a resolution of 2 meters using a cubic convolution interpolation. Several band ratios were computed to assist with classification. Band ratios were selected based on exploratory analysis using visual interpretation and the feature optimization tool in eCognition. The selected band ratios were NIR/Red (i.e. Simple Ratio) and NIR/Blue for the Quickbird imagery, and NIR2/Red, Red Edge/Green, and Yellow/Coastal Blue for the Worldview-2 imagery.

Table 1.2: Sensor Specifications for Quickbird and Worldview-2

| Sensor | Dynamic Range | Resolution (m) | | Channels (nm) | | | | | | | |
		Pan	MSS	Coastal Blue	Blue	Green	Yellow	Red	Red Edge	NIR-1	NIR-2
Quickbird	11 bits / pixel	0.6	2.4	N/A	450 - 520	520 - 600	N/A	630 - 690	N/A	760 - 900	N/A
Worldview-2	11 bits / pixel	0.46*	1.83*	400 - 450	450 - 510	510 - 585	585 - 625	630 - 690	705 - 745	770 - 895	860 - 1040

* Distribution and use of imagery at better than .50 m GSD pan and 2.0 m GSD multispectral is subject to prior approval by the U.S. Government.

Spectral Separability

        Spectral separability analysis compares the spectral signature of classes and determines the degree to which those classes can be distinguished. Spectral separability analysis is a commonly used exploratory analysis approach for selecting classes and training data for classification. Spectral separability was calculated using Jeffries-Matusita (J-M) Distance that measures the divergence between spectral means (Schmidt and Skidmore, 2003; Swain, 1986). The J-M distances in ENVI is squared so that the distance values range from 0 to 2, where values greater than 1.9 are highly separable, and value less than 1.0 require class clumping or new training data for traditional mean-based classification methods.

Object-Based Image Analysis

        Image segmentation and decision-tree classification were conducted using eCognition Developer 8. eCognition groups pixels based on spectral and spatial properties (Benz et al., 2004). A two-level segmentation was used to first classify general land cover classes, and then refine the coastal vegetation classes. The first-level segmentation used shape = 0.5, compactness = 0.5, and scale = 25.

Decision-Tree Classification

        The decision tree classification is shown in figure 3.5. Class rules were identified using interactive visual interpretation of threshold values based on training data, existing map, and expert knowledge of the study area. Upland and coastal vegetation were separated using a distance rule of 250 meters from open water based on field observations. While there was little confusion between these general land cover classes, there was considerable confusion between lava and shallow water over lava (e.g. ponds, coastline). In these cases, objects were manually edited using expert image interpretation.

67
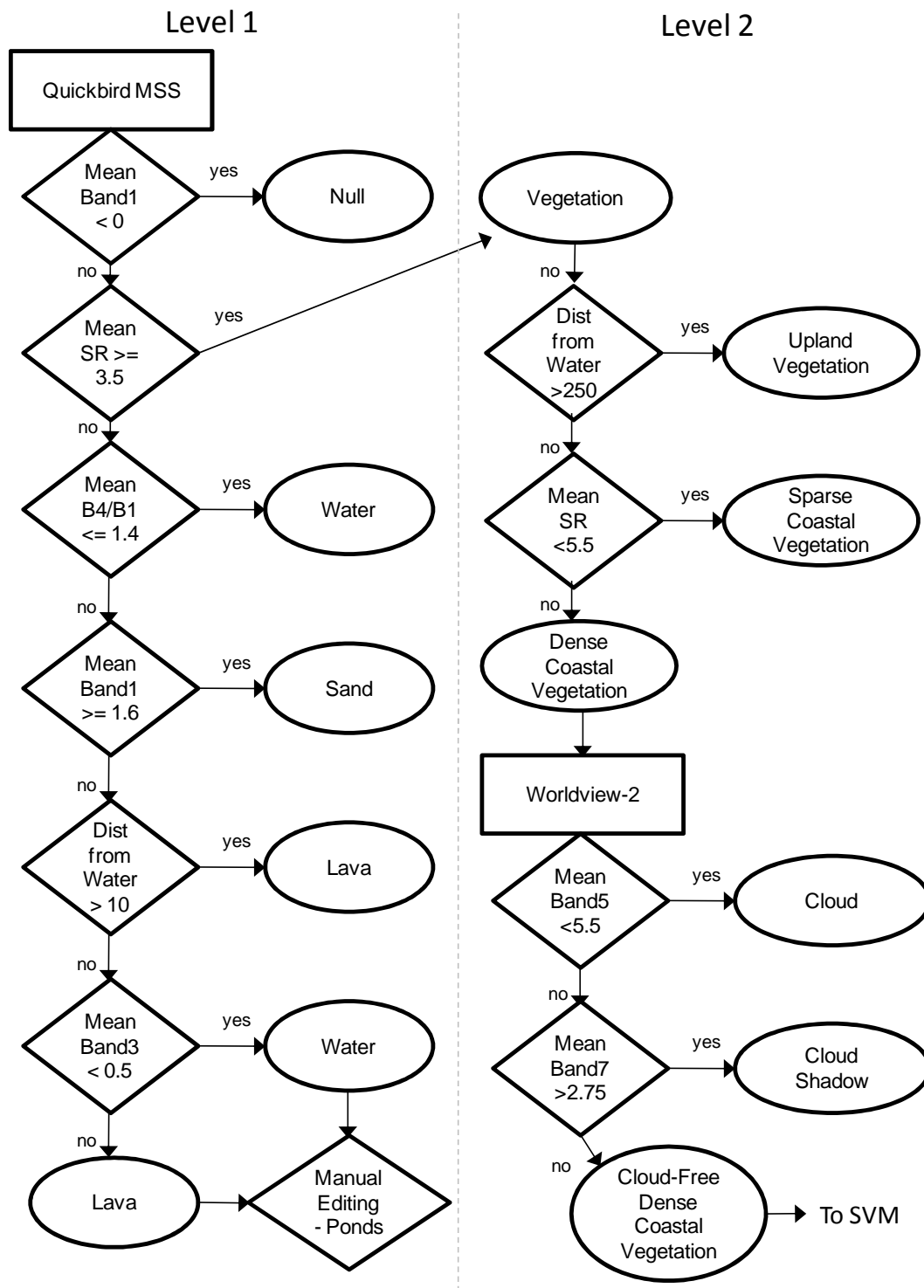
Figure 1.5: OBIA Decision Tree (rectangle = image; diamond = rule; oval = class)

A second image level was segmented based on the Worldview-2 imagery using shape = 0.5, compactness = 0.9, and scale = 10 for only the dense coastal vegetation classification from level 1. Although overall cloud cover was less than 15%, clouds and cloud-shadow were classified and removed from the vegetation analysis. The remaining dense coastal vegetation objects were exported to ArcGIS 9.3.1 with the mean values of each band and band ratio for each object. In ArcGIS, the shapefiles were converted to raster stacks for analysis in ENVI 4.8. It should be noted that during exploratory analysis, object-level standard deviation and texture (i.e. grey-level co-occurrence matrix) were also calculated, but they were not found to substantially improve classification results, while raising concerns of model over-fitting with higher data dimensionality. Additionally, the eCognition fuzzy nearest neighbor classification, using the feature optimization tool to select input data for the classification, did not produce acceptable results for the true mangrove classification. When using only mean spectral information, there was insufficient separabiltiy between classes. The addition of standard deviation or skewness of spectral data or image texture, separability increased, but classification results showed strong overfitting of the classification to training data.

Support Vector Machine Classification

The SVM classification was conducted using ENVI. Calibration and validation objects were selected based on field data; homogenous objects were verified through visual assessment. The distribution of the objects is shown in table 3.3. The objects were systematically divided between calibration and validation datasets to ensure an even geographic distribution. An SVM radial basis function(RBF) kernel was applied using the default parameters (gamma = 0.091 and a penalty parameter of 100). The penalty parameter is particularly important for non-separable classes. Equation (1) shows the RBF kernel:

$K(x_i, x_j) = \exp(-g||x_i - x_j||^2), g > 0$ (1)

where g is the user-defined gamma

ENVI conducts pair-wise iterations of SVM and assigns fuzzy class membership. Classes are assigned using the highest membership. Exploratory analysis did not show improved results with other gamma or penalty values.

Table 1.3: Distribution of objects used to calibrate and validate the SVM classification

	True Mangroves	Mangrove Associates	Total
Calibration	143	54	197
Validation	73	24	101
Total	216	78	298

Accuracy Assessment

The accuracy of the SVM classification was assessed in several ways. First, accuracy is assessed at the object-level using an error confusion matrix. The overall, producer's, and user's accuracy was calculated, in addition to the kappa statistic. The area under the curve (AUC) of the receiver operating characteristic (ROC) (Metz, 1978) was also computed based on fuzzy membership. This statistic illustrates the accuracy of the classification relative to a perfect classification (AUC =1) and a random classification (AUC = 0.5) based on the rate of false positives. Second, an error confusion matrix was created for the individual vegetation types at the field point level and all classes from both the decision tree and SVM classification. To further illustrate the relationship between the field data and SVM, a boxplot distribution of fuzzy membership to true mangroves was computed for each field vegetation class.

Results and Discussion

Spectral Separability Analysis

Class spectral separability at the pixel level for all vegetation field data points is shown in table 3.4 for the Quickbird (A) and Woldview-2 (B) imagery. The spectral

separability between vegetation classes for the Quickbird imagery was moderate to poor. Not a single value was found to be greater than the suggested threshold of 1.9, though many values were greater than 1.8. More importantly, there was not a consistently high separability for any individual species. This indicates that the ability to discriminate vegetation types with high accuracy using Quickbird imagery is very unlikely. Although the Worldview-2 imagery had better spectral separability than the Quickbird imagery (Table 3C), likely due to the greater number of spectral bands, only manzanillo (MZ) was consistently separable from mangroves. Separability between mangrove species was particularly low, especially between red and white mangroves. This result is consistent with field measurements taken from a handheld spectroradiometer during the field campaign (unpublished data, Conghe Song, University of North Carolina at Chapel Hill). The spectral overlap and confusion between species was consistent with the accuracy assessment of previous studies using various classification techniques. Neukermans et al. (2008) reported an overall accuracy of 72% using a fuzzy classification and Wang et al. (2004b) reported an overall accuracy of 75% using a maximum likelihood technique, although the user's accuracy for some species was as low as 55%. During the exploratory analysis of this study, a MLC classification failed to detect two separate true mangrove and mangrove associate classes.

Table 3.4D shows spectral separability of true mangroves (TM) and mangrove associates (MA) for all vegetation field points and dense vegetation objects from OBIA segmentation and decision tree classification. In most cases, spectral separability increased with the inclusion of band ratios and spatial information through image segmentation into objects. However, the maximum value of 1.665 demonstrates that there is considerable spectral overlap between the two classes and that non-traditional classification methods are likely required (i.e. SVM). The use of an object-based approach worked best for dense vegetation objects. Results for sparse vegetation objects (not shown) did not improve the separability results and were sometimes worse than the pixel-based analysis due to the

inclusion of background substrate reflectance. Moreover, the moderate to poor spectral separability indicates the in ability to discern between species using this imagery which includes noise from non-leaf surfaces such as braches and background substrate. Given, pure leaf reflectance from finer scale imagery or spectral unmixing, spectral separabiltiy may be higher.

Classification

The classification is illustrated in figure 3.6. Table 3.5 shows the proportion of each land cover type. For both study areas, lava and ocean are the dominant cover types and coastal vegetation comprises about 5.5 sq. km or 12% and 8% of Puerto Villamil and Cartago images, respectively. The composition of coastal vegetation differs between the two study areas. The Puerto Villamil study area is mostly sparse vegetation with mangrove associates and true mangroves comprising a minority of coastal vegetation. The Cartago study area is mostly true mangroves with much less sparse vegetation and almost no mangrove associate species present. However, much of the dense coastal vegetation was obstructed by clouds or cloud shadow in the Worldview-2 image (24.8%).

The satellite classification has shown that true mangroves are widespread and the dominant vegetation cover in the Cartago study area, while true mangroves are part of a wider range of vegetation in the Puerto Villamil study area. In both study areas, mangroves grow along the sheltered coastline and thrive where there is likely subsurface freshwater from the humid highlands emerging along the coast as springs. Several of these springs are found near the town of Puerto Villamil and these reflect the large dense mangrove patches observed.

The differences in land cover reflect the differences in the climatic and geomorphic environment. The Puerto Villamil study area is along the southern edge of the Sierra Negra volcano and has considerably more cloud cover during the year than the Cartago study area

72

(unpublished MODIS data). Furthermore, elevation increases rapidly from the coast to the area west of Puerto Villamil, where mists and fog increase with elevation providing moisture to plants. In the Cartago study area, the elevation remains near sea-level with little available moisture, as observed from the barren lava beds, except along the coast where there are likely isolated fresh water springs fed by rain in the humid highlands on Sierra Negra.

Table 1.4: Spectral Separability (Jeffries-Matustia Distance) for individual species using Quickbird (A) or Worldview(B) pixels, and true mangroves vs. mangrove associates using pixels and objects(D)

A- Quickbird

	AC	MZ	OV	BW	RM	WM	BM
AC		1.892	1.342	1.455	1.837	1.703	1.543
MZ	1.892		1.734	1.690	1.593	1.814	1.355
OV	1.342	1.734		0.994	1.725	1.673	1.233
BW	1.455	1.690	0.994		1.256	1.185	0.702
RM	1.837	1.593	1.725	1.256		0.508	1.129
WM	1.703	1.814	1.673	1.185	0.508		1.258
BM	1.543	1.355	1.233	0.702	1.129	1.258	

B- Worldview-2

	AC	MZ	OV	BW	RM	WM	BM
AC		**1.963**	1.647	1.698	1.820	1.498	1.785
MZ	**1.963**		1.861	**1.925**	**1.900**	**1.943**	1.647
OV	1.647	1.861		1.532	1.622	1.584	1.381
BW	1.698	**1.925**	1.532		1.617	1.336	1.634
RM	1.820	**1.900**	1.622	1.617		0.866	1.226
WM	1.498	**1.943**	1.584	1.336	0.866		1.540
BM	1.785	1.647	1.381	1.634	1.226	1.540	

C- Difference

	AC	MZ	OV	BW	RM	WM	BM
AC		0.071	0.304	0.243	-0.017	-0.205	0.242
MZ	0.071		0.127	0.235	0.307	0.129	0.292
OV	0.304	0.127		0.537	-0.103	-0.089	0.148
BW	0.243	0.235	0.537		0.361	0.151	0.932
RM	-0.017	0.307	-0.103	0.361		0.358	0.097
WM	-0.205	0.129	-0.089	0.151	0.358		0.282
BM	0.242	0.292	0.148	0.932	0.097	0.282	

D- Pixel vs. Object for TM and MA

	QB	QB w/ BR	WV	WV w/ BR	
All Veg Points	0.664	1.141	0.734	1.084	QB = Quickbird
Dense Veg Objects	0.839	1.118	1.321	1.665	WV = Worldview-2
					BR = Band Ratios

<u>Mangrove Associates - MA</u>

AC = Acacia

MZ = Manzanillo

OV = Other Vegetation

BW = Buttonwood

<u>True Mangroves - TM</u>

RM = Red Mangrove

WM = White Mangrove

BM = Black Mangrove

SVM Classification

- True Mangrove
- Assoc. Species
- Quickbird Cloud
- Sparse Coastal Vegetation
- Dense Coastal Vegetation - Clouds
- Lava
- Ocean
- Pond
- Sand / Urban
- Upland Vegetation

Puerto Villamil

0   0.5   1   2 Kilometers

0   1.5   3   6 Kilometers

0   0.5   1   2 Kilometers

0   0.5   1   2 Kilometers

- Upland Vegetation
- Sand
- Ocean
- Lava
- Dense Vegetation - Clouds
- Sparse Vegetation
- True Mangroves
- Mangrove Associate

Figure 1.6: Land Cover Classification for Puerto Villamil (top) and Cartago (bottom)

Table 1.5: Land Cover Classification for all classes (A) and coastal vegetation (B)

A	Puerto Villamil		Cartago	
Cover	Area	Percent	Area	Percent
OC	17.9304	38.1463	29.2249	43.4184
PD	1.5400	3.2763	*	
LV	14.1150	30.0291	32.4511	48.2114
SD	0.8032	1.7087	0.0397	0.0589
UV	6.8491	14.5712	0.2722	0.4043
QBC	0.0985	0.2096	0.0000	0.0000
SCV	2.8796	6.1262	1.2552	1.8648
DCVC	0.1785	0.3798	1.0119	1.5033
MA	1.5091	3.2106	0.0006	0.0009
TM	1.1010	2.3423	3.0544	4.5379
Total	47.004	12.0588	67.310	7.9069

Indicates coastal vegetation classes

B	Puerto Villamil		Cartago	
Cover	Area	Pct CV	Area	Pct CV
SCV	2.8796	0.5080	1.2552	0.2358
DCVC	0.1785	0.0315	1.0119	0.1901
MA	1.5091	0.2662	0.0006	0.0001
TM	1.1010	0.1942	3.0544	0.5739
Total	5.668		5.322	

OC = Ocean	UV = Upland Vegetation
PD = Pond	QBC = Quickbird Clouds
LV = Lava	SCV = Sparse Coastal Veg
SD = Sand	DCVC = Dense Coast Vegetation w/ Clouds
TM = True Mangrove	MA = Mangrove Associates

Another major difference between the two study areas is the presence of ponds and lagoons. The Puerto Villamil study area contains the largest lagoon system in the Galapagos Islands. The hydrologic connectivity of these lagoons is complex as some lagoons are hyper-saline and others are nearly fresh water (unpublished data, Brian White, University of North Carolina at Chapel Hill). The range of hydrologic conditions near Puerto Villamil are likely the cause of the range of vegetation types (i.e. true mangroves vs. mangrove associates) and vegetation conditions (i.e. LAI and canopy height) observed. As Song et al. (2011) observed

in this study area, salinity can have an observable impact on remote sensing-derived photosynthetic productivity.

The lagoon complex is the result of volcanic topographic features seemingly unique to that area. In contrast, the structure of the Cartago coastline reflects a more fluvial pattern of inter-tidal channels. The relatively simple topography and hydrology and more arid environment near Cartago has led to isolated but large, dense mangrove patches around protected coves and likely fresh water springs. Future research is needed to investigate the link between hydrologic conditions including subsurface flow and coastal vegetation.

<u>Accuracy Assessment</u>

The accuracy assessment was considered at two levels - 1) validation objects for a typical assessment of just the SVM classification, and 2) validation field points to understand the accuracy from the decision tree classification and the sub-object level.

OBIA

The overall accuracy of the SVM classification between true mangroves and mangrove associates was 94.4% with a kappa statistic of 0.863. The greatest source of error was the misclassification of mangrove associates as true mangroves (Table 3.6). The producer's and user's error were consistent for each class and greater than 90% in all cases. The AUC-ROC was 0.991 for true mangroves and 0.987 for mangrove associates. The overall accuracy of the classification was very good and better than most previous mangrove studies (Heumann, 2011) and thus demonstrates the ability of this approach to accurately distinguish between true and associate mangroves in fringe and basin environments.

Table 1.6: Classification confusion matrix (A) and classification accuracy (B) of SVM classification

A	TM (Pix)	TM (%)	MA(Pix)	MA(%)	Total
Unclassified	0	0	0	0	0
TM	3152	96.04	128	9.69	3280
MA	130	3.96	1193	90.31	1323
Total	3282	100	1321	100	4603

B	Prod. (Pix)	Prod.(%)	User (Pix)	User (%)
TM	3152/3282	96.04	3152/3280	96.1
MA	1193/1321	90.31	1193/1323	90.17

Table 1.7: Accuracy Assessment of Decision Tree and SVM Classification from Field Data by number of points (A) and percent of points (B)

Remote Sensing Classes

A	TM	MA	QBC	SCV	DCVC	LV	OC	PD	SD	UV	Total
AC	2	0	0	18	0	11	0	0	0	0	31
MZ	5	27	0	2	0	0	0	0	0	0	34
OV	4	9	0	14	0	10	0	0	0	0	37
BW	18	6	0	52	0	12	0	4	0	0	92
RM	84	8	0	71	0	23	1	18	0	0	205
WM	43	1	0	159	0	120	7	7	0	0	337
BM	9	22	0	16	0	6	0	0	0	0	53
Total	165	73	0	332	0	182	8	29	0	0	789

(Field Data Classes)

Remote Sensing Classes

B	TM	MA	QBC	SCV	DCVC	LV	OC	PD	SD	UV	Total
AC	6.45	0.00	0.00	58.06	0.00	35.48	0.00	0.00	0.00	0.00	100
MZ	14.71	79.41	0.00	5.88	0.00	0.00	0.00	0.00	0.00	0.00	100
OV	10.81	24.32	0.00	37.84	0.00	27.03	0.00	0.00	0.00	0.00	100
BW	19.57	6.52	0.00	56.52	0.00	13.04	0.00	4.35	0.00	0.00	100
RM	40.98	3.90	0.00	34.63	0.00	11.22	0.49	8.78	0.00	0.00	100
WM	12.76	0.30	0.00	47.18	0.00	35.61	2.08	2.08	0.00	0.00	100
BM	16.98	41.51	0.00	30.19	0.00	11.32	0.00	0.00	0.00	0.00	100
Total	0.209	0.093	0	0.421	0	0.231	0.010	0.037	0	0	1

(Field Data Classes)

Field Points

Table 3.7 shows the distribution of validation vegetation field data points (i.e. points that did not fall within objects used for the SVM classification). The majority of field points were classified either as sparse coastal vegetation or lava. This is indicative of the arid environment of the study area, particularly in an OBIA classification framework where the spectral signature of the object and not individual pixels are used for classification. Furthermore, given the sparse nature of the vegetation, the spectral signal strength of these vegetation points was relatively weak, preventing further classification with detailed spectral unmixing, requiring hypersepctral data. Of the true mangrove species, about 50% of red and black mangroves points were classified as sparse vegetation, while nearly all of the white mangrove points were classified as sparse. It should be noted that since the field sampling scheme was opportunistic due to Galapagos National Park regulations about cutting vegetation, sampling was likely biased towards less dense and more accessible vegetation, especially for the field plots.

Figure 3.7 shows the fuzzy SVM true mangrove classification distribution for each vegetation type. Manzanillo, other vegetation, red mangrove, and white mangrove had appropriate membership to true mangroves. However, black mangrove and buttonwood had low and high membership, respectively, indicating misclassification of these vegetation types.

There are many aspects to this error. First, there is a spatial scale mismatch between the field points and the objects in that many points may occur in a single object. For example, field plots dominated by black mangroves (~11 of 29 dense black mangrove points) were misclassified as mangrove associates due to the misclassification of a single object. Moreover, single points may not be representative of a whole object, especially near object edges where geometric uncertainty of both field and satellite data could be factors. Second,

79

fuzzy classification or mixed classes were not explicitly considered. Only pure objects were used for calibrating the classification as the exact composition of mixed objects was unknown due to the lack of a tree census. While mangroves often have detectable patterns of zonation, this is not always observed (Ellison et al., 2002). This was certainly the case in some parts of the study area where edaphic and topographic conditions changed rapidly over small distance such that for a given field plot, multiple species were present.
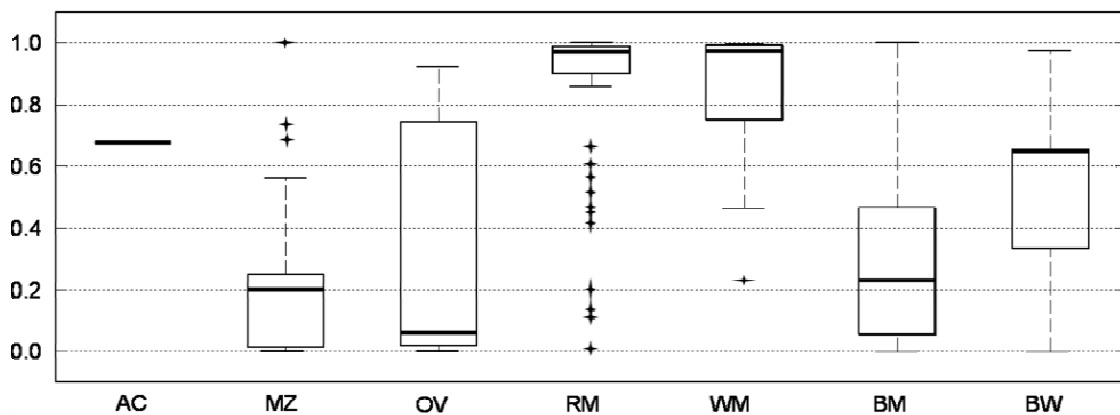
Figure 1.7: Boxplot of TM Fuzzy Membership for Validation Field Points

This second point demonstrates a gap in the current knowledge of methods in remote sensing. While there are several papers that assess methods of image segmentation and object classification (Blachke et al., 2008), there is not a good assessment of linking field sampling schemes with OBIA of natural landscapes where visual interpretation is not as straight forward as human landscapes (e.g. buildings, roads, impervious surfaces). Field sampling protocols for remote sensing have been largely designed for pixel-based analysis from a legacy of 25-meter pixels from Landsat and SPOT. The type of sampling for pixel based analysis does not lend itself to assessing whole objects created after field data collection, especially fuzzy membership of heterogeneous objects. Two alternative sampling schemes such as large-scale quadrat sampling or mapping boundaries of homogeneous

patches may be more appropriate of OBIA, but this type of field data collection is difficult and time-consuming in the best of conditions, let alone in dense mangrove swamps. Furthermore, this type of sampling would be prohibitively destructive in the Galapagos National Park. Future research is needed to assess effective and efficient field sampling schemes for use with OBIA.

Conclusions

Effective monitoring and management of mangrove forests requires accurate and repeatable measures of forest extent and species composition. While previous studies have successfully mapped mangrove extent and species, these studies have largely ignored fringe mangroves. This study has addressed this issue. Spectral separability analysis revealed that the spectral signatures between mangrove species and even associate species were not only moderately separable using Quickbird or Worldview-2 imagery at both the pixel and object level. The best separability was found using dense vegetation objects, indicating that even for very high resolution imagery, the multispectral signature of non-vegetation components for sparse vegetation produce mixed pixel effects that seriously limit multispectral analysis. Using a hybrid decision-tree and SVM approach, true mangrove species and associate mangrove species were classified with an accuracy of 94% at the object level. However, when class accuracy was considered at the species level, black mangrove and buttonwood were often misclassified, indicating that certain species of true and associate mangroves are better classified than others. This research has demonstrated the need and application of non-linear machine-learning classification schemes with OBIA and highlighted remaining challenges including the classification of sparse vegetation as well as image segmentation over natural landscapes as objects are less distinct than in human-managed landscapes. Given these challenges, future research should focus on hyperspectral image analysis to

improve spectral separability between species and LiDAR to enhance image segmentation

based on canopy structure as well as spectral properties.

References

Al Habshi, A., T. Youssef, M. Aizpuru & F. Blasco (2007) New mangrove ecosystem data along the UAE coast using remote sensing. *Aquatic Ecosystem Health & Management,* 10**,** 309-319.

Alongi, D. M. (2002) Present state and future of the world's mangrove forests. *Environmental Conservation,* 29**,** 331.

Benfield, S. L., H. M. Guzman & J. M. Mair (2005) Temporal mangrove dynamics in relation to coastal development in Pacific Panama. *Journal of environmental management,* 76**,** 263.

Benz, U. C., P. Hofmann, G. Willhauck, I. Lingenfelder & M. Heynen (2004) Multi-resolution, object-oriented fuzzy analysis of remote sensing data for GIS-ready information. *Isprs Journal of Photogrammetry and Remote Sensing,* 58**,** 239-258.

Blaschke, T., S. Lang & G. Hay. 2008. *Object-based image analysis: spatial concepts for knowledge-driven remote sensing applications*. Springer.

Chubey, M. S., S. E. Franklin & M. A. Wulder (2006) Object-based analysis of Ikonos-2 imagery for extraction of forest inventory parameters. *Photogrammetric Engineering and Remote Sensing,* 72**,** 383-394.

Conchedda, G., L. Durieux, P. Mayaux & Ieee. 2007. Object-based monitoring of land cover changes in mangrove ecosystems of Senegal., In *4th International Workshop on the Analysis of Multi-Temporal Remote Sensing Images*, 44-49. Louvain, BELGIUM.

Desclee, B., P. Bogaert & P. Defourny (2006) Forest change detection by statistical object-based method. *Remote Sensing of Environment,* 102**,** 1-11.

Foody, G. M. & A. Mathur (2006) The use of small training sets containing mixed pixels for accurate hard image classification: Training on mixed spectral responses for classification by a SVM. *Remote Sensing of Environment,* 103**,** 179-189.

Gao, J. (1998) A hybrid method toward accurate mapping of mangroves in a marginal habitat from SPOT multispectral data. *International Journal of Remote Sensing,* 19**,** 1887-1899.

Giri, C., E. Ochieng, L. L. Tieszen, Z. Zhu, A. Singh, T. Loveland, J. Masek & N. Duke (2011) Status and distribution of mangrove forests of the world using earth observation satellite data. *Global Ecology and Biogeography,* 20**,** 154-159.

Hay, G. J., G. Castilla, M. A. Wulder & J. R. Ruiz (2005) An automated object-based approach for the multiscale image segmentation of forest scenes. *International Journal of Applied Earth Observation and Geoinformation,* 7**,** 339-359.

Hogarth, P. 2007. The Biology of Mangroves and Seagrasses. Oxford University Press.

Hsu, C., C. Cahng & C. Lin. 2010. A Practical Guide to Support Vector Classification. Department of Computer Science, National Taiwan Univeristy.

Huang, C., L. S. Davis & J. R. G. Townshend (2002) An assessment of support vector machines for land cover classification. *International Journal of Remote Sensing,* 23, 725-749.

Huang, X., L. P. Zhang & L. Wang (2009) Evaluation of Morphological Texture Features for Mangrove Forest Mapping and Species Discrimination Using Multispectral IKONOS Imagery. *Ieee Geoscience and Remote Sensing Letters,* 6, 393-397.

Krause, G., M. Bock, S. Weiers & G. Braun (2004) Mapping land-cover and mangrove structures with remote sensing techniques: A contribution to a synoptic GIS in support of coastal management in North Brazil. *Environmental management,* 34, 429.

Li, H. T., H. Y. Gu, Y. S. Han & J. H. Yang (2010) Object-oriented classification of high-resolution remote sensing imagery based on an improved colour structure code and a support vector machine. *International Journal of Remote Sensing,* 31, 1453-1470.

Manson, F. J., N. R. Loneragan, I. M. McLeod & R. A. Kenyon (2001) Assessing techniques for estimating the extent of mangroves: topographic maps, aerial photographs and Landsat TM images. *Marine and Freshwater Research,* 52, 787-792.

Metz, C. E. (1978) BASIC PRINCIPLES OF ROC ANALYSIS. *Seminars in Nuclear Medicine,* 8, 283-298.

Myint, S. W., C. P. Giri, W. Le, Z. L. Zhu & S. C. Gillette (2008) Identifying mangrove species and their surrounding land use and land cover classes using an object-oriented approach with a lacunarity spatial measure. *Giscience & Remote Sensing,* 45, 188-208.

Neukermans, G., F. Dahdouh-Guebas, J. G. Kairo & N. Koedam (2008) Mangrove species and stand mapping in GAzi bay (Kenya) using Quickbird satellite imagery. *Journal of Spatial Science,* 53, 75-86.

Ramsey, E. W. & J. R. Jensen (1996) Remote sensing of mangrove wetlands: Relating canopy spectra to site-specific data. *Photogrammetric Engineering and Remote Sensing,* 62, 939.

Schmidt, K. S. & A. K. Skidmore (2003) Spectral discrimination of vegetation types in a coastal wetland. *Remote Sensing of Environment,* 85, 92-108.

Simard, M., G. De Grandi, S. Saatchi & P. Mayaux (2002) Mapping tropical coastal vegetation using JERS-1 and ERS-1 radar data with a decision tree classifier. *International Journal of Remote Sensing,* 23, 1461-1474.

Song, C., White, B., Heumann, BW. (2011) Hyperspectral Remote Sensing of Salinity Stress on Red (*Rhizophora mangle*) and White (*Laguncularia racemosa*) Mangroves on Galapagos Islands. *unpublished data.*

Swain, P. (1986) Remote Sensing. In *The handbook of pattern recognition and processing,* eds. T. Young & K. Fu, 613 - 627. Orlando: Academic Press.

Tomlinson, P. B. (1986) *The botany of mangroves.* Cambridge Cambridgeshire; New York: Cambridge University Press.

Vaiphasa, C., S. Ongsomwang, T. Vaiphasa & A. K. Skidmore (2005) Tropical mangrove species discrimination using hyperspectral data: A laboratory study. *Estuarine Coastal and Shelf Science,* 65, 371-379.

Vaiphasa, C., A. K. Skidmore & W. F. de Boer (2006) A post-classifier for mangrove mapping using ecological data. *Isprs Journal of Photogrammetry and Remote Sensing,* 61, 1.

Van Der Werff, H. H. & H. Adsersen (1993) Dry coastal ecosystems of the Galapagos Islands. *Ecosystems of the World; Dry coastal ecosystems: Africa, America, Asia and Oceania*, 459-475.

Vapnik, V. (1995) *The Nature of Statistical Learning Theory.* Springer.

Wang, L., J. L. Silvan-Cardenas & W. P. Sousa (2008) Neural network classification of mangrove species from multi-seasonal ikonos imagery. *Photogrammetric Engineering and Remote Sensing,* 74, 921-927.

Wang, L. & W. P. Sousa (2009) Distinguishing mangrove species with laboratory measurements of hyperspectral leaf reflectance. *International Journal of Remote Sensing,* 30, 1267-1281.

Wang, L., W. P. Sousa & P. Gong (2004a) Integration of object-based and pixel-based classification for mapping mangroves with IKONOS imagery. *International Journal of Remote Sensing,* 25, 5655-5668.

Wang, L., W. P. Sousa, P. Gong & G. S. Biging (2004b) Comparison of IKONOS and QuickBird images for mapping mangrove species on the Caribbean coast of Panama. *Remote Sensing of Environment,* 91, 432-440.

Woodcock, C. E. & A. H. Strahler (1987) The factor of scale in remote sensing. *Remote Sensing of Environment,* 21, 311-332.

Wulder, M. A., J. C. White, G. J. Hay & G. Castilla (2008) Towards automated segmentation of forest inventory polygons on high spatial resolution satellite imagery. *Forestry Chronicle,* 84, 221-230.

Yang, X. (2011) Parameterizing Support Vector Machines for Land Cover Classification. *Photogrammetric Engineering & Remote Sensing,* 77, 27 - 38.

Chapter 4 : Comparison of Spectral and Spatial Techniques to Map Mangrove Forest Leaf Area

Abstract

The aim of this chapter is to investigate and compare the ability of spectral and spatial remote sensing techniques to determine canopy cover and leaf area in fringe mangrove forests. The motivation for this research is prompted by the need for spatial canopy structure data for ecosystem and habitat modeling in the Galapagos Islands, Ecuador. Fractional canopy cover, effective LAI (leaf area index) and true LAI were calculated using digital hemispherical under-canopy photographs at 48 sites composed of red (*Rhizophora mangle*), white (*Laguncularia racemosa*), black (*Avicennia germinans*), or mixed mangrove forest canopies with black lava, white sand, or leaf litter substrates. Spectral vegetation indices (SVI) were calculated using Quickbird and Advanced Land Imager multispectral imagery. Texture metrics from grey-level occurrence (GLOM) and co-occurrence matrices (GLCM) were calculated using panchromatic Quickbird imagery to predict canopy structure. Results show the relationships between SVI and canopy structure are statistically significant but weak ($r < 0.45$). Moderate to strong relationships ($r^2 > 0.6$) were found for GLCM-derived texture. However, the results indicate that spatial texture metrics are sensitive to the canopy structure of individual species, variation in the reflectance of the different background substrate, or possibly both. Empirical models of fractional canopy cover and true LAI based on GLCM texture relationships for substrate, and species, respectively, are presented. This paper demonstrates the that *a priori* knowledge of species composition or substrate is needed but represent a serious challenge to mapping mangrove forest LAI using the parametric models.

Introduction

The amount of canopy cover or leaf area is an important biophysical parameter related to ecological processes such as habitat selection, evapotranspiration, and carbon cycling. Given that large-scale ground-based measurements of canopy cover or leaf area are

unfeasible, remote sensing methods are required to produce the spatial data essential for spatially-explicit habitat or ecological models. Relatively little research has investigated the use of satellite remote sensing to characterize mangrove forest beyond areal extent mapping and change detection (Heumann, 2011) despite the known ecological importance of mangrove forests in terms of ecological services, such as nurseries for economically important fisheries, biofiltration of pollution, and the potential for reduce the impacts of tsunami and hurricanes (Hogarth, 2007).

Many studies have investigated the empirical relationships between spectral vegetation indices (SVI) and leaf area for terrestrial boreal, temperate, and tropical forests (e.g. Turner et al., 1999; Eklundh et al., 2003; Lu et al., 2004; Boyd and Danson, 2005) using high resolution (e.g. Landsat ETM+) or very high resolution imagery (e.g. IKONOS or Quickbird). Although the normalized difference vegetation index (NDVI) and simple ratio (SR) have been shown to have moderate to strong relationships with LAI for red, white, and black mangroves (Kovacs et al., 2004; Kovacs et al., 2009), the geographical extent of this research has been limited to a single study area. Despite evidence from terrestrial ecosystems that spectral information from short-wave infrared (SWIR) is significantly related to canopy cover and leaf area (e.g. Brown et al., 2000; Pu et al., 2005; Twele et al., 2008), the use of SVI that incorporate SWIR wavelengths have not been investigated for mangrove forests.

The rise of widely available very high resolution imagery has lead to a novel approach to characterize canopy cover and leaf area based on spatial information. This approach relies upon a relationship between the pattern of canopy tree crowns and gaps with canopy cover and leaf area (Woodcock and Strahler, 1987; Wulder et al., 1998; Bruniquel et al., 1998). Several studies have investigated the link between image spatial information and canopy cover or leaf area in boreal and temperate regions (e.g. Wulder et al., 1998; Bruniquel et al., 1998; Moskal and Franklin, 2004; Kayitakire et al., 2006; Song and Dickison, 2008; Gray,

2009). Kraus et al. (2009) found in mature tropical forests (eLAI > 5.0) that in the absence of any significant relationship between SVI and LAI, texture metrics had a strong and significant relationship with LAI (r^2 = 0.71). While image texture has been used to classify mangrove species, it has not been used to determine canopy structure to date.

Objectives and Contents of the Study

The aim of this research is to investigate the use of spectral vegetation indices (SVI) and image texture to determine fractional canopy cover and leaf area index in fringe-type mangrove forests in the Galapagos Islands, Ecuador. The motivation of this study is the ability to map either leaf as an input for ecosystem modeling or habitat modeling for species such as the mangrove finch. This paper is organized in two parts. First, SVIs are examined using very high spatial resolution, Quickbird imagery and the enhanced spectral sensitivity and resolution of Advanced Land Imager (ALI) imagery to test differences in spatial resolution and spectral bands. In addition, spectral unmixing is conducted to examine if reducing mixed pixel effects in ALI imagery improves prediction of canopy structure. Second, image texture is examined using Quickbird panchromatic data. As a preliminary step, variance is calculated using the grey-level occurrence matrix (GLOM) is used to rapidly examine the effects of image resolution and window size, species composition, and substrate background conditions on the relationship between texture and canopy structure. Seven grey-level co-occurrence matrix (GLCM) image texture statistics are tested based on sub-groups of species composition and background substrate. Results describe the exploratory analysis of SVI and texture metrics and conclude with a suggested parameterized model to predict canopy structure. The results are discussed in terms of previous research and real-world challenges to mapping canopy structure from satellite remote sensing. The paper concludes by describing areas of future remote sensing research for the Galapagos Islands and mangrove forests in general.,

Background

<u>Definitions of Canopy Cover and Leaf Area Index</u>

Fraction Canopy Cover (FCC) and Leaf Area Index (LAI) provide two measures of vegetation canopy structure. FCC is the planimetric faction of the canopy covered with leaves and is often used because it is simple to define and relatively easy to measure using indirect methods. LAI for broadleaf vegetation is the one-sided area of all leaves for a given areal unit (i.e. leaf area (m^2) / ground area (m^2) and provides a more accurate measurement of functioning green elements in the canopy. Due to leaf clumping and overlap, indirect measurement of LAI is more challenging than FCC. Jonckheere et al. (2004) and Weiss et al. (2004) provide a detailed review of *in-situ* LAI theory and methods and conclude that digital hemispherical photography (DHP) offers many advantages to other sensors such as color, *in-situ* and post-processing lighting adjustments, spatially-explicit calculations and the option for automated, semi-automated or manual assessment. The various techniques used to estimate LAI result in different LAI definitions (Zheng and Moskal, 2010). eLAI can be calculated using gap fraction measurements using a hemispherical light sensor (e.g. LiCOR LAI-2000 Plant Canopy Analyzer) or hemispherical photography based on an inversion model of light interception assuming a random distribution of leaf clumping (Baret, 2006). Without direct measurement such a leaf litter traps, tLAI can only be estimated. tLAI can be estimated from eLAI by accounting for the effect non-random of leaf clumping on canopy gaps. The modeling of leaf clumping can be difficult without spatially-explicit measurements of canopy-gap distribution (i.e. DHP). Given measurement constraints, eLAI is more commonly used for ecosystem modeling of evapotrainspiration and primary productivity rather than tLAI. For a more detailed review of LAI definitions and theory, see Zheng and Moskal (2009).

While eLAI is commonly used for ecosystem modeling, it is unknown which description of leaf area, FCC, eLAI, or tLAI, is best suited to characterize mangrove finch habitat. Dvorak et al. (2004) found that fraction canopy cover was a significant characteristic of mangrove finch habitat. Since Dvorak et al. (2004) only used a visual assessment to estimate canopy cover, it is unclear if canopy cover, the amount of light interception (i.e. eLAI) or the amount of green leaf material (i.e. tLAI) best characterizes mangrove finch habitat.

Broadband Spectral Vegetation Indices

Spectral Vegetation Indices (SVI) have a strong tradition in biophysical remote sensing (Boyd and Danson, 2005). The basic theory behind SVI is the existence of a characteristic response between two or more spectral bands that strongly relate to biophysical properties of vegetation (Jordan, 1969). Many commonly used SVI rely on the relationship between red and near-infrared (NIR) reflectance to indicate the relative amount of photosynthetic pigment. Photosynthetically active leaves characteristically absorb red light for photosynthesis and highly reflect NIR light (Tucker, 1979). Other common SVI, such as the normalized difference moisture index (NDMI), utilize shortwave infrared (SWIR) reflectance that is sensitive to other aspects of leaf physiological responses such as water stress (Ceccato et al., 2001) and can be less sensitive to background conditions (Brown et al., 2000).

Despite widespread use, SVI present several challenges for determining LAI including mixed pixel effects, non-linear spectral relationships, and site- or species-specific empirical relationships. While it is possible for SVI to determine LAI in continuous land cover situations, multiple land cover types often occur within a single pixel for high or moderate resolution sensors (i.e. Landsat or MODIS). Thus, the SVI value of a given pixel does not represent a single vegetation component, but other land cover types not necessarily

91

capture by ground-based measurements. Methods to reduce the influence of mixed pixels include attempts to remove the effect of non-vegetation components through spectral unmixing or using SWIR spectral properties to estimate the fraction of vegetation cover (see section 1.3.4). The spectral relationship to leaf area is often non-linear over the full range of LAI, particularly saturation effects at high LAI values (e.g. Turner et al., 1999; Eklundh et al., 2001). Thus non-linear approaches and multiple regression techniques are useful in predicting canopy structure from SVI (e.g. Fassnacht et al., 1997). Finally, the use of SVI to determine LAI largely relies on empirical relationships. The response of SVI to LAI can vary between biomes, vegetation types, and even individual species due to differences in leaf spectral properties and canopy structure (Turner et al., 1999; Boyd and Danson, 2005; Glenn et al., 2005).

Spectral Unimixing

Spectral unmixing estimates the fractional proportion of endmembers within a pixel from the mixed spectral measurements based on each endmember's unique spectral signature as in the following equation:

$$\lambda_{Pixel} = f_1\lambda_1 + f_2\lambda_2 + ... + f_n\lambda_n \qquad \text{(Eq. 1)}$$

where the reflectance value (λ) of a pixel for a given wavelength is the sum of the spectral reflectance of endmembers, 1 to n, weighted by the fraction cover (f). Spectral unmixing can also be applied to SVI using the sub-pixel endmember fractions derived from a spectral unmixing model and replacing the reflectance value with SVI, assuming the non-vegetation SVI are distinct (Brown, 2001). Linear modeling approaches can be used to solve this equation if the spectral signature of each endmember is known (GarciaHaro et al., 1996). Non-linear model approaches can also be used, but are often difficult to solve due to their complex equations. Spectral signatures can be obtained from field collection or from

"pure" pixels in existing imagery using manual approaches such as visual interpretation from very high resolution imagery (e.g. satellite or aerial photography) or automated approaches such as Purity Pixel Index (Boardman et al., 1995).

Since the SVI of the vegetation component of Eq.1 varies depending on vegetation parameters such as leaf area, the contribution of vegetation to the pixel SVI is unknown. Eq. 1 can be solved algebraically to calculate the SVI of vegetation by subtracting the other SVI components from the pixel SVI, assuming all the SVI of the other components are known and consistent across the image (Brown, 2001). Previous studies have shown that this approach greatly improves the relationship between SVI and LAI in mixed pixels of discontinuous forest (Brown, 2001, Sonnentag et al., 2007). This approach has not been applied to mangrove forests.

<u>Image Texture</u>

Image texture describes the spatial pattern and relationship among and between pixels and is controlled by the geometric relationship between objects and pixel resolution (Woodcock and Strahler, 1987). In high resolution imagery, individual tree crowns and canopy gaps consist of multiple pixels, producing spatial-autocorrelation within objects that can be detected using image texture (Woodcock and Strahler, 1987). The panchromatic pattern of bright tree crowns and dark canopy gaps and shadows across a canopy can be used to determine canopy structure attributes such as crown diameter and LAI (Song and Dickinson, 2008).

Image texture can be described using statistical metrics based on the GLOM or GLCM. GLOM measures image texture using all pixel grey-levels in a given window. GLCM measures image texture using all pairs of pixel grey-levels. While only a single parameter, window size, is used with GLOM, three parameters control the selection of GLCM pixel pairs - moving window size, lag distance, and direction. Haralick et al. (1973) describe several first and second order metrics to measure image texture using GLCM (see Table 4.1).

While several studies have used GLCM texture to describe canopy structure and estimate LAI (Wulder et al., 1998, Colombo et al., 2003, Moskal and Franklin 2004, Kayitakire et al., 2006), only one study has been conducted on tropical forests. Kraus et al. (2009) use SVI and GLCM image texture to determine LAI in various stages of tropical forest. They found that only the GLCM image texture could determine LAI for mature forest stands.

The novelty of the image texture approach to determine leaf area is both a challenge and an opportunity. To date, there has not been a peer-reviewed study that has investigated the use of GLCM image texture for determining LAI in mangrove forests. Therefore, the type of statistical metric or the ideal set of parameters to apply is unknown. Specifically, the spatial scale of image texture, in terms of lag distance, image resolution, or window size, is largely untested and previous research provides little guidance. Furthermore, unlike many SVI which have been specifically designed to be insensitive to background conditions (e.g. SAVI, EVI), image texture of panchromatic imagery is likely to be sensitive to differences in background conditions because texture relates differences in intensity and spatial arrangement of canopy and gap pixel reflectance.

Table 4.1: Grey-level co-occurrence matrix statistics (after Haralick et al., 1973). P(i,j) is the proportional frequency of compared pixels with grey-levels i and j.

Statistic	Equation
Homogeneity	$\displaystyle\sum_{i,j=0}^{N-1}\frac{P_{i,j}}{1+(i-j)^2}$
Contrast	$\displaystyle\sum_{i,j=0}^{N-1}P_{(i,j)}*(i-j)^2$
Dissimilarity	$\displaystyle\sum_{i,j=0}^{N-1}P_{(i,j)}*\left|i-j\right|$
Mean	$\displaystyle\sum_{i,j}^{N-1}i*P_{(i,j)}$
Standard Deviation	$\displaystyle\sqrt{\sum_{i,j}^{N-1}P_{(i,j)}*(i-\sum_{i,j}^{N-1}i*P_{(i,j)})^2}$
Correlation	$\displaystyle\sum_{i,j=0}^{N-1}\frac{P_{(i,j)}*(i-\sum_{i,j}^{N-1}i*P_{(i,j)})*(j-\sum_{i,j}^{N-1}j*P_{(i,j)})}{\sqrt{\sum_{i,j}^{N-1}P_{(i,j)}*(i-\sum_{i,j}^{N-1}i*P_{(i,j)})^2)*(\sum_{i,j}^{N-1}P_{(i,j)}*(j-\sum_{i,j}^{N-1}j*P_{(i,j)})}}$
Inverse Difference	$\displaystyle\sum_{i,j=0}^{N-1}\frac{P_{(i,j)}}{\left|i-j\right|^2};i\neq j$

where $\displaystyle\sum_{i,j=0}^{N-1}P_{(i,j)}=1$

Methods

Study Area

The research was conducted near the town of Puerta Villamil on Isabela Island in the Galapagos Archipelago, Ecuador. The Galapagos Islands, located 1000-km off the coast of Ecuador, are an archipelago consisting of 13 large islands, 4 of which have human populations, and 188 small islands and rocks (Figure 4.1). The Galapagos Islands were declared a national park in 1959 (the park consists of 97% of land area), a UNESCO World Heritage Site in 1978, and a UNESCO Biosphere Reserve in 1987. The Galapagos Islands lie on the western edge of the

Atlantic-East Pacific mangrove complex. Mangrove forests consist of three true species common in this region: *Rhizophora mangle* (red), *Avicennia germinans* (black), *and Laguncularia racemosa* (white), and as well as the associate species *Conocarpus erectus* (button or buttonwood mangrove) and *Hippomane mancinella* (manzanillo). In the Galapagos Islands, mangroves form dense, but small patches in protected coves and lagoons along an otherwise barren or arid coast. Mangrove forests in the study site can be described primarily as fringe mangroves, although some forest patches occur along inland brackish lagoons and ponds. Salinity varies greatly across the study site as both fresh water springs and hyper-saline ponds occur in relatively close proximity. Field observations show that while mangrove species form patterns of zonation based on salinity and/or wave action, the mangrove and associate species can co-occur in close proximity.
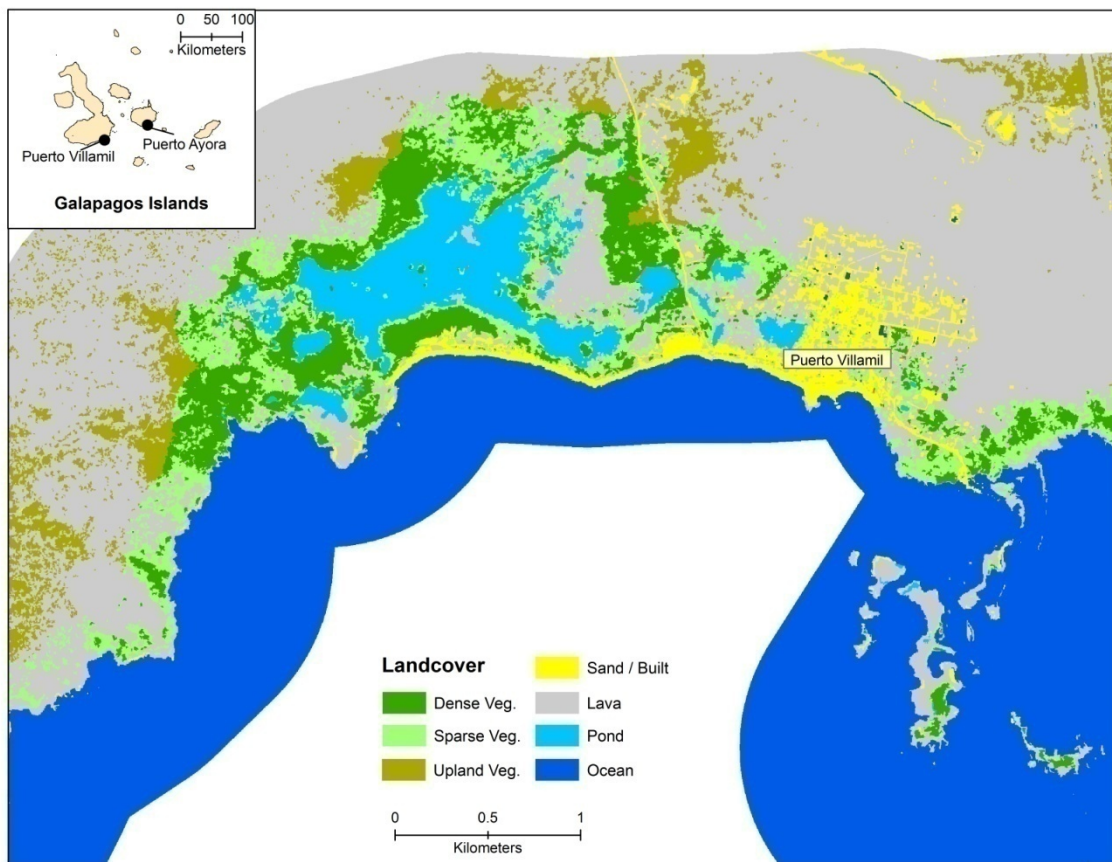
Figure 4.1: Land cover classification of the study area near Puerto Villamil, Galapagos Islands, Ecuador (see Chapter 3)

<u>Field Data and Processing</u>

Field data was collected during summer 2009. Due to conservation policies within the Galapagos National Park, non-destructive sampling was required. Mangroves form stands with dense aerial roots and branches, making many areas inaccessible without destructive measures. An opportunistic sampling scheme was conducted due to logistical constraints. Efforts were made to sample a wide range of leaf area for each species. Digital Hemispherical Photographs (DHP) were taken at the center of 10-meter diameter field plots. A 5 megapixel, Nikon Coolpix 5000 camera and a FC-E8 fisheye lens with equidistant projection were used. Additionally, canopy height, substrate conditions, and mangrove species were recorded at nine points in each plot. Plot location was recorded using a Trimble GeoXT GPS unit and differentially corrected to a 95% horizontal positional accuracy of less than 1.5 meters.

The DHP was used to calculate canopy cover, effective leaf area index (eLAI), and true LAI (tLAI) using the Can-EYE software. Previous studies indicate this software-hardware configuration provides accurate estimates of FCC and LAI in tropical forests (Kraus et al., 2009). Images were subset and cropped to above 65° from the zenith to remove the effects of blurred and mixed pixels at higher zenith angles. Branches and direct sunlight were manually masked to improve the classification of leaf area and canopy gap. Can-EYE software calculates fraction canopy cover as the proportion of non-gap area in the nadir direction from 0° to 10°, the default setting in the Can-EYE software. eLAI was calculated based an inverse light diffusion model look-up-table based on a poisson distribution model of leaf distribution. eLAI was converted into rLAI based on an estimation of non-random leaf clumping from the DHP by the Can-EYE software. The results from the Can-EYE software analysis were linked to the GPS plot locations to link field and remote sensing data.

Figure 4.2 illustrate the distribution of FCC and LAI among species. FCC and LAI were similar among species with the following exceptions: white mangroves had canopy cover well below 50% and red mangrove had a much lower effective LAI range than the other species (see figure 4.2). In terms of canopy height, white mangroves were distinct from the other species. All white mangroves were less than 10 meters in height, while the mean height of red and black mangroves was greater than 10 meters in height and some red mangrove trees exceeded 15 meters. These results illustrate that a wide range of canopy conditions were sampled, but do not suggest any statistically significant differentiation between species based on canopy cover, LAI or height. However, these results are not necessarily representative of the entire study area due to the opportunistic sampling scheme that sought to capture a range of canopy conditions rather than a representative sample.
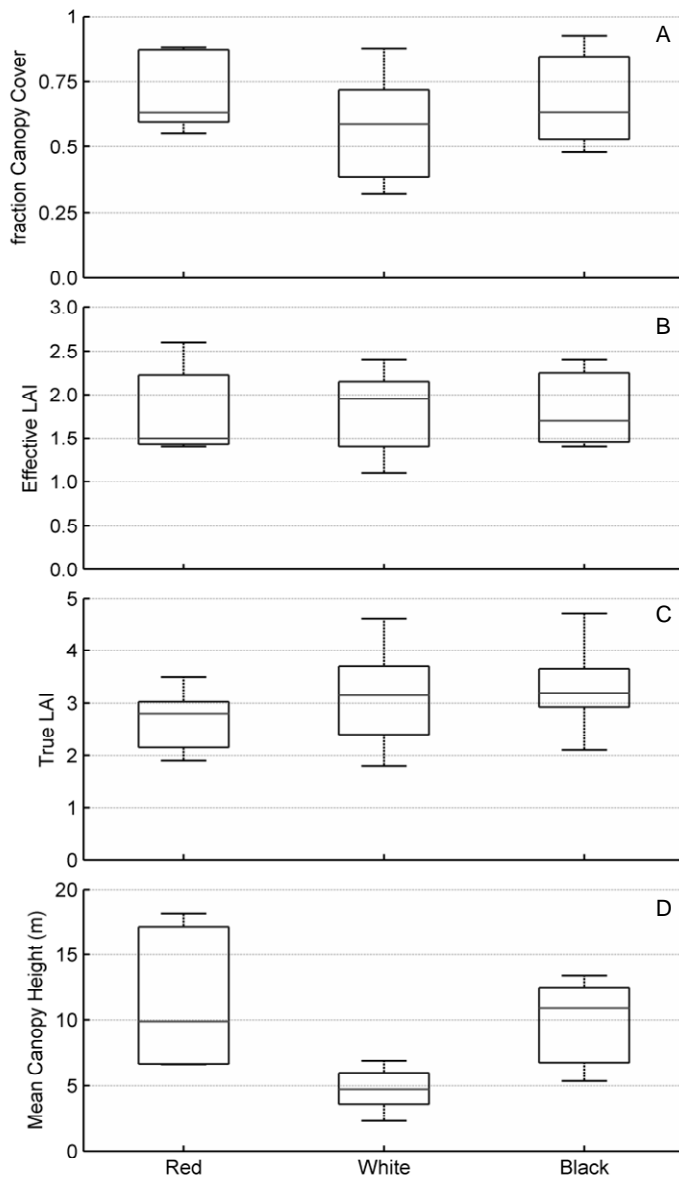
4.2: Boxplot in-situ measured fraction Canopy Cover (A), effecctive LAI (B), true LAI (C), and height (D) by mangrove species

Remote Sensing Data

Details of the remote sensing data are shown in Table 4.2. The Quickbird Standard

Product imagery was geometrically corrected using ENVI RPC with GCP orthogeometric

correction algorithm. The corrected imagery has a Root Mean Square Error (RMSE) of less

than 2-meters based on 16 independent validation GCPs. The RMSE of the Quickbird

imagery is similar to the uncertainty of the differentially corrected GPS points used as GCPs.

The ALI image was geometrically corrected with an RSME less than 15m (i.e. half a pixel) using a 3rd order polynomial based on tiepoints from the corrected Quickbird image. The digital numbers were converted to radiance and atmospherically corrected using a Dark Object Subtraction (DOS) model in ENVI.

Table 4.2: Details of the ALI and Quickbird data

Sensor	Resolution	Bands	Wavelength (nm)	Landsat ETM+ Equivalent
Feb. 24th, 2008				
ALI	30 m	Blue'	433 - 453	
		Blue	450 - 515	x
		Green	525 - 605	x
		Red	630 - 690	x
		NIR	775 - 805	x
		NIR'	845 - 890	
		SWIR'	1200 - 1300	
		SWIR	1550 - 1750	x
		MIR	2080 - 2350	x
Aug. 27th, 2008				
Quickbird	2.4 m	Blue	450 - 520	
		Green	520 - 600	
		Red	630 - 690	
		NIR	760 - 900	
	0.6 m	Panchromatic	450 - 900	

' indidcates ALI specific-band

Spectral Vegetation Indices

Table 4.3 lists the SVI used in this study. The Quickbird SVIs were calculated for 1x1, 3x3, 5x5, and 7x7 pixel windows. The 10 SVI selected for the ALI imagery include the Quickbird SVIs as well as several that incorporate SWIR data or ALI-unique data. Since the ALI imagery has two channels in the NIR and SWIR wavelengths, the SVI were tested using ETM+ equivalent bands and using only the unique ALI bands.

Table 4.3:Spectral vegetation indices for Quickbird and Advanced Land Imager

	Spectreal Vegetation Index	Sensor Specific Equation	Source
QB	Simple Ratio	$SR=[B4]/[B3]$	Jordan, 1969
	Normalized Difference Vegetation Index	$NDVI=\dfrac{([B4]-[B3])}{[B4]+[B3]}$	Rouse et al. 1973
ALI	Simple Ratio (Landsat Equivalent)	$SR=\dfrac{[B7]+[B6]/2}{[B5]+[B4]/2}$	Jordan, 1969
	Simple Ratio' (ALI Unique)	$SR'=[B6]/[B5]$	
	Normalized Difference Vegetation Index (Landsat Equivalent)	$NDVI=\dfrac{[B7]+[B6]/2-[B5+B4]/2}{[B7]+[B6]/2+[B5+B4]/2}$	Rouse et al. 1973
	Normalized Difference Vegetation Index' (ALI Unique)	$NDVI'=\dfrac{[B6]-[B5]}{[B6]+[B5]}$	
	Enhanced Vegetation Index (Landsat Equivalent)	$EVI=2.5*\dfrac{[B7]+[B6]/2-[B5]+[B4]/2}{[B7]+[B6]/2+6*[B5]+[B4]/2-7.5*[B2]+1}$	Huete et al. 2002
	Infrared Simple Ratio (Landsat Equivalent)	$IRSR=\dfrac{[B6]+[B5]}{[B8]}$	Fiorella and Ripple, 1993
	Infrared Simple Ratio' (LAI-Unique)	$IRSR'=[B5]/[B9]$	
	Normalized Difference Moisture Index (Landsat Equivalent)	$NDMI=\dfrac{[B8]-([B7]+[B6])/2}{[B8]+([B7]+[B6])/2}$	Hardisky, 1983
	Normalized Difference Moisture Index' (ALI-Unique)	$NDMI'=\dfrac{[B9]-[B6]}{[B9]+B6}$	

Spectral Unmixing

Linear mixture modeling was conducted in ENVI. Endmembers' spectra were

identified by selecting a minimum of four "pure" pixels in the ALI image using visual

interpretation Quickbird multispectral and panchromatic data. Automated acquisition of

endmember spectra using the Purity Pixel Index (Boardman et al., 1995) did not yield

realistic endmembers as determined by visual assessment of the mapped endmembers. Pure

vegetation pixels were selected based on homogeneous brightness of the false color

composite (i.e. dense vegetation without visible gaps). All ten ALI bands were used to

identify the endmember spectra. Selected endmembers initially included lava, sand,

vegetation, pond, and ocean. Preliminary results using all five endmembers showed

confusion between lava with ocean and sand with pond. In both cases, the water

endmembers were found not to be pure due to the contribution of substrate endmembers

(i.e. sand under the ponds, and lava under the ocean). The endmembers were reduced to

vegetation, lava, and sand. Once the fractional component of each endmember was

calculated, the ALI SVIs were calculated for each pure endmember. The "pure" SVI and

fractional components were used to estimate the vegetation component of SVI using

MATLAB. Mixed and unmixed SVI are compared to test the effect of spectral unmixing.

GLOM Variance

The GLOM variance was used as a preliminary rapid assessment of the potential

effects of image resolution, window size, species and background substrate on the

relationship between image texture and FCC or LAI (after Song and Dickinson, 2008). Since

variance is computed based on grey-level occurrence, i.e. a single statistic based on all pixels,

the computational demand is far less than statistics based on GLCM, a statistic based on the

many pair-wise comparisons. The relationship of variance to canopy cover and LAI was

tested using 19 different image resolution and window size parameter sets.

GLCM Image Texture

Seven image texture metrics were calculated using Quickbird panchromatic imagery

with PCI Geomatica v. 10.3 (see table 4.1). All GLCM texture statistics were calculated using

16 grey levels and a window size of 11 x 11 pixels (~6.6m). The statistics were computed from

GLCM in each direction (i.e. 0°, 45°, 90°, and 135°) and non-zero (i.e. error) values were

averaged across directions to obtain omni-directional values. If zero-values were found in all

four directions, then the data point was removed from further analysis. Four lag distances,

1, 3, 5, and 7 pixels, were tested, producing 28 possible metrics of GLCM texture.

The statistical analysis was conducted using MATLAB. The non-parametric

Spearman's ranked correction (r_s) was used to identify significant relationships without the

stringent assumptions of data normality, linear relationships, or outliers required of a

Pearson's correlation or Ordinary Least-Squares Regression. Due to the coarse spatial

resolution of the ALI data, non-overlapping field plots that fell into the same pixel were

averaged, reducing the sample size at the individual species level such that red and black

mangroves could not be tested individually.

Subsets of the data based on individual species (e.g. red (R), white (W), black (B),

groupings of species (e.g. all vegetation including associate species (AV), all mangroves

including button(AM), true mangroves (TM)), and substrate background were separately

tested (see table 4.4). The best models identified by the Spearman's ranked correlation were

used to create parametric models using OLS. In the case of non-linear relationships, a least-

squares nonlinear curve fitting optimization tool in MATLAB was used to identify the

equation parameters and the r^2 and p-value statistics were calculated.

Table 4.4: Field plots by species and substrate

	Lava	Sand	Leaf Litter	Total
Red	3	6	1	10
White	7	6	1	14
Black	0	1	4	5
Mix*	3	1	2	6
Button	0	3	3	6
Other*	0	1	4	5
Total	13	18	15	46

* mix of 2 or more true mangroves
** other associate species

Results

Spectral Vegetation Indices

       The Quickbird SVI results are shown in table 4.5. NDVI had the strongest

relationship with FCC and eLAI. The strength of the relationship was weak (r_s ~ 0.4 or less)

and similar for all three aggregated species groupings (i.e. AV, AM, TM). The window size

5x5 was consistently among the strongest, although in some cases 3x3 and 7x7 were also

significant. For tLAI, SR with a 3x3 window had the strongest correlation, though the

relationship was still weak (r_s < 0.38). Overall, SVI were not significantly correlated with

FCC, eLAI, or tLAI at the individual species level with the exception of white mangrove eLAI.

For the white mangrove eLAI, SR with a 7x7 window had the highest correlation (r_s = 0.634),

much greater than any other Quickbird SVI result.

Table 4.5: Quickbird SVI correlation results for all vegetation (AV), all mangroves including associates (AM), true mangroves (TM), and white mangroves.

		Canopy Cover					Effective LAI					True LAI		
	r	p	SVI	Window		r	p	SVI	Window		r	p	SVI	Window
AV	0.407	0.0050	NDVI	5x5	**AV**	0.454	0.0017	NDVI	7x7	**AV**	0.355	0.0168	SR	3x3
n = 46	0.401	0.0058	NDVI	3x3	n = 46	0.448	0.0020	NDVI	5x5	n = 46	0.333	0.0256	SR	5x5
	0.397	0.0063	SR	5x5		0.442	0.0024	SR	7x7		0.349	0.0188	SR	7x7
	0.397	0.0064	SR	3x3		0.436	0.0028	NDVI	3x3		0.348	0.0191	NDVI	3x3
	0.387	0.0079	NDVI	7x7		0.429	0.0033	SR	3x3		0.322	0.0307	NDVI	5x5
	0.381	0.0089	SR	7x7		0.421	0.0039	SR	5x5		0.325	0.0295	NDVI	7x7
	0.352	0.0163	SR	1x1		0.354	0.0170	SR	1x1					
	0.352	0.0163	NDVI	1x1		0.354	0.0170	NDVI	1x1	**AM**	0.379	0.0174	SR	3x3
										n = 40	0.351	0.0285	SR	5x5
AM	0.363	0.0215	NDVI	5x5	**AM**	0.387	0.0148	NDVI	7x7		0.362	0.0233	SR	7x7
n = 40	0.352	0.0258	SR	5x5	n = 40	0.379	0.0173	NDVI	5x5		0.367	0.0215	NDVI	3x3
	0.351	0.0264	NDVI	3x3		0.370	0.0203	SR	7x7		0.332	0.0388	NDVI	5x5
	0.346	0.0286	SR	3x3		0.364	0.0228	NDVI	3x3		0.334	0.0374	NDVI	7x7
	0.338	0.0331	NDVI	7x7		0.357	0.0255	SR	3x3					
	0.334	0.0354	SR	7x7		0.349	0.0296	SR	5x5	**TM**	0.350	0.0426	SR	3x3
										n = 35	0.345	0.0454	SR	7x7
TM	0.364	0.0314	NDVI	5x5	**TM**	0.357	0.0380	NDVI	5x5					
n = 35	0.361	0.0333	SR	5x5	n = 35	0.348	0.0436	NDVI	7x7					
	0.346	0.0420	SR	7x7		0.348	0.0437	SR	7x7					
	0.344	0.0433	NDVI	3x3										
	0.342	0.0445	SR	3x3	**White**	0.634	0.0201	SR	7x7					
	0.340	0.0460	NDVI	7x7	n = 13	0.614	0.0255	SR	5x5					
						0.606	0.0281	NDVI	5x5					
						0.579	0.0383	NDVI	3x3					
						0.576	0.0395	NDVI	7x7					

The results of the ALI spectral vegetation indices are shown in table 4.6a. The SWIR indices (i.e. NDWI and IRSR) had the strongest relationships for all three canopy structure parameters at an aggregate species grouping and these relationships were stronger than any of the Quickbird SVI results. Interestingly, when considering only white mangrove data, the SR and EVI were the best SVI. Again, the white mangrove relationships were much stronger than the aggregate species relationships. The ALI-unique SVI did not perform better than the Landsat equivalent SVI.

The spectral unmixed SVI results are shown in table 4.6b. The spectral unmixing improved a few SVI relationships, but most changes were marginal., For FCC, not a single SVI had a significant relationship (p <0.05), despite two significant unmixed SVI. For white mangroves, all of the unmixed SVI had a significant relationship with eLAI and tLAI. However, this improvement was not observed for other species groups. For example, the "all vegetation" group and "true mangrove" group did not have a single significant SVI-eLAI relationship. For "true mangrove", two signification SVI-tLAI relationships were found, but the SVI differ from the unmixed results and the strength of the relationship was weaker.

Due to the coarse resolution of the ALI imagery, some field plots fell into the same pixel and were averaged. The effect of the pooling of plots was also tested with the Quickbird imagery to examine the ALI results were cause by data pooling. Data pooling did not have any substantial effect on the Quickbird data (data not shown).

Table 4.6: Advanced Land Imager SVI correlation results for spectrally mixed (A) and unmixed (B) data. ' indicates ALI-unique SVI (NS = not significant p < 0.05).

Mixed

Canopy Cover

SPP	r	p	SVI
TM	0.551	0.006	NDWI
n = 23	0.551	0.006	IRSR

Effective LAI

SPP	r	p	SVI
AV	0.436	0.014	NDWI
n=31	0.373	0.039	NDWI'
	0.373	0.039	IRSR'
	0.436	0.014	IRSR'
TM	0.490	0.018	NDWI
n = 23			
White	0.829	0.008	SR
n=9	0.829	0.008	SR'
	0.829	0.008	EVI
	0.807	0.011	NDVI
	0.807	0.011	NDVI'

True LAI

SPP	r	p	SVI
TM	0.456	0.029	NDWI
n = 23	-0.456	0.029	IRSR
White	0.833	0.008	SR
n=9	0.833	0.008	SR'
	0.833	0.008	EVI
	0.803	0.012	NDVI
	0.803	0.012	NDVI'

Unmixed

Canopy Cover

SPP	r	p	SVI
		NS	

Effective LAI

SPP	r	p	SVI
White	0.829	0.008	SR
n=9	0.829	0.008	SR'
	0.829	0.008	NDVI
	0.787	0.015	IRSR
	0.778	0.017	NDVI'
	0.778	0.017	EVI
	0.736	0.028	IRSR'
	0.736	0.028	NDWI
	0.736	0.028	NDWI'

True LAI

SPP	r	p	SVI
TM	0.453	0.045	SR'
n = 23	0.451	0.046	SR
White	0.833	0.008	SR
n=9	0.833	0.008	SR'
	0.833	0.008	NDVI
	0.817	0.011	IRSR
	0.767	0.021	NDVI'
	0.767	0.021	EVI
	0.750	0.026	NDWI
	0.733	0.031	IRSR'
	0.733	0.031	NDWI'

Grey-Level Occurrence Matrix Variance

Overall, variance was not significantly related to fraction canopy cover, eLAI, and tLAI at any species grouping. Interestingly, when considering the relationship between variance and eLAI by substrate background, several significant models were found for the lava and leaf litter substrates, but not sand (see table 4.7). Results described here are for the "All Mangrove" species group as the "True Mangrove" group had an insufficient sample size for the leaf litter substrate group.

The results show that canopy structure can be detected at multiple resolutions within a range of window sizes. For lava, there were significant models ($p < 0.05$) across image resolutions (i.e. 0.6m, 1.2m, and 2.4m) and window sizes (5.4m, 9.0m, 8.4m, and 7.2m). Similarly, the variance models for the leaf litter substrate group had significant models at different resolutions (e.g. 1.2m and 1.8m), but at similar window sizes (e.g. 6.0m and 5.4m). The results for tLAI were similar for the lava substrate group although more models were found to be significant and the relationships were stronger, but the leaf litter group did not have any significant relationships (data not shown). The results for FCC were found to be overall not significant (data not shown).

Table 4.7: Results for grey-level occurrence matrix variance for "All Mangroves" eLAI by substrate.

Model	Res. (m)	Win (pix)	Win (m)	All (r)	Lava (r)	Sand (r)	Leaf Litter (r)
1	0.6	3	1.8	0.026	-0.123	0.173	-0.056
2	0.6	5	3	-0.150	-0.363	0.106	-0.397
3	0.6	7	4.2	-0.230	<u>-0.609</u>	0.158	-0.471
4	0.6	9	5.4	<u>-0.289</u>	**-0.702**	0.061	-0.496
5	0.6	11	6.6	-0.207	-0.542	0.201	<u>-0.569</u>
6	0.6	13	7.8	-0.158	<u>-0.603</u>	0.252	-0.559
7	0.6	15	9	-0.155	<u>**-0.788**</u>	0.239	-0.496
8	1.2	3	3.6	-0.112	-0.258	0.106	-0.172
9	1.2	5	6	-0.254	-0.388	0.034	**-0.671**
10	1.2	7	8.4	-0.237	**-0.634**	0.108	<u>-0.524</u>
11	1.2	9	10.8	-0.142	-0.535	0.228	-0.489
12	1.8	3	5.4	**-0.328**	-0.154	-0.054	**-0.591**
13	1.8	5	9	-0.151	<u>-0.591</u>	0.211	-0.422
14	1.8	7	12.6	-0.039	-0.363	0.205	-0.151
15	2.4	3	7.2	-0.208	**-0.677**	0.157	<u>-0.524</u>
16	2.4	5	12	-0.074	-0.406	0.119	-0.105
17	3.0	3	9	-0.126	<u>-0.591</u>	0.192	-0.257
18	3.0	5	15	-0.074	-0.382	0.006	-0.246
19	3.6	3	10.8	-0.010	-0.209	0.173	-0.197
n				40	10	18	12

<u>p-value</u> < 0.1, **p-value** < 0.05, <u>**p-value**</u> < 0.01

Grey-Level Co-Occurrence Matrix

At the aggregate species level, GLCM had weak and insignificant relationships with FCC and LAI, respectively (Table 4.8). However, there were strong significant relationships at the individual species level. While GLCM texture had significant relationships with FCC for red and white mangroves, the relationship with any GLCM texture metric was insignificant for black mangroves (Table 4.8a). However, significant relationships with tLAI were found for all three species (Table 4.8b). The correlation statistic with a lag of 7 pixels was significant for each of the three species, although the relationship was positive for red and white mangroves and negative for black mangroves. The only other significant GLCM statistic was dissimilarity, but only for red mangroves.

Table 4.8: Grey-level co-occurrence matrix results for fraction Canopy Cover by species (A), true LAI by species (B), and fraction Canopy Cover by substrate (C).

A	r_s	p	statistic	lag (pix)	n
ALL	0.426	0.019	Inverse Difference	5	32
AM	0.318	0.046	Homogeneity	3	41
TM	0.584	0.007	Inverse Difference	5	21
	0.39685	0.02222	Homogeneity	2	34
Red	-0.843	0.013	Contrast	1	9
	-0.735	0.047	Contrast	3	9
White	-0.565	0.038	Mean	3	14
Black	Not Significant				5

B	r_s	p	statistic	lag (px)	n
Red	-0.797	0.003	Dissimilarity	7	8
	0.706	0.015	Correlation	7	8
White	0.704	0.005	Correlation	7	14
Black	-1.000	0.017	Correlation	7	5

C	r_s	p	statistic	lag (px)	n
Lava	0.943	0.017	Inverse Difference	5	6
	-0.671	0.024	Contrast	1	11
Sand	0.732	0.007	Correlation	7	13
	-0.711	0.010	Mean	7	13
	-0.599	0.040	Mean	1	13
Leaf Litter	0.803	0.005	Homogeneity	3	10

FCC was the only canopy structure variable with significant models for all three substrate types. The p-value of the best relationships for each substrate was well below the 0.05 threshold (see table 4.8c), although each substrate had a different statistic and lag distance. The strength of the best relationships ranged from moderate for sand (r_s = 0.732) to strong for lava (r_s = 0.943).

<u>Parameterized Model</u>

The goal of the previous analysis was to identify the best metrics and parameters from which to create a parameterized model to predict leaf area in mangrove forests. Since none of the spectral or texture methods had moderate or strong relationships at the aggregate species and substrate level, models based on the individual species or substrate relationships were developed. Only the GLCM texture had moderate to strong relationships for all individual species or substrates. Two composite models have been identified, assuming linear relationships, non-interacting components (e.g. mixed or overlapping species or substrates within the texture window). The first predicts tLAI based on mangrove species texture, the second predicts FCC based on individual substrate texture.

The species model is shown below:

$$tLAI = R * tLAI_R + W * tLAI_W + B * tLAI_B \hspace{2cm} \text{(Eq. 4)}$$

where R, W, and B indicate the species-specific tLAI relationships for red, white, and black mangroves, respectively (see figure 3 a-c). The composite model had an r^2 of 0.6690 and p-value of 0.0342. The strength of the individual species models ranged from $r^2 = 0.46$ to $r^2 = 0.96$.

The composite substrate model is as follows:

$$FCC = LV * FCC_{LV} + SD * FCC_{SD} + LL * FCC_{LL} \hspace{2cm} \text{(Eq. 5)}$$

where LV, SD, and LL, substrate-specific FCC relationships for lava, sand, and leaf litter, respectively (see figure 3 d-f). The composite model had an r^2 of 0.5238 and p-value of 0.0053. The strength of the individual substrate models ranged from $r^2 = 0.45$ to $r^2 = 0.78$. Both the sand and leaf litter substrates had exponential functions. Small changes at low levels of the texture statistic accounted for large changes in LAI, but relatively large changes of the texture statistic were required to predict change at higher LAI values.
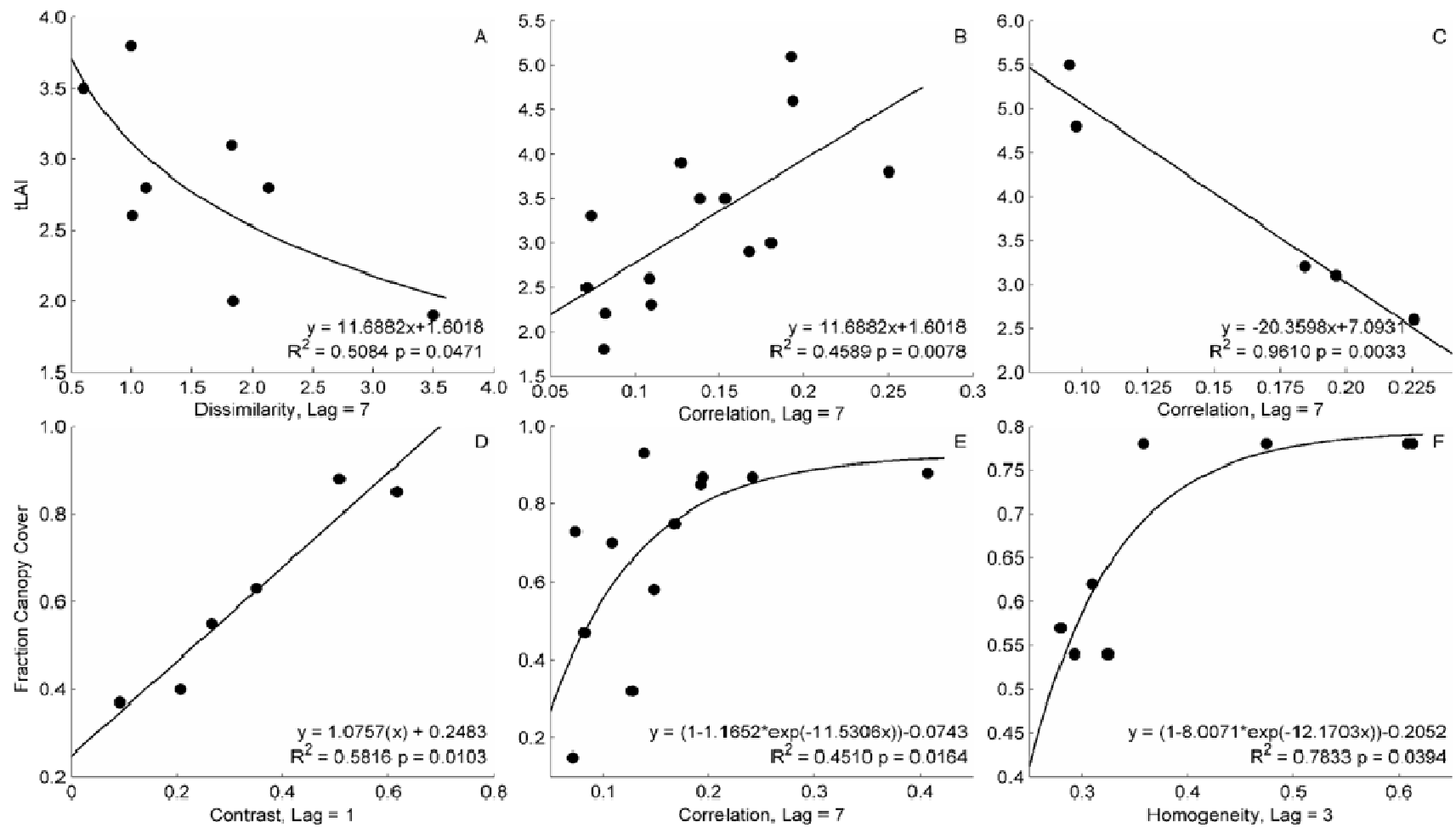
4.3:Scatterplots and OLS regression of true LAI for red (A), white (B), and black mangroves (C) and fraction Canopy Cover for lava (D), sand (E), and leaf litter (F) substrates.

Discussion

<u>Spectral Vegetation Indices</u>

The results have shown that SVIs derived from the Quickbird or Advanced Land Imager sensors did not produce strong relationships with leaf area. These results, specifically the Quickbird results, contrast with findings by Kovacs et al. (2004, 2005, 2009). Although these previous studies have reported strong relationships between SVI using very high resolution imagery such as Quickbird for red, white and black mangroves, here, significant relationships were only found for white mangroves. Differences between this study and previous studies may be due to differences in field methods or inherent difference in mangrove structure due to environmental conditions. Kovacs et al. (2004) used the LAI-2000 instrument to estimate LAI across a degraded mangrove swamp. In this study, we used DHP to estimate LAI along in fringe mangroves that ranged from healthy to degraded. Mangroves can have very different forms and structure based on salinity, nutrients and other factors associated with the hydroperiod (Tomlinson, 1986). For example, Hardisky et al. (1983) found that salinity and growth form can affect remotely sensed radiance in vegetation. The range of environmental conditions in the Galapagos such as lava or sand substrate and freshwater, brackish, or hypersaline lagoons, may produce a greater than the range of conditions than the study site of Kovacs et al., This high variation in environmental conditions may have resulted in greater variation in mangrove structure and spectral properties for this study. Kovacs et al. (2005) found a difference between mangrove species based on LAI, but this study did not find any distinction in LAI between species. Although the field data collected for this study was not collected in a geo-statistically rigorous method due to constraints of working within a protected area, the very similar mean and range of LAI between species demonstrates that mapping of species using LAI would have considerable ambiguity between species in this study area.

The Advanced Land Imager had stronger relationships with canopy structure than Quickbird, despite the order of magnitude difference in spatial resolution. While the Quickbird

sensor has a higher spatial resolution and a relatively high signal to noise ratio (Rangaswamy, 2003), the Advanced Land Imager has a greater spectral range (e.g. SWIR), spectral resolution with 2 blue, NIR and SWIR bands each, and a higher signal to noise ratio than Quickbird (Bicknell et al., 1999). Given the large ratio of root and stem material to green leaves for some mangrove species, it is not surprising that SVI, without SWIR, would perform poorly. As Asner (1998) found, woody stem material can play a significant role in canopy reflectance for canopies with LAI < 5.0 and moreover, the relationship between NIR and SWIR is very different between green and woody plant material., The contribution of the SWIR is clear for the results at the aggregate species level for canopy cover and true LAI, as ALI outperforms Quickbird (see Tables 5 and 6). Other studies have also found that SWIR SVI improves LAI estimates (e.g. Lu et al., 2004). In contrast to Liang et al. (2003), this study did not find an improvement with the ALI-specific band SVI over the Landsat equivalent band SVI. In fact, the ALI-specific band SVI were either comparable or less significant.

One of the disadvantages of the relatively large pixel size of the ALI imagery is mixed pixels, which is particularly problematic in fringe mangroves (Mason et al., 2001). Spectral unmixing is one method to resolve the effects of multiple landcover types by identifying and separating the individual endmember components. Overall, the results of spectral unmixing to improve estimation of FCC, eLAI, and tLAI demonstrated marginal, if any, improvement. The very limited improvement in SVI using spectral unmixing is consistent with the findings of Brown (2001). Non-linear spectral unmixing techniques, such as neural networks or support machine vectors, or incorporating endmember variability, however, may improve results (Bateson et al., 2000) and should be explored in a future study.

The SVI results from both the Quickbird and ALI sensors suggest that there may be a problem with scale in terms of spatial resolution and spectral resolution. Although the ALI SVI outperformed the Quickbird SVI, the spatial resolution of the ALI sensor is not ideal for the fine-scale analysis required for mapping fringe mangroves. Furthermore, the rise of hyperspectral

remote sensing has demonstrated the limitations of broad-band SVI (Twele et al., 2008). Due to the very limited relationships between broadband SVI and mangrove canopy structure, future research should investigate the use of high resolution, hyperspectral imagery to determine canopy structure in mangrove forests.

Image Texture

The results of grey-level occurrence matrix (GLOM) variance revealed two interesting patterns. First, the results indicate that a range of resolutions can be used to detect canopy structure as long as a certain window size is captured. These results are consistent with the findings of Song and Dickinson (2008). However, in this case, the finest resolution, 0.6m had the best results rather than at coarser resolutions as Song and Dickinson found. This suggests that the importance of fine scale pattern for mangroves canopies. Second, the reflectance of the background substrate can have a serious impact on the calculation of image texture. Dark backgrounds such as black lava and leaf litter produce high contrast to relatively bright canopy surface. Bright backgrounds such as white sand produce both an inverse relationship and lower variation between the canopy and gaps and thus reduce the ability to detect canopy structure using variance as a metric. Although the situation of black lava and white sand maybe limited to mangrove forests on volcanic islands, these results have serious implications for forest where background conditions may vary across the study area or over time. For example, inter-tidal conditions could greatly alter the reflectance depending on tidal level.

At the aggregate species level, the GLCM had similar strength relationships as the Advanced Land Imager SVI. However, the GLCM results provided the strongest relationships for individual species and substrates. This suggests that either the canopy structure of the individual species, the brightness of the background substrate, or both play an important role. The superior performance of the GLCM texture compared to SVI in this study agrees with the

findings of Moskal and Franklin (2004), who also found that GLCM texture outperformed SVI once vegetation-type was subset.

When accounting for variations between species or substrate, moderately strong and significant regression models were found. The species model was stronger than the substrate model (r^2 = 0.669 vs. r^2 = 0.5238), but less significant (p = 0.0342 vs. p = 0.0053) due to differences in sample size as only mixed species and mixed substrate plots were excluded from the species and substrate models, respectively. Thus, while the species model accounts for more variance, the substrate model is statistically more confident.

The species-specific tLAI model is more desirable for several reasons. First, tLAI is a better representation of the canopy for ecosystem modeling. Second, although the tLAI model is species-specific, the GLCM parameters are more consistent between species with the same lag distance and the same or very similar statistic. Although the substrate model is significant, the variation in GLCM parameters between substrates is best interpreted as an indication that the substrate can affect GLCM – LAI relationships than as a predictive model.

White and black mangrove tLAI had significant relationships with GLCM with a lag distance of 7 and the correlation statistic. Interestingly, the direction of this relationship was opposite between species. One potential explanation is the relationship between the scale of the analysis (lag distance 7) and scale of canopy gaps for each species. White mangroves in the study area were much smaller than white mangroves in terms of height and crown size. As LAI increase, the distance between canopy gaps increases, assuming a strong positive allometric relationship between LAI and crown diameter. Since the scale of analysis is fixed and the allometric relationship is species-specific, the image texture is capturing a different change in the scale of canopy gap patterns in the white and black mangroves. However, it should be noted that the black mangrove model is based on only 5 data points as this species is uncommon in the study area and further investigation is needed to confirm these results.

Both models have a serious obstacle for predictive mapping. First, they require spatially-explicit *a priori* knowledge of either the mangrove species or substrate. Unlike SVI, the effects of mixing are less certain for image texture metrics since mixtures of species or substrates may alter the window size or type texture metric. Specifically, the opposite direction of the black and white mangrove tLAI models suggests that it would be highly unlikely that texture could be used over mixed canopies. Previous studies have applied Object-Based Image Analysis (OBIA) to map individual species (e.g. Myint et al., 2008), but this approach has not been largely applied to fringe mangrove forests. However, recent research in this study has not been able to accurately distinguish between mangrove species in a fringe environment (Heumann, 2011). Similarly, Exploratory analysis for this paper using linear spectral modeling of Quickbird imagery revealed that lava and sand endmembers could be accurately mapped. Second, they do not account for a mixture or juxtaposition of species or substrates at any given location. This point is particularly concerning for the tLAI models for white and black mangroves. Specifically, both models use the same GLCM metric and lag distance, but the sign of the relationship is opposite. The implications of this for predictive mapping for juxtaposed or mixed species stands are a serious challenge.

Despite the overall good performance of GLCM texture in this study, this approach has several drawbacks or remaining challenges for future studies. First, texture metrics are very sensitive to edge effects including large gaps. In mangrove forests, there is high edge area and gaps due to geomorphic formations from inter-tidal fluvial processes and lava microtopography. This is especially true for fringe mangroves that grow in relatively thin strips along the shore. Second, the potential number of GLCM metrics is very large. There are approximately a dozen possible spatial statistics that can be computed for any window size, with any lag distance smaller than the window size, at a variety of pixel resolutions, in any or all directions. As Kayitakire et al. (2006) note, the selection of the texture metrics, window size, and lag distance are very important when applying GLCM texture to estimate forest biophysical parameters.

117

While it is possible to calculate hundreds or even thousands of different texture metrics, it is computational expensive to compute GLCM statistics.

Furthermore testing large numbers of possible texture metrics presents a serious statistical problem, thereby reducing the confidence of non-random relationships when comparing multiple hypotheses. Common approaches to account for the multiple hypotheses problem adjust the p-value according to the number of hypotheses being compared (e.g. Bonferroni correction), thus requiring much larger sample sizes to obtain significant results. In this study, the number of statistics was reduced based on previous studies, and the window size and resolution were based on the GLOM results. Further research is needed to better understand how the different statistics, window size, lag distance, resolution, and background substrate affect measurements of image texture and how it relates to canopy structure in mangroves and other types of forests.

Conclusions

This study investigated the use of spectral and spatial methods to map leaf area in mangrove forests with remotely sensed data. Results showed that when species or background substrates were not considered individually, both spectral and spatial methods generally had weak and often insignificant relationships with leaf area. For spectral vegetation indices, namely, SR, NDVI, and EVI, strong relationships were found for white mangrove LAI, but not other individual species. SVI derived from Advanced Land Imager that included SWIR outperformed those from Quickbird both for white mangroves and at the aggregate species level. Image texture produced the best models, but texture metrics were sensitive to either individual species or background substrate. Grey-level occurrence matrix (GLOM) variance of Quickbird panchromatic imagery revealed that a range of image resolutions and window sizes to detect canopy structure. Additionally, the differences in substrate background between black lava, white sand, and leaf litter had substantial effects on the measurement of texture. The strongest

relationships for canopy structure were found using grey-level co-occurrence matrix. A model based on GLCM with a lag distance of 7 for individual species explained 66% of true LAI variance. However, these models only accounted for pure species or substrates and the effect of mixed species and substrates on image texture is unknown. Based on this outcome, future research should focus on alternative remote sensing technologies such as hyperspectral and LiDAR.

References

Asner, G. P. (1998) Biophysical and biochemical sources of variability in canopy reflectance. *Remote Sensing of Environment,* 64**,** 234-253.

Baret, F. (2006) Can-Eye output variable description. http://www.avignon.inra.fr/can_eye/Variables_Meaning_CAN_EYE.pdf (last accessed October, 2009).

Bateson, C. A., G. P. Asner & C. A. Wessman (2000) Endmember bundles: A new approach to incorporating endmember variability into spectral mixture analysis. *Ieee Transactions on Geoscience and Remote Sensing,* 38**,** 1083-1094.

Bicknell, W., C. Digenis, S. Forman & D. Lencioni. (1999) EO-1 Advanced Land Imager. MIT Lincoln Laboratory.

Boardman, J. W., F. A. Kruse & R. O. Green. (1995) *Mapping target signatures via partial unmixing of AVIRIS data*. Pasadena, CA.

Boyd, D. S. & F. M. Danson (2005) Satellite remote sensing of forest resources: three decades of research development. *Progress in Physical Geography,* 29**,** 1-26.

Brown, D. G. (2001) A Spectral Unmixing Approach to Leaf Area Index (LAI) Estimation At The Alpine Treeline Ecotone. In *GIS and remote sensing applications in biogeography and ecology,* ed. A. C. Millington, Walsh, Stephen J. and Osborne, Patrick E., 7 - 21. Springer.

Brown, L., J. M. Chen, S. G. Leblanc & J. Cihlar (2000) A shortwave infrared modification to the simple ratio for LAI retrieval in boreal forests: An image and model analysis. *Remote Sensing of Environment,* 71**,** 16-25.

Bruniquel-Pinel, V. & J. P. Gastellu-Etchegorry (1998) Sensitivity of texture of high resolution images of forest to biophysical and acquisition parameters. *Remote Sensing of Environment,* 65**,** 61-85.

Ceccato, P., S. Flasse, S. Tarantola, S. Jacquemoud & J. M. Gregoire (2001) Detecting vegetation leaf water content using reflectance in the optical domain. *Remote Sensing of Environment,* 77**,** 22-33.

Colombo, R., D. Bellingeri, D. Fasolini & C. M. Marino (2003) Retrieval of leaf area index in different vegetation types using high resolution satellite data. Remote Sensing of Environment, 86, 120-131.

Dvorak, M., H. Vargas, B. Fessl & S. Tebbich (2004) On the verge of extinction: a survey of the mangrove finch Cactospiza heliobates and its habitat on the Galapagos Islands. *Oryx,* 38**,** 171.

Eklundh, L., L. Harrie & A. Kuusk (2001) Investigating relationships between Landsat ETM plus sensor data and leaf area index in a boreal conifer forest. *Remote Sensing of Environment,* 78**,** 239-251.

Fassnacht, K. S., S. T. Gower, M. D. MacKenzie, E. V. Nordheim & T. M. Lillesand (1997) Estimating the leaf area index of North Central Wisconsin forests using the Landsat Thematic Mapper. *Remote Sensing of Environment,* 61**,** 229-245.

Fiorella, M. & W. J. Ripple (1993) Determining successional stage of temperate coniferous forests with Landsat satellite data. *Photogrammetric Engineering and Remote Sensing,* 59**,** 239-246.

GarciaHaro, F. J., M. A. Gilabert & J. Melia (1996) Linear spectral mixture modelling to estimate vegetation amount from optical spectral data. *International Journal of Remote Sensing,* 17**,** 3373-3400.

Glenn, E. P., A. R. Huete, P. L. Nagler & S. G. Nelson (2008) Relationship between remotely-sensed vegetation indices, canopy attributes and plant physiological processes: What vegetation indices can and cannot tell us about the landscape. *Sensors,* 8**,** 2136-2160.

Gray, J. (2009) Mapping LAI using image texture and spectral vegetation indices. In *Association of American Geographers Annual Meeting*. Las Vegas, NV.

Haralick, R. M., Shanmuga.K & I. Dinstein (1973) Textural features for image classification. *Ieee Transactions on Systems Man and Cybernetics,* SMC3**,** 610-621.

Hardisky, M., V. Klemas & R. Smart (1983) The influence of soil salinity, growth form, and leaf moisture on the spectral radiance of *Spartina alterniflora* canopies. 49**,** 77-83.

Heumann, B. (2011) Satellite remote sensing of mangrove forests: Recent advances and future opportunities. *Progress in Physical Geography,* 35**,** 87-108.

Hogarth, P. (2007) The Biology of Mangroves and Seagrasses. Oxford University Press.

Huete, A., K. Didan, T. Miura, E. P. Rodriguez, X. Gao & L. G. Ferreira (2002) Overview of the radiometric and biophysical performance of the MODIS vegetation indices. *Remote Sensing of Environment,* 83**,** 195-213.

Jonckheere, I., S. Fleck, K. Nackaerts, B. Muys, P. Coppin, M. Weiss & F. Baret (2004) Review of methods for in situ leaf area index determination - Part I. Theories, sensors and hemispherical photography. *Agricultural and Forest Meteorology,* 121**,** 19-35.

Jordan, C. F. (1969) Derivation of leaf-area index from quality of light on forest floor. *Ecology,* 50**,** 663-&.

Kayitakire, F., C. Hamel & P. Defourny (2006) Retrieving forest structure variables based on image texture analysis and IKONOS-2 imagery. *Remote Sensing of Environment,* 102**,** 390-401.

Kovacs, J. M., F. Flores-Verdugo, J. F. Wang & L. P. Aspden (2004) Estimating leaf area index of a degraded mangrove forest using high spatial resolution satellite data. *Aquatic Botany,* 80**,** 13.

Kovacs, J. M., J. M. L. King, F. F. de Santiago & F. Flores-Verdugo (2009) Evaluating the condition of a mangrove forest of the Mexican Pacific based on an estimated leaf area index mapping approach. *Environmental Monitoring and Assessment,* 157**,** 137-149.

Kovacs, J. M., J. F. Wang & F. Flores-Verdugo (2005) Mapping mangrove leaf area index at the species level using IKONOS and LAI-2000 sensors for the Agua Brava Lagoon, Mexican Pacific. *Estuarine Coastal and Shelf Science,* 62**,** 377.

Kraus, T., M. Schmidt, S. W. Dech & C. Samimi (2009) The potential of optical high resolution data for the assessment of leaf area index in East African rainforest ecosystems. *International Journal of Remote Sensing,* 30**,** 5039-5059.

Liang, S. L., H. L. Fang, M. Kaul, T. G. Van Niel, T. R. McVicar, J. S. Pearlman, C. L. Walthall, C. S. T. Daughtry & K. F. Huemmrich (2003) Estimation and validation of land surface broadband albedos and leaf area index from EO-1 ALI data. *Ieee Transactions on Geoscience and Remote Sensing,* 41**,** 1260-1267.

Lu, D. S., P. Mausel, E. Brondizio & E. Moran (2004) Relationships between forest stand parameters and Landsat TM spectral responses in the Brazilian Amazon Basin. *Forest Ecology and Management,* 198**,** 149-167.

Manson, F. J., N. R. Loneragan, I. M. McLeod & R. A. Kenyon (2001) Assessing techniques for estimating the extent of mangroves: topographic maps, aerial photographs and Landsat TM images. *Marine and Freshwater Research,* 52**,** 787-792.

Moskal, L. M. & S. E. Franklin (2004) Relationship between airborne multispectral image texture and aspen defoliation. *International Journal of Remote Sensing,* 25**,** 2701-2711.

Myint, S. W., C. P. Giri, W. Le, Z. L. Zhu & S. C. Gillette (2008) Identifying mangrove species and their surrounding land use and land cover classes using an object-oriented approach with a lacunarity spatial measure. *Giscience & Remote Sensing,* 45**,** 188-208.

Pu, R., Q. Yu, P. Gong & G. S. Biging (2005) EO-1 Hyperion, ALI and Landsat 7 ETM+ data comparison for estimating forest crown closure and leaf area index. *International Journal of Remote Sensing,* 26**,** 457-474.

Rangaswamy, M. (2003) Quickbird II Two-dimensional On-orbit Modulation Transfer Function Analysis Using Convex Mirror Array. In *Electrical Engineering*. South Dakota State University.

Rouse, J. W. J., R. H. Haas, J. A. Schell & D. W. Deering. (1973) Monitoring vegetation systems in the Great Plains with ERTS. In *Third ERTS Symposium*, 309–317. Washington D.C.: NASA.

Song, C. & M. B. Dickinson (2008) Extracting forest canopy structure from spatial information of high resolution optical imagery: tree crown size versus leaf area index. *International Journal of Remote Sensing,* 29**,** 5605-5622.

Sonnentag, O., J. M. Chen, D. A. Roberts, J. Talbot, K. Q. Halligan & A. Govind (2007) Mapping tree and shrub leaf area indices in an ombrotrophic peatland through multiple endmember spectral unmixing. *Remote Sensing of Environment,* 109**,** 342-360.

Tomlinson, P. B. (1986) *The botany of mangroves*. Cambridge Cambridgeshire; New York: Cambridge University Press.

Tucker, C. J. (1979) Red and photographic infrared linear combination for monitoring vegetation. *Remote Sensing of Environment,* 8**,** 127-150.

Turner, D. P., W. B. Cohen, R. E. Kennedy, K. S. Fassnacht & J. M. Briggs (1999) Relationships between leaf area index and Landsat TM spectral vegetation indices across three temperate zone sites. *Remote Sensing of Environment,* 70**,** 52-68.

Twele, A., S. Erasmi & M. Kappas (2008) Spatially explicit estimation of leaf area index using EO-1 hyperion and landsat ETM+ data: Implications of spectral bandwidth and shortwave infrared data on prediction accuracy in a tropical montane environment. *Giscience & Remote Sensing,* 45**,** 229-248.

Weiss, M., F. Baret, G. J. Smith, I. Jonckheere & P. Coppin (2004) Review of methods for in situ leaf area index (LAI) determination Part II. Estimation of LAI, errors and sampling. *Agricultural and Forest Meteorology,* 121**,** 37-53.

Woodcock, C. E. & A. H. Strahler (1987) The factor of scale in remote sensing. *Remote Sensing of Environment,* 21**,** 311-332.

Wulder, M. A., E. F. LeDrew, S. E. Franklin & M. B. Lavigne (1998) Aerial image texture information in the estimation of northern deciduous and mixed wood forest leaf area index (LAI). *Remote Sensing of Environment,* 64**,** 64-76.

Zheng, G. & L. M. Moskal (2009) Retrieving Leaf Area Index (LAI) Using Remote Sensing: Theories, Methods and Sensors. *Sensors,* 9**,** 2719-2745.

Chapter 5 : Mapping Mangrove Canopy Height: A Comparison of Space-based InSAR and Stereo

Optical Products

Abstract

Canopy height is an important structural parameter for monitoring ecosystem goods and services such as timber, standing biomass, and habitat. This paper compares globally available space-based InSAR (SRTM) and stereo optical (ASTER GDEM) imagery to a digital surface model created from ALOS PRISM for estimating canopy height in mangrove forests. This paper emphasizes the challenges of mapping canopy height for mangroves with small extents such as fringe mangroves. The results show that SRTM, PRISM, and a hybrid SRTM-PRISM DSM has RMSE of 3.47m, 3.74m, and 2.92m, respectively. These results have greater error than previous mangrove studies using 90-meter SRTM data, but similar to IceSAT/GLAS estimates of canopy height of terrestrial forests. This approach demonstrates the potential for mangrove canopy height mapping and monitoring using ALOS PRISM but highlights the need for very high resolution InSAR DSM products

Introduction

Mangroves are woody halophytes (i.e. salt tolerant plants) that grow in tropical and subtropical areas and form inter-tidal ecosystems that link terrestrial and marine systems. Mangroves provide valuable ecosystem goods and services such as timber and fuel, carbon sequestration, habitat for terrestrial and marine fauna including economically important fisheries, and a potential reduction in the impact of tsunami and storm surge (Alongi 2002, 2008). Costanza et al. (1997) estimated that mangroves are worth about $10,000 per hectare per year in terms of ecosystem goods and services. Despite their demonstrated value, the extent of mangrove forests declined by 25% between 1980 and 2000 (Wilkie and Fortuna, 2003) and a recent remote sensing study found calculated global mangrove area to be 12.3% less than recent Food and Agriculture Organization estimates. While extent is an important aspect of monitoring mangroves, other parameters such as canopy height are also critical., Canopy height is an important parameter for characterizing forest structure (Shugart et al., 2010), estimating

standing biomass (Wulder et al., 2008), and describing habitat (Bradbury et al., 2005). Thus mapping and monitoring canopy height is of great importance to a wide range of science questions and applications from forest ecology, to biogeochemistry, to conservation.

At the landscape scale, measuring and predicting canopy height requires remote sensing. Mangrove canopy height has been primarily mapped using SRTM - Shuttle Radar Topographic Mission (Simard et al., 2006, Simard et al., 2008; Fatoyinbo et al., 2008). However, the coarse 90-meter spatial resolution of this product outside of the United States makes it generally unsuitable for all but large, continuous mangrove forests. In many parts of the world, especially in arid environments such as the Galapagos Islands, mangroves form small patches along the fringe of protected coves and lagoons. Despite their limited extent, these mangrove are important ecosystems that link terrestrial and marine systems. The objective of this study is to examine the potential of finer resolution stereo optical elevation products with SRTM for mapping small extent fringe and basin mangroves.

Background

There are a number of indirect and direct methods to estimate canopy height from remote sensing. Indirect methods rely on empirical relationships between canopy height, or highly correlated proxy structural parameters such as leaf area index (LAI) or above ground biomass, and optical multispectral (Helmer et al., 2010) or hyperspectral (Lefsky et al., 2001; White et al., 2010), synthetic aperture radar (SAR) signal backscatter (e.g. Hyyppa et al., 2000, Woodhouse, 2006), or image texture (e.g. Bruniquel-Pinel et al., 1998). There are three basic types of direct methods - stereo imagery from passive or active sensors, SAR interferometry (InSAR), and LiDAR. Each of these approaches has advantages and disadvantages (Table 5.1). Each of these methods seeks to create a digital surface model (DSM) or digital elevation model (DEM). A DSM is a representation of the earth's surface including non-terrain features such as

vegetation and buildings, where a DEM is a representation primarily of the bare earth surface. This study is primarily concerned with DSMs.

Table 0.1: Advantages and Disadvantages of Digital Surface Model Techniques

Technique	Advantages	Disadvantages
Stereo Optical/SAR	High to Very High Resolution	Accuracy limited by base-height ratio and image resolution
	Detailed orbital information	Optical affected by cloud cover
	Standardized Radiometric Correction	SAR backscatter can be sensitive to canopy volume, understory, and soil conditions over space and time
	SAR not affected by cloud cover	High accuracy for vegetation requires good GCPs
	Software for automated DSM extraction widely available	
InSAR	Moderate to Very High Resolution	Very complex processing
	Sub-Centimeter Accuracy (Terrain)	Requires special training and software
		For vegetation, requires multi base-pair acquisitions
		Accuracy for canopy height dependent on signal coherence
		Global products limited to moderate resolution
LiDAR	Variable Footprint Size or Posting Distance	Limited extent (airborne and satellite)
	Sub-Centimeter Accuracy (Terrain)	Affected by cloud cover

The use of stereo imagery has a long tradition in remote sensing. For decades, stereo photogrammetry has been the primary method of mapping terrain and forest stands. Elevation is estimated through manual interpretation of the parallax displacement of terrain features from overlapping pairs of inline aerial photographs (Lillesand and Kiefer, 1987). Digital stereo air photos are still widely used method for estimating forest stand parameters such as canopy height (e.g. Lucas et al., 2002; Mitchell et al., 2007; Vega and St-Onge, 2008). The extracted elevation accuracy is determined by the base to height ratio of the stereo image pair and the resolution or grain size of the image, assuming perfect orthorectification. However, aerial

photography has many constraints including variable image brightness, considerable pre-processing and processing to orthorectify and moasic photographs, and limited extent of airborne coverage. Satellite remote sensing offers a means to obtain consistent and repeatable imagery over large areas. DSMs can be extracted from any satellite imagery where two images overlap and the sensor geometry is known. A wide range of satellite optical remote sensing systems have been used to create DSMs including AVHRR (Saraf et al., 2005), Landsat ETM+ (Toutin 2002b), IKONOS (Toutin 2004), ASTER (Toutin 2002a,2008), and ALOS PRISM (Takaku and Tadono, 2009). DSMs can also be generated from stereo pairs of SAR imagery (Toutin 2000; Peng et al., 2005; d'Ozouville et al., 2008).

SAR can also be used to calculate elevation using interferometry. InSAR is similar to stereo methods in that two overlapping images from different locations, called base pairs, are needed. However, instead of comparing difference in image geometry between images, InSAR compares the return signal phase between base pairs for the same target. For a detailed description of InSAR concepts, see Rott (2009). Since InSAR analyzes the phase of the SAR signal, InSAR can have sub-centimeter accuracy and it commonly used for geological deformation studies. However, the application of InSAR can be more difficult for vegetation applications since the SAR signal can scatter in the canopy resulting in low coherence. This challenge can be overcome by using multiple base pairs. For example, Simard et al. (2006) found the interferometric center from multiple base pairs could be used to estimate canopy height. Previous studies have found that the SRTM phase center lies between 1 and 6 meter below the top of the canopy surface (Kellndorfer et al., 2004; Simard et al., 2006). Currently, there are a number of satellite SAR missions suitable for InSAR including ALOS PALSAR, Enivsat ASAR, RADARSAT-2, and TerraSAR-X. The obvious challenge to InSAR is the very technical nature of InSAR processing that is beyond typical remote sensing training and software and is thus available at a very limited number of research institutions or commercial vendors.

Another form of active remote sensing is LiDAR. LiDAR calculates the distance of an object from the sensor by measuring the time it takes for a light pulse to be sent from the sensor, reflect off the object, and return. Height is then calculated based on sensor elevation and pulse geometry. There are two forms of LiDAR - discrete return and waveform. Discrete return LiDAR measures the distance for each pulse, usually over a small footprint size. Small-footprint discrete LiDAR is most suitable for terrain modeling or to delineate urban features. Waveform LiDAR analyzes proportional timing of the light pulse over the entire pulse footprint and thus provides a more detailed distribution of heights over the footprint that is particularly useful for vegetation studies. For a more detailed examination of LiDAR for DEM or forestry applications, see Liu, (2008) or Wulder et al. (2008), respectively.

While airborne LiDAR is now commonly used, to date there is only one satellite LiDAR sensor - IceSAT/GLAS. IceSAT/GLAS was designed to track changes in glacier and icesheets but like SRTM, have been adapted for vegetation analysis. IceSAT/GLAS has been shown to accurately describe mangrove canopy height (Simard et al., 2008). However, the ability for global continuous LiDAR coverage is still unavailable.

One of the major challenges to mapping canopy height using direct methods, is subtracting the elevation of the canopy from the ground elevation. Both stereo and InSAR methods cannot detect the ground surface where there is vegetation cover. As Hyde et al. (2006) found, estimation of the ground surface using interpolated DEM products can introduce serious error. Thus, accurate mapping of canopy height for terrestrial forests requires LiDAR (St-Onge et al., 2008). However, mangroves grow by definition in the inter-tidal zone. As long at the tidal range is relatively small, the base elevation of mangroves can be assumed to be at mean sea level (Simard et al., 2006). Yet, despite this simplification for mapping mangrove canopy height, relatively few studies have addressed this topic (Heumann, 2011). Lucas et al. (2002) and Mitchell et al. (2007) both used stereo aerial photography to estimate ground elevation and canopy height with relatively good reported success, although an overall accuracy statistic was

not reported. Though airborne remote sensing data are not suitable for global assessments due to limited areal extent, this approach demonstrates the potential for satellite-based stereo optical techniques.

The first space-borne approach estimated mangrove canopy height using the SRTM (Simard et al., 2006). The SRTM DSM was produced using C-band synthetic aperture radar interferometry (InSAR) to provide a global snapshot of surface elevation. The SRTM DSM was calibrated using airborne waveform LiDAR and field data. To calculate canopy height, it was assumed that the inter-tidal mangroves had a ground elevation of mean sea level. Simard et al. (2006) found that the SRTM could predict canopy height with a root mean square error (RSME) of 2.0m over the 30m pixel. Simard et al. (2008) applied a similar methodology using field data to calibrate SRTM canopy height. They found that despite the 90m pixel, canopy height could be estimated with a RMSE of 1.9m. Furthermore, they demonstrated that the IceSAT/GLAS waveform LiDAR could be used to calibrate SRTM, providing a global methodology for mangrove canopy height mapping. This approach was applied to mapping canopy height and biomass for all of Mozambique (Fatoyinbo et al., 2008).

While the SRTM approach provides the first globally available technique for mapping mangrove canopy height, there are some limitations. First, the 90m pixel is suitable only for large scale studies across continuous, dense canopy mangrove forests. In fact, Simard et al. (2006) found substantially lower correlations between SRTM and field data over short and sparse canopies. In locations with fringe mangroves where forest patches may be less than 100m wide, the 90-meter spatial resolution of the SRTM DSM is insufficient. Second, the SRTM was a single mission to create a global digital elevation model in the year 2000. This product is now a decade old, making it difficult to link to contemporary field data. Furthermore, this single mission was not design for repeat collection, hindering monitoring applications. While other SAR data suitable for vegetation InSAR are available (e.g. RADARSAT-2, ALOS PALSAR, TerraSAR-X), the processing requirements for InSAR are very complicated and requires

specialized training and software beyond typical remote sensing and image analysis capacity of most universities or geo-spatial companies.

This study compares the 90m SRTM DSM product with two stereo optical products – the 30m Global ASTER (Advanced Spaceborne Thermal Emission and Reflection Radiometer) DSM and a 5m ALOS PRISM DSM. The objective is to identify a suitable space-based DSM product that can be used to map mangrove canopy height, particularly for fringe mangroves, at a finer resolution and accuracy than SRTM with the potential for global coverage. Additionally, several different techniques to generate ALOS (Advanced Land Observing Satellite) PRISM (The Panchromatic Remote-sensing Instrument for Stereo Mapping) DSM are tested as well as a hybrid SRTM-PRISM DSM.

Methods

<u>Study Area</u>

The research was conducted on Isabela Island in the Galapagos Archipelago, Ecuador. The Galapagos Islands, located 1000-km off the coast of Ecuador, are an archipelago consisting of 13 large islands, 4 of which have human populations, and 188 small islands and rocks (Figure 5.1). The Galapagos Islands were declared a national park in 1959 (the park consists of 97% of land area), a UNESCO World Heritage Site in 1978, and a UNESCO Biosphere Reserve in 1987. The Galapagos Islands lie on the western edge of the Atlantic-East Pacific mangrove complex. Mangrove forests consist of three true species common in this region: *Rhizophora mangle* (red), *Avicennia germinans* (black), *and Laguncularia racemosa* (white), and as well as the associate species such as *Conocarpus erectus* (button or buttonwood mangrove) and *Hippomane mancinella* (manzanillo), or other halophytes growing on nearby sand flats or dunes (Van der Werff and Andsersen, 1993). In the Galapagos Islands, mangrove forest form dense, but small patches in protected coves and lagoons along an otherwise barren or arid coast. Mangrove forests in the study site can be described primarily as fringe mangroves forming along the coastline or basin mangroves along hyper-saline lagoons.

Mangroves grow on a range of substrates from aa lava to sand or silty-clay. Mangrove canopy height is primarily short except for a few small areas with fresh water springs were trees can reach over a 1m in diameter and 20 m in height. For a more detailed description of the arid coastal environment in the Galapagos Islands, see Van der Werff and Andersen (1993).
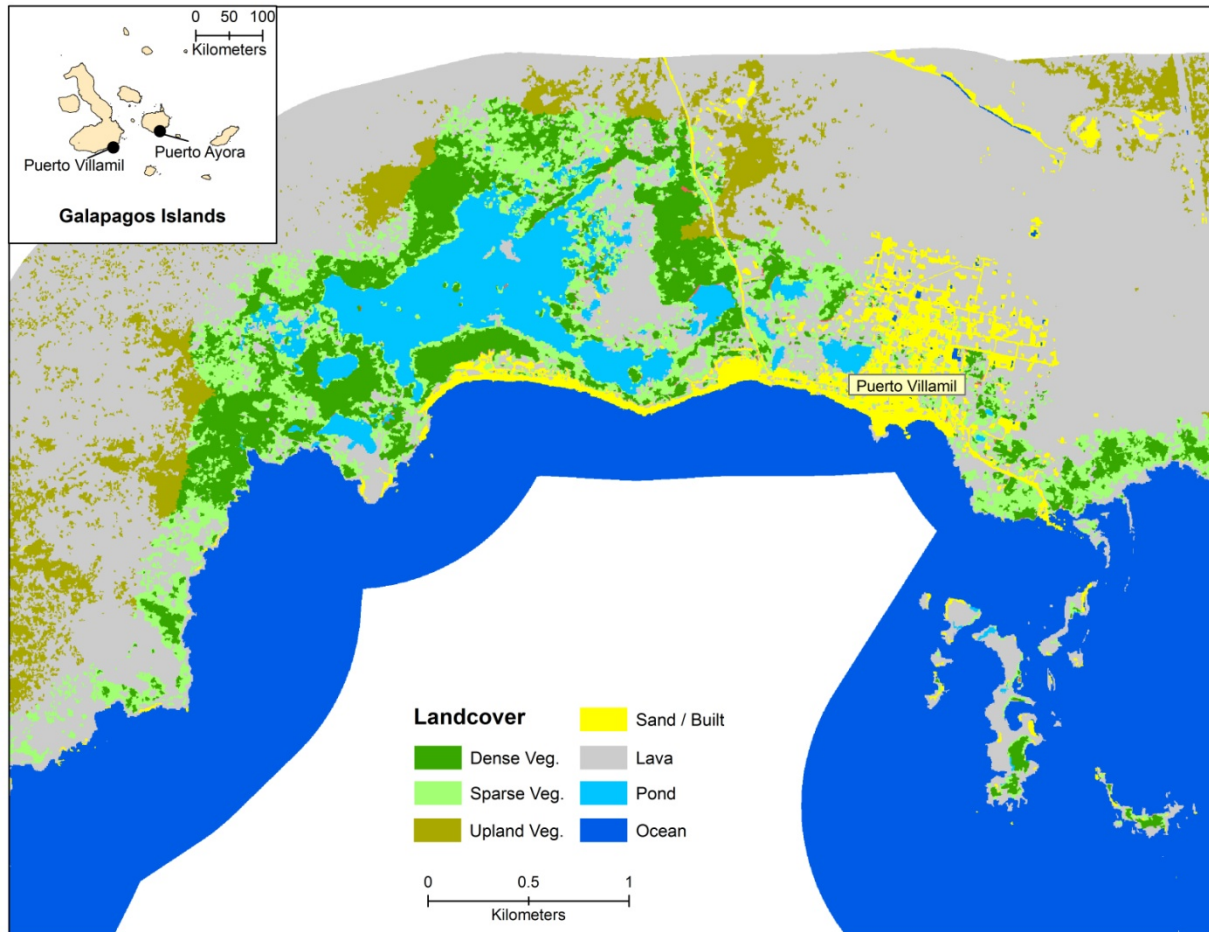

Figure 0.1: Land cover classification of the study area near Puerto Villamil on Isabela Island (see Chapter 3).

Field Data

Field data were collected during the summer of 2009 near the village of Puerta Villamil on Isabela Island. Non-destructive sampling was required in the Galapagos National Park, including the removal of vegetation to access the interior of mangroves. Due to these access restrictions imposed by the Park, only 35 field plots were sampled. Due to the difficulty and

limitations of establishing field plots within mangroves, an additional 461 point measurements of species and canopy height, representing 2-m diameter areas were taken. This paper uses this point dataset because of its larger sample size and areal coverage. Figure 5.2 shows the distribution of species and canopy heights of the field data. Canopy height was measured using an Optilogic ® laser range finder. Height locations were linked to a differentially corrected GPS location (95% confidence < 1.5m) using the laser range finder and a field compass. A maximum distance of 100m was established to reduce location error from the precision of the compass reading (1 degree). The height of the observer was referenced to mean sea-level for all measurements and thus all canopy height values are height above mean sea level.
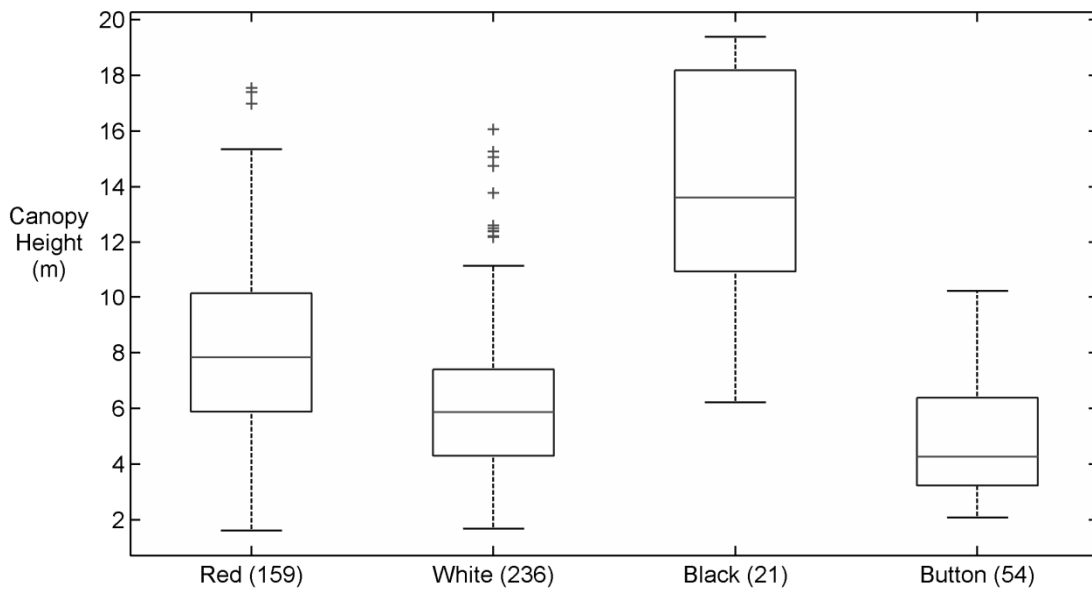
Figure 0.2: Boxplot of canopy height (m) by species (number of sample point in parenthesis).

Base Digital Elevation Model

A base DEM was purchased from the Instituto Geografico Militar (IGM) of Ecuador. This 1:24,000 DEM was generated using true color stereo air photos collected in 2007. The DEM has a contour interval of 10m. A continuous DEM with a 10m resolution was created by

133

interpolating the contour intervals in ArcGIS 9.3 using the Spatial Analyst TopoToRaster tool. In addition to the DEM, urban and natural features were digitized from the orthophotos.

Remote Sensing Data

Land Cover Classification

Land cover was classified using a hybrid decision-tree / support vector machine in an object-based image analysis environment using Quickbird and Worldview-2 imagery. The classification included lava, sand, pond, ocean, upland vegetation, sparse coastal vegetation, true mangroves, and mangrove associates, as well as cloud affected pixels. The image was segmented using e-Cognition 8.1 with shape, compactness, and scale parameters of 0.5, 0.5, and 25, respectively. Coastal vegetation objects were classified using the following rules: 1) simple ratio (NIR/Red) > 3.5 and 2) distance from water < 250m. The accuracy of this classification was greater than 85% for red, black, and buttonwood mangroves. However, 40% of white mangroves were classified as non-vegetation, likely due to sparse vegetation conditions in many locations. Details of the land cover classification are described in Chapter 4.

SRTM

The STRM DEM version 2 is a 90-meter InSAR product produced by the NASA Jet Propulsion Laboratory. The SRTM product was created using several sets of base pairs to estimate surface elevation. The overall accuracy of the SRTM product for terrain was found to be less than 10m (90% height error) for all continents (Rodriguez et al., 2005). Although the radar signal scatters in the vegetation canopy, the interferometric center from multiple base pairs can be used to estimate canopy height (Simard et al., 2006). Previous studies have found that the SRTM phase center lies between 1 and 6 meter below the top of the canopy surface (Kellndorfer et al., 2004; Simard et al., 2006). For a detailed description of InSAR concepts, see Richards (2007).

ASTER GDEM

The Advanced Spaceborne Thermal Emission and Reflection Radiometer Global Digital Elevation (ASTER GDEM) is a 30-meter stereo optical product produced by the Ministry of Economy, Trade and Industry (METI) of Japan and the United States National Aeronautics and Space Administration (NASA). The GDEM was produced from 1.5 million stereo pairs collected by the ASTER sensor. The overall accuracy of the ASTER GDEM is 20m (95% confidence) although the accuracy may be worse in some areas (ASTER GDEM Validation Team, 2009). To date, the ASTER GDEM has not been applied to canopy height.

ALOS PRISM DSM Extraction

The Advanced Land Observation Satellite (ALOS) Panchromatic Remote-sensing Instrument for Stereo Mapping (PRISM) is a 2.5 meter panchromatic radiometer that produces triplet sets of forward, nadir, and backward images (+/- 1.5 degrees). Though PRISM data is widely available, to date, a global or regional DSM product from ALOS PRISM is not available. Five triplet sets of ALOS PRISM images was obtained from the Alaska Satellite Facility for January 17th, 2008, April 18th, 2008, and September 17th, 2007 to cover the entire study area. This paper focuses on a single triplet set that covers the study area and field data (see figure 5.1).

The DSMs were extracted using PCI Geomatica 10.2 Orthoengine using Toutin's model (Toutin, 2006). Toutin's model is a 3-dimensional physical model used to process imagery for orthorectification or the creation of epipolar images for DSM extraction. Toutin (2006) reported that the Toutin's model was equivalent or better than IKONOS or Quickbird rational function models (RFM) for DSM extraction over forest, urban, and bare surfaces. Although a RFM is available for ALOS PRISM, the RFM is not available from the Alaska Satellite Facility, necessitating the use of the Toutin's model. The processing steps for DSM extraction include selection of ground control points (GCP) and tiepoints between images, image

orthorectification, creation of epipolar image pairs, extraction of the DSM, and post-extraction processing (e.g. filtering, merging, error removal).

GCPs were gathered from differentially corrected GPS locations (90% confidence interval < 1.5m) collected during previous field campaigns (2007 - 2009) and surface features digitized from orthophotos by IGM obtained as part of the IGM DEM data. Elevation values for GCPs not at the coast were extracted from the IGM DEM. The horizontal positional RMSE of control and check points was less than 0.7 pixels for all images. Processing must be computed for the entire raw scene and cannot be subset to a small study area (e.g. coastal areas) or edited (e.g. cloud removal). The triplet set of images allows for three DSM to be computed as well as a correlation score for each pixel. The final DSM is a composite of the three DSMs using the value with the highest correlation score for each pixel and averaged to a 5m horizontal resolution. Errors created during the automated DSM extraction process as well as unrealistic values caused by isolated clouds and cloud shadow were removed post-extraction.

Three PRISM DSM products were generated. The first product, PRISM-B, was created using 8 bare-ground GCPs. The second product, PRISM-CH, was created using 11 bare ground GCPs and 9 additional canopy height GCPs. The third product, PRISM-OBIA, was created by taking the average PRISM-CH value for each coastal vegetation object polygon, both dense and sparse, created from the OBIA land cover classification (see Chapter 3). The RMSE of the PRISM-CH compared to the IGM elevation data was 8.07 meters based on 927 elevation points.

Hybrid DSM

A hybrid DSM was created using the SRTM and PRISM-CH datasets. The two DSMs were merged by minimizing the RMSE using the following equation:

$$H = x * SRTM + (1 - x) * PRISM \qquad\qquad\qquad (eq.\ 1)$$

The equation was solved iteratively using intervals of 0.01 for x = 0-1. A similar approach was used by d'Ozouville et al. (2008) to improve their stereo SAR DEM on Santa Cruz Island, Galapagos.

DSM Calibration and Analysis

Calibration and analysis of data was conducted using MATLAB. DSM and field data were geographically linked and extracted using ArcGIS 9.3. Each DSM was compared and calibrated using the field data. Systematic errors were removed using a simple linear 1:1 model, finding the offset that minimized the RMSE. The offset added to the SRTM and the PRISM DSMs was +0.5m and +3.1m, respectively.

Results and Discussion

Figure 5.3 illustrates the relationship between the observed and predicted canopy height. Figure 5.4 maps each of the DSM products. The RMSE of the SRTM was 3.47 meters. The coarse spatial resolution of the SRTM data manifests itself in two ways as observed in figure 5.3(A). First, there was considerable range of observed canopy height for any given SRTM value. Second, the upper range of canopy height (greater than 15m) appears to be omitted from the SRTM data. This demonstrates the loss of sub-pixel variability in canopy height, especially tall trees that are a minority the of overall canopy. While previous studies have used the SRTM DSM for mangrove canopy height, the scale of those analyses were much larger than this study (e.g. country-wide) and for largely estuarine mangroves and not specifically fringe mangroves (Fatoyinbo et al., 2008).
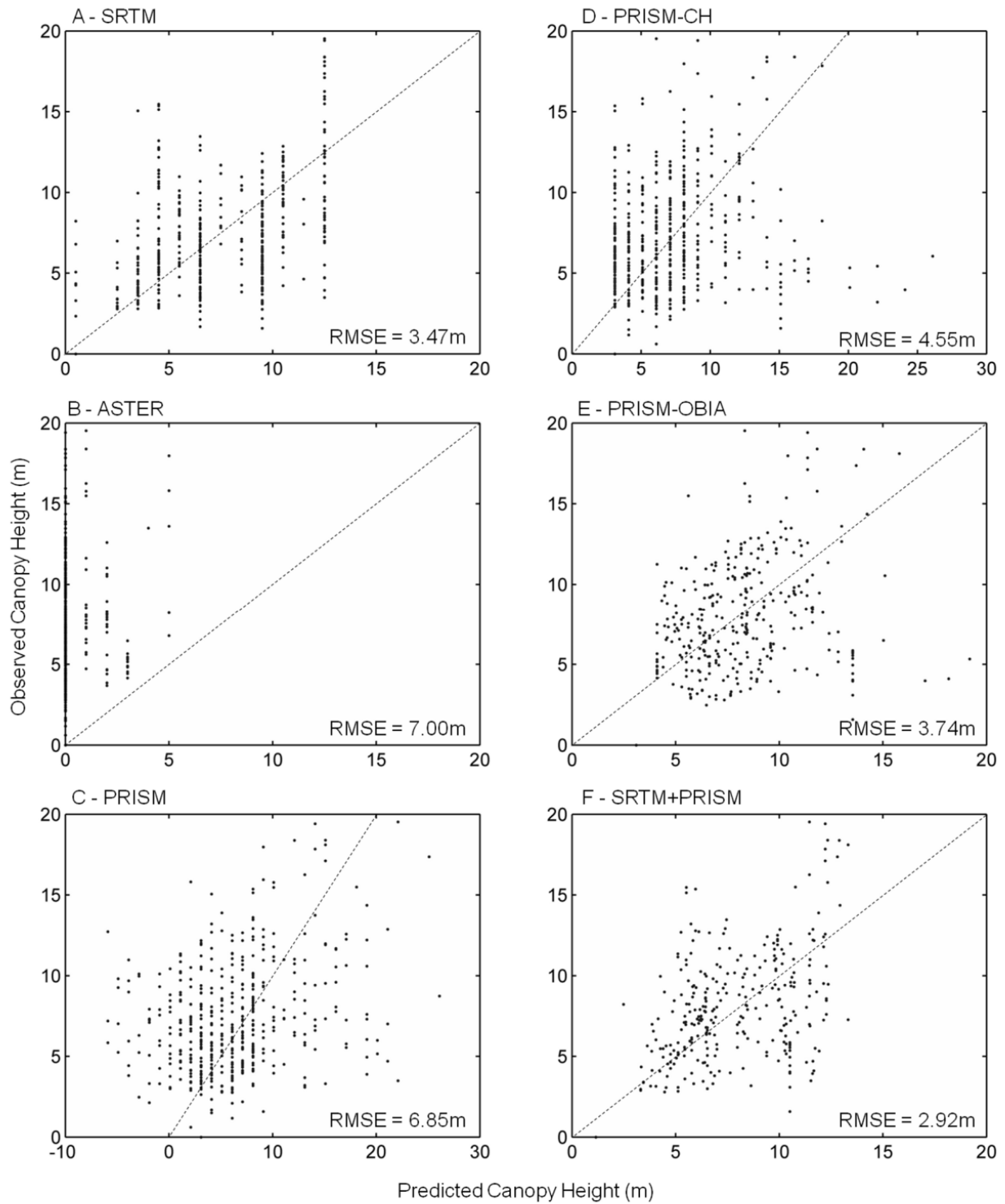
Figure 0.3: Scatterplots of observed canopy height (y-axis) and predicted canopy height (x-axis) for SRTM (A), ASTER GDEM (B) , PRISM with only bare ground GCP (C), PRISM with canopy height GCP (D), PRISM using OBIA objects (E), and hybird SRTM-PRISM DSM (F).

138
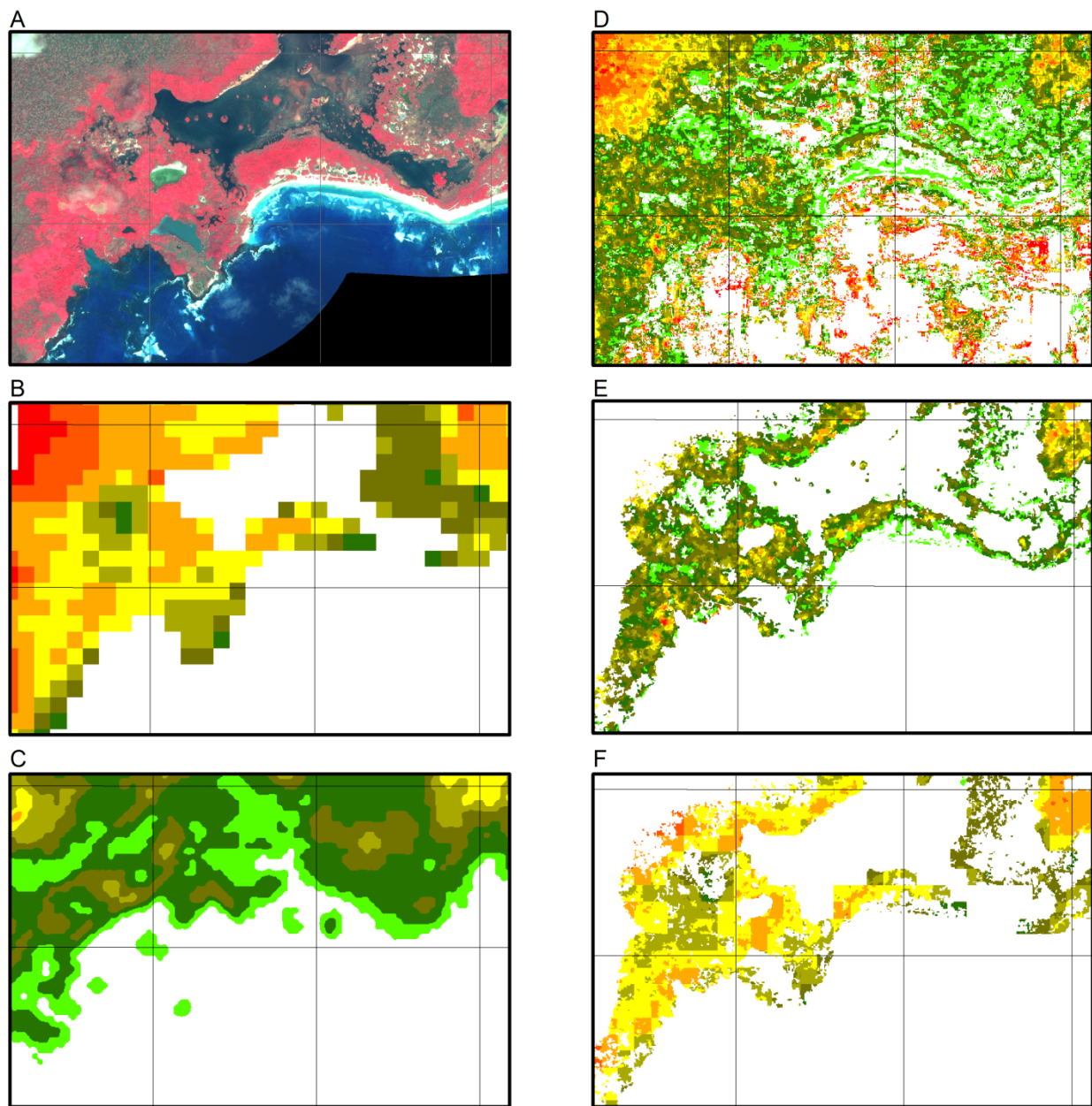
Surface Elevation including Canopy Height (m)

0 - 2	8 - 10
2 - 4	10 - 13
4 - 6	13 - 16
6 - 8	16 - 19

Figure 0.4: Maps of VHR false colour composite(A), SRTM (B), ASTER GDEM(C), PRISM-CH (D), PRISM-OBIA(E), SRTM+PRISM(F). Note that PRISM-CH has not had a water mask applied.

139

The ASTER GDEM had serious errors for the coastal areas of Galapagos. Almost all values were at sea-level or near sea-level and do not reflect the ground or vegetation surface (see figure 5.4C). The likely causes of this error is the global coastline definition around the Galapagos Islands or persistent cloud cover of the images in those areas. Although further information on this problem could not be found in any product documentation, this problem was reported on several online technical forums. Given the recent release of the ASTER GDEM product, these issue may be addressed in future product versions. Due to the nature of the errors, this product was not considered for further analysis. However, even if the ASTER GDEM was available for the study, the accuracy results of previous terrain studies suggest that it may be unacceptable for canopy height modeling. For example, Hirt et al. (2010) found that the vertical accuracy of the ASTER GDEM was 15m over Western Australia, more than twice that of SRTM. The authors conclude that despite the improved horizontal resolution, the vertical accuracy may impede research applications.

The three versions of the PRISM DSM showed improved accuracy with each level of processing. The PRISM DSM using only bare ground GCPs had considerable error, similar to that of the ASTER GDEM product. The GCPs were all located on or very near the coast with an elevation close to mean sea level, or in the highlands with an elevation above 500 meters. As such, there was not sufficient information to create accurate epipolar images of the forest canopy. The addition canopy height GCPs (PRISM-CH) reduced the RMSE by 2.29 meters. When the PRISM-OBIA DSM values were averaged over vegetation objects from the OBIA land cover classification, the RMSE was reduce to 3.74 meters producing a reasonable looking canopy height model (see figure 5.4E)).

The production of the PRISM-OBIA DSM created some strange errors (Figure 5.3E). Although there is a dense point cloud toward the center of the image, there are a number of points illustrating gross under-prediction for tall observed points or gross over-prediction for medium heights. One possible reason for this is heterogeneous canopies within image objects.

Another possible reason is error produced during the averaging process where missing data values were excluded from the mean calculation. For some objects, the majority of pixels may have been classified as missing data (i.e. calculation errors or unrealistic values during DSM generation) leading to a mean object height due to a few pixels that might not be representative.

Theoretically, the best RMSE possible for ALOS PRISM is 1.25m for the front-back stereo pair and 2.5m for the nadir-back or nadir-front pairs (Maruya and Ohyama, 2007). The PRISM DSM created in this study was through a merging of the backward-nadir, and forward-nadir DSMs as the forward-backward DSM had considerable errors during the DSM generation, likely due to matching errors. While a RMSE of 3.74m is about 50% greater than the theoretical value, the results here are better than the RMSE reported for terrain studies using ALOS PRISM. For example, Takaku (2009) reported RMSE values ranging from 4.72m to 20.78m over various terrain conditions. To date, there are not any canopy height studies using ALOS PRISM to compare the results with.

However, as Imai et al. (2008) outlined, actual results will deviate from theoretical results due to errors in geometric accuracy, triplet matching accuracy, and height calculation accuracy. Additionally, there were errors in the field measurements due to instrument error as well as the definition of canopy height by the observer. Although Simard et al. (2008) found that the random tree height error using a laser range finder was 10%, defining the point that represents canopy height from the ground, especially for sparse canopies, can be difficult and a major source of error.

Ultimately, these models are only useable if they provide a better estimate of canopy height than a null model (i.e. mean observed canopy height). The RMSE between the mean observed canopy height and observed canopy height is 3.41 meters, less than both the SRTM and PRISM-OBIA. Thus, neither of these products is suitable for predicting mangrove canopy height.

To potentially reduce the effects spatial averaging of the SRTM and the error of the PRISM-CH model, a combination of SRTM and PRISM was tested. The hybrid digital surface model was a composite of 75% of the SRTM and 25% of the PRISM. The resulting 2.92m RMSE was lower than the SRTM or PRISM independently, better than the mean canopy height model. The final model is mapped in figure 5.4(F). While the RMSE is higher than those reported by Simard et al. (2006) and Simard et al. (2008), the overall RMSE is reasonable considering the range of RMSE values reported by previous studies measuring canopy height using LiDAR. While some studies reported RMSE less than 2-meters (Clark et al., 2004; Coops et al., 2007; Tesfamichael et al., 2010), Rosette et al., 2008 reported a RMSE of 2.86m using IceSAT/GLAS. Thus the results of the hybrid model here have similar error to a large footprint waveform LiDAR demonstrating that the hybrid DSM may provide a viable solution for a finer scale canopy height mapping.

Conclusions

This research compared the capability of InSAR SRTM and optical stereo digital surface model products for estimating canopy height mangroves of fringe mangroves. The results demonstrate that the 90-meter SRTM and object-level ALOS PRISM DSMs have similar error for estimating canopy height for 10-meter diameter field plots. The ASTER GDEM product was unusable for the study area due to serious errors in the data possibly from either cloud cover or incorrect coastline editing. A hybrid model of SRTM and ALOS PRISM achieved the best results (RMSE = 2.92m), with similar error to previous studies using large footprint waveform LiDAR. These results suggest that a combination of SRTM and ALOS PRISM could be used to map canopy height of mangroves at finer scales. However, a stereo optical DSM requires cloud free images and high quality GCPs to create epipolar images that may present serious challenges for global mapping. Ultimately, there is a clear and demonstrated need for a global, high resolution

InSAR DSM product suitable for vegetation studies that can provide the accuracy demonstrated

by SRTM but at a finer spatial resolution suitable to fringe mangroves or fine scale analysis.

Reference

Alongi, D. M. (2002) Present state and future of the world's mangrove forests. *Environmental Conservation,* 29**,** 331.

--- (2008) Mangrove forests: Resilience, protection from tsunamis, and responses to global climate change. *Estuarine Coastal and Shelf Science,* 76**,** 1.

Bradbury, R. B., R. A. Hill, D. C. Mason, S. A. Hinsley, J. D. Wilson, H. Balzter, G. Q. A. Anderson, M. J. Whittingham, I. J. Davenport & P. E. Bellamy (2005) Modelling relationships between birds and vegetation structure using airborne LiDAR data: a review with case studies from agricultural and woodland environments. *Ibis,* 147**,** 443-452.

Bruniquel-Pinel, V. & J. P. Gastellu-Etchegorry (1998) Sensitivity of texture of high resolution images of forest to biophysical and acquisition parameters. *Remote Sensing of Environment,* 65**,** 61-85.

Clark, M. L., D. B. Clark & D. A. Roberts (2004) Small-footprint lidar estimation of sub-canopy elevation and tree height in a tropical rain forest landscape. *Remote Sensing of Environment,* 91**,** 68-89.

Costanza, R., R. dArge, R. deGroot, S. Farber, M. Grasso, B. Hannon, K. Limburg, S. Naeem, R. V. Oneill, J. Paruelo, R. G. Raskin, P. Sutton & M. vandenBelt (1997) The value of the world's ecosystem services and natural capital., *Nature,* 387**,** 253.

d'Ozouville, N., B. Deffontaines, J. Benveniste, U. Wegmuller, S. Violette & G. de Marsily (2008) DEM generation using ASAR (ENVISAT) for addressing the lack of freshwater ecosystems management, Santa Cruz Island, Galapagos. *Remote Sensing of Environment,* 112**,** 4131-4147.

Fatoyinbo, T. E., M. Simard, R. A. Washington-Allen & H. H. Shugart (2008) Landscape-scale extent, height, biomass, and carbon estimation of Mozambique's mangrove forests with Landsat ETM+ and Shuttle Radar Topography Mission elevation data. *Journal of Geophysical Research-Biogeosciences,* 113.

Helmer, E. H., T. S. Ruzycki, J. M. Wunderle, S. Vogesser, B. Ruefenacht, C. Kwit, T. J. Brandeis & D. N. Ewert (2010) Mapping tropical dry forest height, foliage height profiles and disturbance type and age with a time series of cloud-cleared Landsat and ALI image mosaics to characterize avian habitat. *Remote Sensing of Environment,* 114**,** 2457-2473.

Heumann, B. (2011) Satellite remote sensing of mangrove forests: Recent advances and future opportunities. *Progress in Physical Geography,* 35**,** 87-108.

Hyde, P., R. Dubayah, W. Walker, J. B. Blair, M. Hofton & C. Hunsaker (2006) Mapping forest structure for wildlife habitat analysis using multi-sensor (LiDAR, SAR/InSAR, ETM plus , Quickbird) synergy. *Remote Sensing of Environment,* 102**,** 63-73.

Hyyppa, J., H. Hyyppa, M. Inkinen, M. Engdahl, S. Linko & Y. H. Zhu (2000) Accuracy comparison of various remote sensing data sources in the retrieval of forest stand attributes. *Forest Ecology and Management,* 128**,** 109-120.

Kellndorfer, J., W. Walker, L. Pierce, C. Dobson, J. A. Fites, C. Hunsaker, J. Vona & M. Clutter (2004) Vegetation height estimation from shuttle radar topography mission and national elevation datasets. *Remote Sensing of Environment,* 93**,** 339-358.

Lefsky, M. A., W. B. Cohen & T. A. Spies (2001) An evaluation of alternate remote sensing products for forest inventory, monitoring, and mapping of Douglas-fir forests in western Oregon. *Canadian Journal of Forest Research-Revue Canadienne De Recherche Forestiere,* 31**,** 78-87.

Lillesand, T. & R. Kiefer. (1987) *Remote Sensing and Image Interpretation.* Wiley.

Liu, X. Y. (2008) Airborne LiDAR for DEM generation: some critical issues. *Progress in Physical Geography,* 32**,** 31-49.

Lucas, R. M., J. C. Ellison, A. Mitchell, B. Donnelly, M. Finlayson & A. K. Milne (2002) Use of stereo aerial photography for quantifying changes in the extent and height of mangroves in tropical Australia. *Wetlands Ecology and Management,* 10**,** 161-175.

Mitchell, A. L., R. M. Lucas, B. E. Donnelly, K. Pfitzner, A. K. Milne & M. Finlayson (2007) A new map of mangroves for Kakadu National Park, Northern Australia, based on stereo aerial photography. *Aquatic Conservation-Marine and Freshwater Ecosystems,* 17**,** 446-467.

Peng, X. L., J. F. Wang & Q. F. Zhang (2005) Deriving terrain and textural information from stereo RADARSAT data for mountainous land cover mapping. *International Journal of Remote Sensing,* 26**,** 5029-5049.

Rodriguez, E., C. S. Morris, J. E. Belz, E. C. Chapin, J. M. Martin, W. Daffer & S. Hensley (2005) An assessment of the SRTM topographic products. *Technical Report JPL D-31639***,** 143.

Rosette, J. A. B., P. R. J. North & J. C. Suarez (2008) Vegetation height estimates for a mixed temperate forest using satellite laser altimetry. *International Journal of Remote Sensing,* 29**,** 1475-1493.

Rott, H. (2009) Advances in interferometric synthetic aperture radar (InSAR) in earth system science. *Progress in Physical Geography,* 33**,** 769-791.

Saraf, A. K., B. P. Mishra, S. Choudhury & P. Ghosh (2005) Digital elevation model (DEM) generation from NOAA-AVHRR night-time data and its comparison with USGS-DEM. *International Journal of Remote Sensing,* 26**,** 3879-3887.

Shugart, H. H., S. Saatchi & F. G. Hall (2010) Importance of structure and its measurement in quantifying function of forest ecosystems. *Journal of Geophysical Research-Biogeosciences,* 115.

Simard, M., V. H. Rivera-Monroy, J. E. Mancera-Pineda, E. Castaneda-Moya & R. R. Twilley (2008) A systematic method for 3D mapping of mangrove forests based on Shuttle Radar Topography Mission elevation data, ICEsat/GLAS waveforms and field data: Application to Cienaga Grande de Santa Marta, Colombia. *Remote Sensing of Environment,* 112**,** 2131-2144.

Simard, M., K. Q. Zhang, V. H. Rivera-Monroy, M. S. Ross, P. L. Ruiz, E. Castaneda-Moya, R. R. Twilley & E. Rodriguez (2006) Mapping height and biomass of mangrove forests in Everglades National Park with SRTM elevation data. *Photogrammetric Engineering and Remote Sensing,* 72**,** 299-311.

St-Onge, B., Y. Hu & C. Vega (2008) Mapping the height and above-ground biomass of a mixed forest using lidar and stereo Ikonos images. *International Journal of Remote Sensing,* 29**,** 1277-1294.

Takaku, J. & T. Tadono (2009) PRISM On-Orbit Geometric Calibration and DSM Performance. *Ieee Transactions on Geoscience and Remote Sensing,* 47**,** 4060-4073.

ASTER Global Validation Team (2009) ASTER Global DEM Validation Summary Report. http://www.ersdac.or.jp/GDEM/E/image/ASTERGDEM_ValidationSummaryReport_Ver1.pdf

Tesfamichael, S. G., F. B. Ahmed & J. A. N. Van Aardt (2010) Investigating the impact of discrete-return lidar point density on estimations of mean and dominant plot-level tree height in Eucalyptus grandis plantations. *International Journal of Remote Sensing,* 31**,** 2925-2940.

Toutin, T. (2002a) DEM from stereo Landsat 7 ETM+ data over high relief areas. *International Journal of Remote Sensing,* 23**,** 2133-2139.

--- (2002b) Three-dimensional topographic mapping with ASTER stereo data in rugged topography. *Ieee Transactions on Geoscience and Remote Sensing,* 40**,** 2241-2247.

--- (2004) DTM generation from Ikonos in-track stereo images using a 3D physical model. *Photogrammetric Engineering and Remote Sensing,* 70**,** 695-702.

--- (2006) Comparison of 3D physical and empirical models for generating DSMs from stereo HR images. *Photogrammetric Engineering and Remote Sensing,* 72**,** 597-604.

--- (2008) ASTER DEMs for geomatic and geoscientific applications: a review. *International Journal of Remote Sensing,* 29**,** 1855-1875.

Vega, C. & B. St-Onge (2008) Height growth reconstruction of a boreal forest canopy over a period of 58 years using a combination of photogrammetric and lidar models. *Remote Sensing of Environment,* 112**,** 1784-1794.

White, J. C., C. Gomez, M. A. Wulder & N. C. Coops (2010) Characterizing temperate forest structural and spectral diversity with Hyperion EO-1 data. *Remote Sensing of Environment,* 114**,** 1576-1589.

Wilkie, M. L. & S. Fortuna. (2003) S*tatus and trends in mangrove area extent worldwide*. In *Forest Resources Assessment Working Paper*. Rome: <st1:place w:st="on">Forest Resources Division. FAO.

Woodhouse, I. H. (2006) Predicting backscatter-biomass and height-biomass trends using a macroecology model. *Ieee Transactions on Geoscience and Remote Sensing,* 44**,** 871-877.

Wulder, M. A., C. W. Bater, N. C. Coops, T. Hilker & J. C. White (2008) The role of LiDAR in sustainable forest management. *Forestry Chronicle,* 84**,** 807-826.

Chapter 6 : Conclusions

The aim of this research was to investigate new earth observation sensors and methods for characterizing mangrove forest composition and structure. Emphasis was placed on globally available very high resolution imagery suitable for mapping fringe mangroves like those found in the Galapagos Islands. Three characteristics were examined: **1)** species composition, **2)** leaf area, and **3)** canopy height. These parameters are important factors for monitoring or modeling ecosystem goods and services such as habitat for biodiversity, standing biomass, and nutrient or water flux.

A review of previous literature in Chapter 2 found that there are a number of areas of remote sensing methods that have not been investigated for mangroves. Image classification has not explicitly considered fringe mangroves and the Woldview-2 sensor has not been applied to mangrove studies. Image texture and SWIR SVI have not been investigated to predict LAI. VHR stereo imagery has not been used to estimate and map mangrove canopy height.

Image classification in Chapter 3 found that the spectral separability between mangrove and mangrove associate species was higher using Worldview-2 than Quickbird imagery. When comparing true mangroves with mangrove associates, spectral separability was higher at the object level than individual pixel-level. However, at both a pixel and object-level, most individual species could not be spectrally separated likely due to subtle spectral differences between species and the effects of noise from non-leaf surfaces. The inclusion of object spectral standard deviation or image texture (GLCM) did not substantially improve classification accuracy.

An analysis of SVI and image texture to detect LAI in Chapter 4 found that image texture predicted LAI better than spectral vegetation indices. In contrast to previous studies, spectral vegetation indices poorly predicted leaf area. Spectral vegetation indices from ALI outperformed those from Quickbird demonstrating that spectral range and sensor sensitivity may be more important than spatial resolution, despite potential mixed pixel effects. Unmixing of spectral vegetation indices did not improve the results. Although image texture explained 66% of tLAI

149

variance, the nature of the species-specific relationships presents a serious challenge for predicting tLAI over mixed canopies using these results.

A comparison of DSM to map canopy height in Chapter 5 found that the ALOS PRISM DSM better predicted canopy height at the object level than at the pixel level and that this object-level PRISM DSM has similar error compared to the 90-meter SRTM InSAR DSM product. A data fusion of these two DSM produced the least error, reducing error to less than 3-meters, similar to level of error reported for space-based large footprint waveform LiDAR.

There were several results that were surprising and unexpected. First the limited improvement of Worldview-2 over Quickbird for pixel-level spectral separability was found despite the addition of 4 new spectral channels, although the WV-2 band ratio of RE/G did highlight manzanillo tree very well compared to other vegetation. Second, there were two unexpected results in the SVI LAI analysis. 1) It was surprising that the spectral unmixing of the ALI imagery did not improve the results with LAI even for the SVI that are known to be sensitive to background conditions. 2) It was interesting to find that the Quickbird SVI results did not replicate those of Kovacs et al. for red and black mangroves, although the sample size of black mangroves was small. Third, the optimal resolution of image texture in relation to LAI was found to be 0.6 meters where previous studies indicated that a coarser resolution of approximately one half the crown diameter was best. Forth, results from both the classification and canopy height analysis demonstrated that the quality of the data was more important than spatial resolution. Specifically, the spectral range and sensitivity of ALI was superior to Quickbird and the SRTM DSM was superior to ALOS PRISM despite the order of magnitude difference in spatial resolution between the respective sensors.

There were several avenues of research that were explored during this research that were not described in the research chapters as they were discarded during exploratory analysis including lacunarity for LAI or species mapping, spectral variation or image texture within object for species classification, and spectral unmixing of background substrate using Quickbird.

Lacurarity, a measure of spatial pattern, was calculated using panchromatic and NIR Quickbird imagery. Despite testing a wide range of parameters (e.g., window size and direction), lacunarity was not found to be significantly related to LAI. Previous studies have also used lacunarity as an input to segment imagery into objects. In the highly fragmented vegetation in this study area, lacnarity was not found to produce useful or realistic objects.

In the image classification at the object-level, only mean spectral reflectance was used in the reported classification. Image texture (GLCM), and spectral standard deviation were explored but they were not found to improve spectral separability using J-M distance. Similarly, tt was found using the feature optimization tool in eCognition that spectral information alone could not distinguish between major land cover classes. The major problem was the confusion between water and the substrate below the water (e.g. sand or lava). However, it was found that a rule-based classification with some minor manual editing could accurate classify these areas. While the inclusion of image texture or object spectral variability did greatly improve separabiltiy between classes using the feature optimization tool, the nearest neighbour classifier in eCognition over fit the object characteristics producing very unrealistic and inaccurate classifications. Similarly, using other object statistics or shape properties also produced an overfit classification that did not capture non-training objects of the same land cover type.

Spectral unmixing of background substrates was examined in hopes of mapping FCC using the substrate-specific models. While lava and sand could be easily detected, leaf litter could not. Furthermore, without either coastal blue or SWIR, shallow water over sand or lava could not be detected and thus this line of research was abandoned. The Worldview-2 imagery was acquired after the LAI analysis was completed and thus the use of this imagery, specifically for new SVI or spectral unmixing, was not explored.

Much of the research use multi-step methods. In this context, it is important to consider the impact of error at each step to understand error propagation. For the mangrove classification, a decision tree was used prior to the SVM classification. The use of a decision tree

can be very useful as a step-wise method of classification. However, with each step, the errors of the previous step compound. For example, the accuracy of the true mangrove classification is dependent on the accuracy of the vegetation, coastal vegetation, and the dense coastal vegetation decision rules. To account for this error propagation, an accuracy assessment after each decision rule would be required.

For the LAI research, the multi-step analysis did not lead to a propagation of error. In this analysis, the exploratory analysis was used only to identify the best set of variable to be used on a parametric statistical model and thus served only to inform the variables in the model but did not contribute any data directly to the final model. That said, there were other sources of error such as the field measurements of LAI, but these errors were additive rather than multiplicative.

The canopy height analysis also included a multi-step component. In this analysis, the different DSMs were primarily considered independent of each other. However, the final hybrid model was a form of data fusion. Specifically, the PRISM DSM averaged of the dense vegetation objects and the SRTM DSM. However, since the model was explicitly the addition of the two datasets, it can be reasonable to assume the any error was random and thus does not compound between the two datasets.

This research sought to address many of the areas of missing gaps in the remote sensing of mangroves outlined in Chapter 2. This research has contributed to the remote sensing of mangroves to characterize mangrove forests that could eventually be used to parameterize models of ecosystem goods and services in several ways. First, issues of spatial resolution, scale and accuracy were addressed around the need to globally assess fringe mangroves using available remote sensing. This research also demonstrated improved results of OBIA over pixel-based analysis further demonstrating the need to shift from pixel to object-based analysis. Second, the application of new sensors for mangrove forest mapping, namely ALOS-PRISM and Worldview-2, was investigated. ALOS-PRISM was not shown to produce reliable estimates of

canopy height, but Worldview-2 did show marked improvement over Quickbird for mangrove mapping. Third, the adaptation of methods, such as image texture, to mangrove forests was tested. Image texture for mapping leaf area has shown good results. This research has contributed to the on-going search for the best metrics and parameters of image texture for mapping canopy structure. This research has also demonstrated some of the limitations of image texture such as species-specific relationships.

Based on the findings of this research, the following research areas for the global mapping and monitoring of mangroves should be addressed: **1)** Given the limitations of Worldview-2 to spectrally distinguish between mangrove species, hyperspectral remote sensing, especially at very high spatial resolutions, should be investigated for mapping mangrove species. **2)** Image texture has shown promise for mapping canopy structure, but it is sensitive for edge effects. Image texture should be examined at the object level to help alleviate these issues. Furthermore, more research is needed into the use of image texture with different spectral bands, possibly including background insensitive SVI, especially over areas with varying background conditions such as mangroves. **3)** Although a hybrid ALOS PRISM - SRTM DSM had reasonable accuracy, neither sensor alone is sufficient for accuracy mapping of canopy height at finer resolutions required for fringe mangroves. Given that SRTM outperformed ALOS PRISM, despite an order of magnitude difference in spatial resolution, InSAR is clearly the better method for mapping canopy height. There is a great need for a global, high resolution InSAR DSM product suitable for vegetation studies from sensors like ALOS PALSAR or Radarsat-2. **4)** Results from both the classification and canopy height analysis demonstrated that the quality of the data was more important than spatial resolution. Specifically, the spectral range and sensitivity of ALI was superior to Quickbird and the SRTM DSM was superior to ALOS PRISM despite the order of magnitude difference in spatial resolution.

For the Galapagos Islands, many of the remaining challenges could be solved using airborne LiDAR. LiDAR has been shown to accurately estimate a wide variety of forest structure

parameters including LAI, canopy height, and above ground biomass for terrestrial forests. OBIA can be enhanced using a fusion of LiDAR and VHR optical imagery as VHR imagery can be segmented into more meaningful natural objects using height. Additionally, LiDAR can obtain detailed ground elevation data that would enhance investigations into mangrove finch habitat by identifying higher locations with leaf litter as well as questions around spatial pattern and process of mangrove species and structure. Given the well documented application of LiDAR to forestry studies and the relatively small extent of mangrove forests in the Galapagos, this approach would bring the greatest benefit in the near future to mapping and monitoring mangroves in the Galapagos Islands.